

## Color transparency and final-state interactions in photonuclear charmonium production

S. Gardner\*

*Continuous Electron Beam Accelerator Facility, Newport News, Virginia 23606*

(Received 17 March 1992)

The final-state interactions of quasielastically photoproduced charmonium have been computed in a quantum-mechanical QCD-inspired model for a range of photon energies and nuclear targets. In this model, charmonium in its rest frame interacts with an array of nucleon flux tubes via its color dipole moment as color electric fields “flash” on and off around it. The photoproduction amplitude is modeled as the narrowest superposition of open charmonium channels available at a given photon energy. A complete calculation of the final-state interactions has been performed; this involves retaining all the charmonium states present in the initial amplitude and produced upon interactions with the medium, and allowing them to scatter into each other upon further medium interactions. This work permits the computation of  $A^{\text{eff}}/A$  with and without “transparency”; the results support the utility of a study of the energy dependence of  $A^{\text{eff}}/A$  in elucidating transparency in the exclusive process considered. Moreover, a comparison of the underlying  $J/\psi$ -nucleon cross section with that deduced from a Glauber analysis of the computed  $A$  dependence shows the Glauber analysis to be misleading.

PACS number(s): 24.85.+p, 25.20.Lj

### I. INTRODUCTION

In this paper the final-state interactions of photoproduced charmonium with the nucleus have been calculated in a QCD-inspired model. In QCD, the interactions of a color singlet cluster of quarks with the nuclear medium depend on the relative separation of the quarks in the projectile. Consequently, a “small” color singlet state produced in the nucleus at large energies may interact weakly with the medium. In this case,  $A^{\text{eff}}$ , the total number of nucleons participating in the reaction, is roughly  $A$ . This effect, called color transparency by Brodsky and others, if observed experimentally, would be striking: one can have “weak” strong interactions [1–5]. Color transparency has most often been discussed in the context of quasielastic ( $e, e'p$ ) and ( $p, pp$ ) reactions at large  $Q^2$ , where a “hard” (large  $Q^2$ ) process is presumably followed [and, in the ( $p, pp$ ) case, preceded as well] by “soft” interactions with the nuclear medium. In these reactions,  $p$ QCD arguments indicate that the initial state produced by the hard process is “small” – relative to the size of the proton – and these arguments suggest that  $A^{\text{eff}}/A \rightarrow 1$  at large  $Q^2$  [4,5].

In the present paper quasielastic charmonium production is considered for the exclusive process in which the  $J/\psi$  carries off the maximum momentum consistent with momentum conservation (large  $x_F$ , zero  $p_T$ ), as a function of the photon energy  $E_\gamma$ . By definition, the initial

production process is “soft” [6], yet it will be argued that the initial state in this case may also be small. In what follows, it will be assumed that this produced charmonium state is small relative to the size of the  $J/\psi$ , and the final-state interactions will be computed as a function of photon energy and *Ansatz* for the initial charmonium amplitude in a simple, QCD-inspired model in a numerically exact way. The highest energies explicitly considered here are a few tens of GeV. In this energy regime, the approach of  $A^{\text{eff}}/A$  towards 1 as a function of photon energy would be regarded as a signature of transparency.

This work represents a departure from conventional descriptions of hadronic final-state interactions in two different ways. First, the assumption of a spatially small initial state means that the initial amplitude is a complicated superposition of charmonium eigenstates, rather than an amplitude for  $J/\psi$  production alone. Second, the propagation of the small *superposition* of states through the nuclear medium implies that quantum mechanical coherence effects in the final-state interactions cannot be, and are not, neglected. The Glauber formalism commonly used to treat hadronic final-state interactions assumes that the projectile interacts independently with the nucleons of the nucleus, ignoring these coherence effects. The primary goal of this paper is to compute the final-state interactions in the nucleus when such coherence effects are included. The results will be compared with the conventional formulation where these effects are neglected. In this way, a model calculation of the final-state interactions is realized. The comparison of  $A^{\text{eff}}/A$  with and without “transparency” as a function of energy and initial state *Ansatz* is a unique feature of this work.

One can also use this model study to examine the efficacy of the Glauber analysis in extracting the total  $J/\psi$ -nucleon cross section from the measured  $A$  dependence. That is, the underlying  $J/\psi$ -nucleon cross section is well

---

\*Present address: Nuclear Theory Center, Indiana University, 2401 Milo B. Sampson Lane, Bloomington, IN 47408.  
e-mail: gardner@venus.iucf.indiana.edu

defined, and this cross section can be compared with the cross section deduced from the calculated  $A^{\text{eff}}/A$ , using the Glauber formula. To the extent that transparency effects are present, the Glauber analysis is misleading as it yields cross sections which are smaller than the “known”  $J/\psi$ -nucleon cross section given by the model [7].

The idea is to construct a model in which the computation of the final-state interactions, including coherence effects, can be effected. This computational limitation constrains the complexity of the model which may be considered; indeed, many of the model assumptions are heuristic. The model adopted here is a refinement of the model adopted in Refs. [8–10]. The model will now be outlined; the logic of the various choices is explained in detail in Sec. II.

(1) Charmonium itself is modeled with a non-relativistic harmonic oscillator, so that its rest-frame Hamiltonian is given by

$$H_0(\vec{r}) = -\frac{(\hbar c)^2}{2\mu_c} \nabla_{\vec{r}}^2 + \frac{1}{2}\mu_c \omega^2 r^2 + C. \quad (1.1)$$

Here the values  $\mu_c = 0.92$  GeV and  $\hbar\omega = 0.24$  GeV are used.  $C$  is defined so that Eq. (1.1) reproduces the empirical  $J/\psi$  mass.

(2) The initial state of the charmonium system in coordinate space is chosen to localize the state as well as possible. For a few tens of GeV, threshold effects alter the initial state. Consequently, the initial state is chosen as the smallest state which can be constructed from the available  $s$ -wave channels. At large energies, the initial state is chosen to be

$$\psi_i(r) = \left(\frac{\alpha_i}{\pi}\right)^{3/4} \exp\left(-\frac{\alpha_i}{2}r^2\right) \quad (1.2)$$

where  $\alpha_i$ , and the size of the state, are limited by the Compton wavelength of the heavy quark.

(3) The nucleons in the nucleus are modeled as flux tubes; the color electric field of the flux tube is chosen to be an uniform field in U(1) color with a circular boundary. The radius of this circle is chosen to be 0.8 fm. The field strength in the lab,  $E_{\text{str}}^{\text{lab}}$ , is chosen to be the meson Regge string tension, such that  $|eE_{\text{str}}^{\text{lab}}| = k_{\text{Regge}} \approx 0.9$  GeV/fm. The approximations leading to this choice of geometry are illustrated in Fig. 1.

(4) The interaction of the charmonium wave packet with the field of the flux tube is that of an U(1) color electric dipole. Working in the charmonium rest frame (defined by the mass of the  $J/\psi$ ), the interaction Hamil-

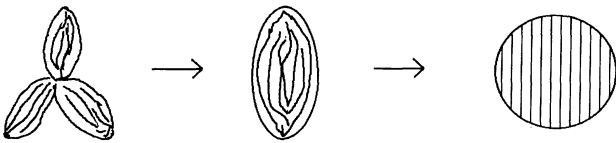


FIG. 1. Successive caricatures of the nucleon. The representation of the nucleon as a “Y-shaped” flux tube is approximated by a quark-diquark geometry, and the field configuration of the latter is represented as a uniform field with circular boundary.

tonian is chosen to be of form

$$H_{\text{int}}(t) = -e\gamma \vec{E}_{\text{str}}^{(1)} \cdot \vec{r} \Theta(t - t_1) \Theta(t_1 + \tilde{\tau}/\gamma - t). \quad (1.3)$$

In this frame, the electric field is assumed to illuminate the  $c\bar{c}$  wave function uniformly for a time given by  $\tilde{\tau}/\gamma$ , where  $\tilde{\tau} = \tau/c$  and  $\tau$  is the width of the flux tube in the laboratory frame. The model is fit to  $\langle E_\gamma \rangle \approx 120$  GeV photoproduction data to yield a flux-tube width of  $\tau = 1.3 \pm 0.3$  fm. The field is assumed to be purely transverse to the direction of motion of the  $c\bar{c}$ ; consequently, the magnitude of the electric field in the laboratory frame is scaled by the Lorentz factor  $\gamma$  in the rest frame.

(5) The multiple scattering of the  $c\bar{c}$  wave packet with the nucleons of the medium is modeled in the following way: the nucleon-flux-tubes are assumed equally spaced, where the spacing of the centers is given by  $D_{\text{spac}} = 2(3/4\pi\rho_{\text{unif}}^A)^{1/3}$  and  $\rho_{\text{unif}}^A$  is the uniform equivalent density of nucleus  $A$ . The charmonium executes straight-line motion through the nuclear medium (see Fig. 2). The fields of the nucleon-flux-tubes are randomly oriented around the transverse axis, so that observables are obtained after averaging over the ensemble of flux-tube orientations.

(6) The observables of interest are the occupation probabilities  $|\langle \psi_f | \psi_{c\bar{c}}(t) \rangle|^2$  of charmonium in its  $J/\psi$ ,  $\chi$ , or  $\psi'$  states after  $N$  flux tube interactions (see Figs. 7–12). These probabilities can be connected to the  $A^{\text{eff}}/A$  associated with the production of a particular  $c\bar{c}$  state. Two possible reaction mechanisms exist at high energies (see Fig. 3).  $J/\psi$  may be produced either via a “shadowed” process, i.e., via a long-lived virtual tower of hadrons [11], or via a “direct” process, in which the  $c\bar{c}$  fluctuation is knocked immediately on-shell – this is the mechanism considered in this paper. The importance of shadowing with energy is estimated in Table II; for photon energies of a few tens of GeV, it is not important. For direct  $J/\psi$  production, so that shadowing is ignored,  $A^{\text{eff}}/A$  is

$$\left[\frac{A^{\text{eff}}}{A}\right]_{J/\psi} = \frac{\int_A dz d^2\vec{b} \rho_A(z, b) \tilde{P}_{J/\psi}(N_{\text{eff}}(z, b))}{\int_A dz d^2\vec{b} \rho_A(z, b)}. \quad (1.4)$$

$\rho_A(z, b)$  is the nuclear density, and  $N_{\text{eff}}(z, b)$  is the effec-

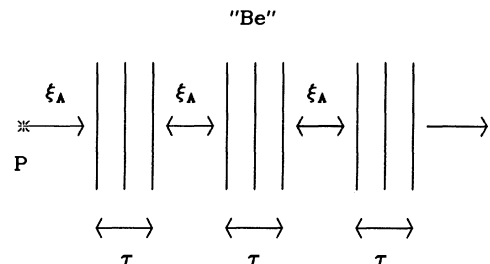


FIG. 2. Schematic of the medium the  $c\bar{c}$  wave packet encounters in its exit through the nucleus after its production at point  $P$ . The field configurations of the successive nucleons may have some orientation  $\theta_j$  with respect to the first, though in this figure all the nucleons are aligned. The schematic is realized with a  $\xi_A : \tau$  ratio commensurate with that of Be.

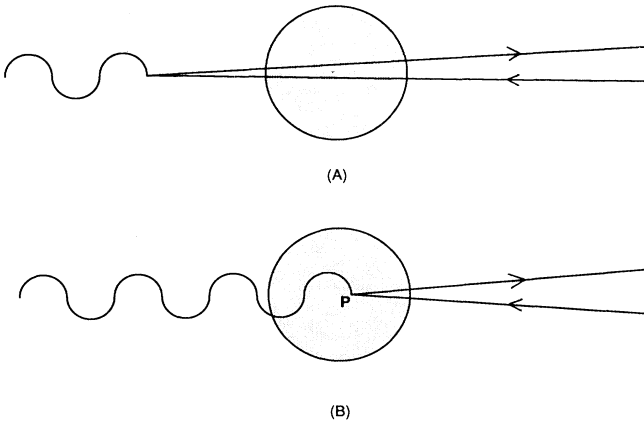


FIG. 3. Charmonium photoproduction at very high (a) and at very low (b) energies. In (a), the photon may fluctuate to  $c\bar{c}$  well in advance of the target, so that the photon's interaction with the nuclear medium is primarily hadronic. In (b), the photon interacts weakly with the nuclear medium and may produce  $c\bar{c}$  at point  $P$ .

tive number of nucleons with which the  $c\bar{c}$  superposition interacts, given an initial production point  $(z, \vec{b})$ .  $z$  and  $\vec{b}$  are defined with respect to the center of the nucleus;  $z$  is the reaction coordinate of the  $c\bar{c}$  tower, parallel to the incoming photon, whereas  $\vec{b}$  is the impact parameter.  $\bar{P}_{J/\psi}(N_{\text{eff}}(z, b))$  is the  $J/\psi$  occupation probability after  $N_{\text{eff}}$  flux tube interactions, normalized to its content in a given initial state.  $N_{\text{eff}}$  is given by

$$N_{\text{eff}}(z, b) \equiv \left[ \left( \frac{t_A(z, b)}{\rho_{\text{unif}}^A D_{\text{spac}}} \right) \right], \quad (1.5)$$

where  $t_A(z, b)$  is the nuclear thickness function,  $t_A(z, b) = \int_z^\infty dz' \rho_A(z', b)$ , and the in-line brackets denote “nearest integer.” Equation (1.4) can be understood as averaging the  $J/\psi$  occupation probability obtained after  $N$  flux tube interactions over the nuclear volume, weighted by the nuclear density. In this way,  $A^{\text{eff}}/A$  for  $J/\psi$ ,  $\chi$ , and  $\psi'$  production can be calculated, and its energy dependence is determined by varying  $\gamma$  in Eq. (1.3) (see Tables X–XII).

The exact numerical calculation is made possible through the structure of Eq. (1.3). One has a time-independent Hamiltonian – either with or without the  $c\bar{c}$ -nucleon interaction – which persists for some finite length of time. The time-dependent development of the wave packet then becomes a superposition problem. Consequently, the exact evolution of the  $c\bar{c}$  wave function with time can be computed from the eigenfunctions and eigenenergies of  $c\bar{c}$  within the nucleon flux tubes. The number of states which must be retained in the evolution matrix for a meaningful calculation greatly increases with energy; this limits the highest energy which may be considered here to a few tens of GeV.

The basic model considered here was adopted previously by Hufner *et al.* [8], Quack [9], and Blaizot *et al.* [10]. The version considered here is more elaborate: the

nucleons are treated as flux tubes of finite, rather than of infinite, length. The probabilities of producing  $J/\psi$ ,  $\chi$ , or  $\psi'$  states as a function of energy and number of nucleon interactions are computed explicitly. In addition, the energy dependence of the shape of the photoproduced charmonium state has been considered, as well as the connection between the evolution of charmonium through a sequence of flux tubes to its passage through a nucleus with some given charge density. The other works were interested, rather generally, in the interaction of a fast  $c\bar{c}$  with the nuclear medium. Here the specific process considered is zero  $p_T$ , quasielastic  $J/\psi$  production from nuclei.

The calculation of  $A^{\text{eff}}/A$  with energy shows the overall change of  $A^{\text{eff}}/A$  to be less than 20% in the energy range  $E_\gamma = 8.5\text{--}20$  GeV, even though many of the model's aspects enhance the effect of transparency. Moreover, in the energy range considered,  $A^{\text{eff}}/A$  may oscillate with energy (see Table X). The overall change of  $A^{\text{eff}}/A$  is not large, yet the relative effect can be enormous. That is, a computation “without transparency” yields less than a 2% change in  $A^{\text{eff}}/A$  in the same energy range, where “without transparency” means that the initial superposition is the  $J/\psi$  eigenstate and that only the  $J/\psi$  state is retained in the propagation of the  $c\bar{c}$  wave packet between nucleons (see Table XI). Again, this comparison is a unique feature of this work: the energy dependence of  $A^{\text{eff}}/A$  with and without transparency is computed in the same model. Although the change of  $A^{\text{eff}}/A$  in the energy range considered is not large, this work supports the use of the empirical behavior of  $A^{\text{eff}}/A$  with energy as a signature of transparency. Another interesting result of this paper is that an increase in  $A^{\text{eff}}/A$  with energy, albeit much weaker, can be seen even if the initial superposition is just the  $J/\psi$  eigenstate. Even if the initial state is an eigenstate, the final-state interactions themselves will produce a superposition of states, which will oscillate in time, with a period (in the wave packet's rest frame) determined by the level spacing of the hadron spectrum (see Figs. 7–9). In the lab frame, this period dilates, so that “snapshots” taken in the lab frame at a distance  $d$  from the initial interaction point at successively increasing momenta show the wave packet at earlier and earlier moments in its rest-frame expansion. Thus, as a nucleus is of finite size, it “sees” more of the initial state as the momentum increases. This illustrates the essential role of the final-state interactions in yielding transparency.

The high energy limit of the model is used in various ways. At high photon energies, the differing time development of the states in the superposition due to the small, but finite, differences in their masses is suppressed by time dilation, so that the expectation value of the relative separation of the quarks becomes stationary in time. Thus, this is called the “frozen” limit. In this model, this limit can be explored analytically. This serves as a useful check of the numerical calculation, provides a convenient way of fitting the flux tube width  $\tau$ , and is useful in providing qualitative insight. In this model in this limit,  $A^{\text{eff}}/A$  is energy independent because the product of the field strength and the interaction time is energy independent. This eventual saturation of  $A^{\text{eff}}/A$  with energy has

been predicted in other models of transparency [12–15]. Here the role of shadowing at very high photon energies is also addressed, albeit superficially, and it is suggested how the additional reaction mechanism might modify the expected saturation of  $A^{\text{eff}}/A$  at hundreds of GeV. In addition, the  $J/\psi$ - and  $\psi'$ -nucleon cross sections can be readily computed in perturbation theory and compared with the exact numerical results. The poor agreement serves as an explicit demonstration of how the existence of transparency and the applicability of perturbation theory need not be linked.

In order to effect the described calculations, many simplifications have been made. It is useful to highlight some of these simplifying assumptions, so that the limitations of the model can be better understood.

This entire work assumes that the physics of the production step can be factorized from that of the final-state interactions. That is, the initial amplitude is taken to be a superposition of *physical* charmonium states. Although some separation of time scale may exist, it is clear that in order to construct a complete description of the process, including the production step, this assumption must be broken, as final-state interactions must act to knock the initial hadronic fluctuation on-shell. Although this is a nontrivial complication, and ultimately an essential one, it is deemed unimportant for a study of the phenomenological impact of such coherence effects, as is the goal here.

The inclusion of open channels, such as  $\bar{D}\Lambda_c$  or  $\pi$  production may have a significant impact, but they have not been included. As it is highly impractical to include all these channels explicitly, some appropriate optical model to describe the loss to the open channels should be constructed. As transparency exists because of rescattering to the  $J/\psi$  channel through final-state interactions, it would seem that the inclusion of open channels should weaken the effect of transparency with energy (see Figs. 13–15).

The charmonium rest frame has been *defined* by the rest mass of the  $J/\psi$ . The mass of the charmonium system, however, varies strongly with excitation, since no strongly bound system is genuinely nonrelativistic. Perhaps additional momentum-dependent phases should be introduced to describe the boosts of the excited states of charmonium in their rest frame to the  $J/\psi$  rest frame, though this has not been done. As the photon energy increases, the relative boosts of adjacent states do become smaller. However, this additional dispersion of the wave packet could also weaken the transparency effect in the energy range of a few tens of GeV.

There are also some computational simplifications: the  $c\bar{c}$ -flux-tube interaction is assumed to “flash” on and off, the flux tubes are treated as if they are purely transverse, and they are assumed to be equally spaced, in order to simplify the Monte Carlo integrations. Probably the first is the most uncontrolled of these approximations. The uniform illumination of the  $c\bar{c}$  wave function by the nucleon’s chromoelectric field in Eq. (1.3) assumes that the nucleon width is large compared to the size of the charmonium wave function in the charmonium rest frame. At very high energies, the Lorentz contraction

of the proton wave function at rest invalidates such an assumption. Seemingly, then, the passage of the narrow proton – here a narrow flux tube – through the  $c\bar{c}$  wave function should be calculated explicitly. However, the appropriate longitudinal dimension to be assigned to a real proton boosted to high momenta is a matter of some question [16–18]. At any rate, the computation of the explicit passage of a narrow flux tube through the charmonium wave function is a much less manageable problem; the choice of Eq. (1.3) is necessary to effect the computation. The interaction choice made is consistent with grafting relativistic kinematics to non-relativistic quantum mechanics. In the laboratory frame, the uniform illumination approximation to the  $c\bar{c}$ -nucleon interaction is an excellent one; Galilean invariance requires that this interaction be equivalent to the physics of the center of mass frame. Certainly, the interaction Hamiltonian used should be at its most meaningful in the near threshold region considered.

The last three limitations discussed may modify the energy dependence of  $A^{\text{eff}}/A$  computed in the  $E_\gamma = 8.5$  to 20 GeV region. The qualitative discussions in the high energy limit should be insensitive to the details of the interaction. Although it is difficult to ascertain the effect of the above computational simplifications on  $A^{\text{eff}}/A$ , the neglect of open channels and the choice of the charmonium rest frame likely enhance the variation of  $A^{\text{eff}}/A$  with energy. These choices, linked with the use of an optimally small initial state, make the final estimate of the energy variation of  $A^{\text{eff}}/A$  rather optimistic. Consequently, the small effect in  $A^{\text{eff}}/A$  seen ( $< 20\%$ ) in the energy range studied strongly suggests that higher energies are required to observe transparency in this process.

In this paper, zero  $p_T$ , large  $x_F$ , quasielastic  $J/\psi$  photoproduction is considered. For this exclusive process, the states of the charmonium superposition are produced more and more nearly on-shell as the photon energy increases. Thus, in contrast to large-angle, quasielastic ( $e, e'p$ ) or ( $p, 2p$ ) reactions, all the interactions are soft. In this case, this behavior makes it reasonable to expect that the initial photoproduced superposition of states becomes small in size as the photon energy increases. That is, since the photon is pointlike, a fluctuation of the photon into charmonium states is also roughly pointlike. Interactions with the nucleon at the point at which the fluctuation is produced could disrupt its initial size, yet this possible effect should be strongly mitigated as the photon energy increases, since the states of the charmonium superposition become more and more nearly on-mass-shell with energy in this exclusive limit. This process is also convenient in that fixing the  $p_T$  and  $x_F$  of  $J/\psi$  to the values desired here (presuming a known photon energy) is sufficient to specify the exclusive process. That is, other processes, involving multiple particle production, could produce a  $J/\psi$  with  $p_T = 0$ ; yet, such  $J/\psi$ 's will always have momenta smaller than the maximum  $J/\psi$  momentum permitted in  $p_T = 0$  quasifree production.

The existence of transparency in  $J/\psi$  photoproduction is not necessarily restricted to this particular exclusive process; however, it can become difficult to “pick out” experimentally. For example, one can also study

quasielastic charmonium production as a function of  $p_T$  and  $x_F$ . For  $x_F$  away from 1, regardless of  $p_T$ ,  $J/\psi$  detection alone is not sufficient to determine the exclusive process uniquely, as various processes, with different final states, could produce a  $J/\psi$  with the same  $p_T$  and  $x_F$ . The exclusive process, in such a case, can be specified only through a coincidence measurement of the produced  $J/\psi$  and knocked-out nucleon. For nonzero  $p_T$  and large  $x_F$ , the exclusive process is well specified, but the argument presented for the “smallness” of the initial state no longer applies. As to other exclusive processes, in which additional particles are present in the final state, the worry is that contributions to the process that result from multiple particle production at the initial production step need not possess a small initial charmonium state.

Color transparency and  $J/\psi$  production were first discussed on general grounds by Brodsky and Mueller, though they were primarily concerned with  $\bar{p} - A$  reactions [12]. Farrar *et al.* considered color transparency in *inclusive*  $J/\psi$  production and computed  $A^{\text{eff}}/A$  as a function of the lab momentum of the  $J/\psi$  in a semi-classical approach [13]. Kopeliovich and Zakharov have recently considered  $c\bar{c}$  photoproduction in the same exclusive limit discussed here [14]. They, too, have a non-relativistic quantum mechanical model, but apply it to photon energies between 20 and 160 GeV. Their interaction is purely imaginary and is of harmonic oscillator form, proportional to the nuclear density. Their model of the initial amplitude is also different. The model presented here is of a more microscopic nature. Though not applied to  $c\bar{c}$  production, a quantum mechanical model of transparency has also been presented by Jennings and Miller [15]. Discussions of other possible phenomenological manifestations of color transparency and an extensive set of references are presented in reviews by Frankfurt and Strikman [19] and by Kopeliovich [20].

The model is described in detail in Sec. II. Its solution in the frozen limit – realized at large  $c\bar{c}$  energies – is presented in Sec. III. Here the  $J/\psi$ - and  $\psi'$ -nucleon cross sections can be readily computed in perturbation theory and compared with the exact numerical results; this serves as an explicit demonstration of how transparency can exist even when perturbation theory fails. The existence of shadowing at very high photon energies is also considered, albeit superficially, and it is suggested how the additional reaction mechanism might modify the expected saturation of  $A^{\text{eff}}/A$  at hundreds of GeV. In Sec. IV the evolution matrix calculation of charmonium’s final-state interactions is presented, and it is shown that the results of this formalism go smoothly to those of the frozen limit as the photon energy increases. The results of the evolution calculation are various, and they are described in Sec. V. That is, as a function of the energy and initial amplitude, the probabilities for the charmonium superposition to be in either a  $J/\psi$ ,  $\chi$ , or  $\psi'$  state are calculated as a function of the distance after the production point for Be, Fe, and Pb nuclei and compared simultaneously to the wave packet’s transverse size. The occupation probabilities can then be converted into an  $A^{\text{eff}}/A$  for  $J/\psi$ ,  $\chi$ , or  $\psi'$  production for a particular nu-

cleus through integration over its nuclear density. The  $J/\psi$ - and  $\psi'$ -nucleon cross sections are also calculated; the model’s  $J/\psi$ -nucleon cross section is compared to that deduced from a Glauber analysis of the computed  $A$  dependence for  $J/\psi$  production. Section V is followed, finally, by a concluding section summarizing this work and future prospects. Technical details essential to a complete description of the work, yet deemed disruptive to the flow of the main discussion, are relegated to appendices. Suggestions as to how information about the quasielastic process discussed here can be extracted from experiment are described in Appendix A, and an evaluation of the various empirical ways the  $J/\psi$ -nucleon cross section may be inferred is given in Appendix B. Appendices C, D, and E contain details specific to the model. The fit to obtain the flux tube width  $\tau$ , the computation of the charmonium eigenenergies and eigenfunction within a flux tube, and the construction of the initial state *Ansätze* are described within respective appendices.

## II. THE MODEL

The model described below combines many features well-known from phenomenological models of confinement motivated by QCD. I shall describe, in turn, the picture of charmonium, the nucleons in the nucleus, and the charmonium-nucleon interaction. I shall then proceed to discuss the nuclear picture, the reaction mechanism, and the model for the initial photoproduced amplitude before turning, in Sec. III, to the computations in the frozen limit.

Nonrelativistic quark potential models with Coulombic and linearly confining potentials have long been successfully applied to the charmonium system [21,22]. Though spin-dependent forces are also required to understand the splitting of the scalar, vector, and tensor  $\chi$  states and that of the  $\eta_c$  and  $J/\psi$  [23], merely the best fit of a simple harmonic oscillator to the vector states is considered in the present application, as the technical complications of spin-dependent forces and linear confinement are deemed inessential.  $\omega$  is determined by choosing  $4\hbar\omega = m_{\psi(4040)} - m_{\psi(3097)}$ , as  $\psi'(3686)$ , due to its closeness to  $D\bar{D}$  threshold, is likely not a pure two-quark state [24]. Following Eichten *et al.*’s fits [21], the charm quark mass is chosen to be 1.84 GeV; a charm quark mass greater than 1.5 GeV is also favored by the relativized quark model calculations of Godfrey and Isgur [23]. With this  $\omega$  and  $m_c$ , the rms  $q\bar{q}$  separation in  $J/\psi$  is 0.52 fm, which is commensurate to but slightly larger than the previously reported values of 0.37–0.47 fm [25]. Finally, the mass of the  $J/\psi$  is reproduced by requiring that the harmonic oscillator potential is shifted by the constant  $-0.937$  GeV. The confining potential is assumed to persist for all  $q - \bar{q}$  separations, so that no open channels have been included. The picture is thus analogous to a “quenched” approximation on the lattice.

Each of the nucleons in the nucleus is modeled as a static flux tube of finite width. The string model of hadrons, once purely phenomenological, is now supported by lattice-gauge-theory calculations [26,27]. That the nu-

cleon may be modeled as a *static* string of definite field orientation is based on strong coupling QCD [28]; in weak coupling, the string fluctuates and the notion of its field orientation becomes ill-posed. Indeed, it is these fluctuations which generate, ultimately, a finite string width and the physical string tension. Here, for tractability, a static string of finite width is presumed. Moreover, it is assumed that the field configuration of the nucleon is similar to that of  $q\bar{q}$ , and that the field of the string is uniform with a circular boundary [29] (see Fig. 1). These approximations would be heuristic even if models of the nucleon strongly supported a quark-diquark geometry [30]; they are made, nevertheless, in the expectation that as the size of the superposition of  $c\bar{c}$  states decreases the field geometry the tower sees should become unimportant – only the field strength and local orientation should matter. The field strength is determined by the string tension, which is chosen to be  $b_{\text{Regge}} = 1/2\pi(0.9 \text{ GeV}^{-2}) \approx 0.18 \text{ GeV}^2$ , the meson Regge string tension. Lattice-gauge-theory and quark-model calculations support this choice [30]. Given that the nucleon can be modeled as a uniform field of strength determined by  $b_{\text{Regge}}$ , it is necessary to determine the parameters which specify its physical extent [33]. The radius of the string configuration is simply chosen to be the proton’s measured charge radius, 0.8 fm [34]. Its width, that is, the thickness of the planar  $qqq$  flux tube configuration, need not be equal to its diameter; this distance  $\tau$  is determined to be  $1.3 \pm 0.3$  fm from a fit in the frozen limit to  $A^{\text{eff}}/A$  of the highest energy ( $\langle E_\gamma \rangle = 120 \text{ GeV}$ ), small  $p_T$ , incoherent (“incoherent” means production from a single nucleon of the nucleus) photoproduction data available [35] (see Sec. III). In principle, though perhaps not yet in practice, the string “thickness” can be measured on the lattice; a recent estimate for  $q\bar{q}$  in  $\text{SU}(2)_c$  is of the order of 1 fm [36]. (All explicit impact parameter averages are ignored here, so that it is meaningful to speak of a single number  $\tau$  as the string width.)

Charmonium’s interaction with the nucleon flux tube is that of a color electric dipole in  $U(1)$  color, i.e., as in QED,

$$V_{\text{int}} = -e\vec{E} \cdot \vec{r} = -\vec{k}_{\text{Regge}} \cdot \vec{r}. \quad (2.1)$$

where  $|\vec{k}_{\text{Regge}}| = b_{\text{Regge}}/(\hbar c)$ . This choice involves two different assumptions. First, interactions via charmonium’s color-magnetic dipole moment are neglected [37]. Chromomagnetic fields may be generated by the nucleon’s chromoelectric field in two possible ways. The string beyond the leading order in the strong coupling expansion fluctuates; the time-varying electric flux generated by the oscillations of the string produces a magnetic field. In the “strong coupling” picture – the straight string is presumed to have finite width – adopted here, these magnetic fields do not exist. Yet, even in this picture, magnetic fields cannot be avoided entirely, as they can also be generated by Lorentz transformations. In the charmonium rest frame, given that its laboratory momentum is parallel to the  $\vec{z}$ -axis,

$$\begin{aligned} E_x^{\text{rest}} &= \gamma E_x, & B_x^{\text{rest}} &= \gamma \beta_{c\bar{c}} E_y, \\ E_y^{\text{rest}} &= \gamma E_y, & B_y^{\text{rest}} &= -\gamma \beta_{c\bar{c}} E_x, \\ E_z^{\text{rest}} &= E_z, & B_z^{\text{rest}} &= 0. \end{aligned} \quad (2.2)$$

Here  $\beta_{c\bar{c}}$  and  $\gamma$  are defined through the mass of the  $J/\psi$ . For the  $c\bar{c}$  momenta considered, the transverse magnetic and electric fields are of the same magnitude, since  $\beta_{c\bar{c}} \sim 1$ . The electric dipole interaction plays a larger role, however, as the strength of the magnetic dipole interaction – when finite – is suppressed by a power of the charm quark mass; this, ultimately, is the basis for the approximation made. As the transverse electric fields in the charmonium rest frame are a factor of  $\gamma$  larger than the longitudinal component, the flux tubes are taken to be purely transverse; this is an excellent approximation for large  $c\bar{c}$  momenta [38].

The second assumption in the interaction choice is that it is sufficient to treat the  $c\bar{c}$ -nucleon interaction in  $U(1)$  color. The process considered in this paper is zero  $p_T$ , large  $x_F$ , quasielastic photoproduction; the produced  $J/\psi$  in this limit carries off the maximum momentum consistent with energy conservation (see Appendix A). In order to conserve momentum at the production point, possibly a nucleon is ejected or soft pions are produced, yet no additional particles are produced via  $c\bar{c}$ ’s final-state interactions, by fiat. The interactions among the  $c\bar{c}$  states in this channel must be, then, color singlet; the  $U(1)$  interaction is chosen for convenience. In perturbative QCD, one can construct a color-singlet interaction from any number of gluon exchanges greater than or equal to two. The analogue in non-Abelian electrodynamics, in this case, is to combine the terms of the perturbative expansion for the interactions of the color-electric dipole with the flux tube’s color-electric field so as to yield a color-singlet interaction. However, including merely the second-order piece cannot be sufficient, as then transitions between parity-odd and -even states are forbidden. As the momentum transfers in the interactions with the medium are infinitesimal by construction, multiple interactions with the medium are not suppressed; in particular, the third-order piece can certainly be finite. Thus, in the “soft” regime studied here, both transitions between like and unlike parity states are allowed; the  $U(1)$  color interaction is a simple realization of this physics. (At high energies, however,  $\chi$  photoproduction in this model will be suppressed, due to the “narrow” initial amplitude used for the photoproduced charmonium state. This effect is consistent with known high-energy phenomenology.) The interaction proposed is purely real, as the potential which describes charmonium is taken to be purely confining. Yet, open channels arise not only from virtual  $q\bar{q}$  pair production, but also from rearrangements within the flux tube to make  $\Lambda_c^+ + \bar{D}^0$  and other charmed baryons. The formalism required to include these rearrangements is described at the end of Appendix D. For the purposes of the current work, however, these complications are simply ignored.

Although the interaction is real, it is to be emphasized that absorptive effects are included in the model. Indeed, explicit numerical calculation of the forward elastic

scattering amplitude in the model after passage through a single flux tube yields a quantity which is predominantly imaginary. The interaction with a single nucleon is such that an incident charmonium ground state has its strength fragmented into many different states. Absorptive effects are included via the production of excited charmonium states. This point deserves further explanation. The coupling of charmonium states of high excitation to the ground state is very small, though it is not zero. If charmonium passed through an infinite nuclear medium, then all the excited charmonium states could return to the ground state. In this situation, no absorptive effects could be said to be included. However, in this case, the length of nuclear matter through which the charmonium must pass is finite. Upon exit from the nucleus, I have assumed that all charmonium excited states are lost from the  $J/\psi$  exit channel. Thus, in this sense, absorption has truly been included. It is true that modeling absorption through the production of charmonium excited states will enhance the significance of the quantum-mechanical coherence effects discussed here. Consequently, it is of marked importance that the effect calculated ( $< 20\%$ ) in the energy range specifically considered is so small.

One final assumption about the interaction, or, rather, its time dependence, must be discussed before I turn to the model of the nucleus. In the laboratory frame, the  $c\bar{c}$  wave packet is “small” relative to the nucleon flux tube width, so that it is appropriate to write the  $c\bar{c}$ -flux-tube interaction as

$$H_{\text{int}}(t) = -e\vec{E}_{\text{str}}^{(1)} \cdot \vec{r} \Theta(t - t_1) \Theta(t_1 + \tilde{\tau} - t), \quad (2.3)$$

where  $t_1$  is the time the  $c\bar{c}$  enters the field and  $\tilde{\tau}$  is the  $c\bar{c}$ 's transit time in the laboratory. Equation (2.3) neglects any edge effects the  $c\bar{c}$  suffers in passage into the flux tube. However, the calculation is performed in the  $c\bar{c}$  rest frame. In this frame, upon neglecting the magnetic interactions discussed above, the interaction as given in Eq. (2.3) becomes

$$H_{\text{int}}(t) = -e\gamma \vec{E}_{\text{str}}^{(1)} \cdot \vec{r} \Theta(t - t_1) \Theta(t_1 + \tilde{\tau}/\gamma - t), \quad (2.4)$$

as the electric field and interaction time are modified by Lorentz transformation. Equation (2.4) is the interaction adopted in this paper. Yet, in the charmonium rest frame, one might think that the passage of the flux tube through the  $c\bar{c}$  wave function should be modeled explicitly. This Hamiltonian is given by

$$H_{\text{int}}(t) = -e\gamma \vec{E}_{\text{str}}^{(1)} \cdot \vec{r} \Theta \left( z - \left[ z_s(t) - \frac{v\tilde{\tau}}{2\gamma} \right] \right) \times \Theta \left( \left[ z_s(t) + \frac{v\tilde{\tau}}{2\gamma} \right] - z \right). \quad (2.5)$$

$z_s(t)$  describes the position of the center of the flux tube with time as it moves along the  $z$  axis, that is,  $z_s(t) = z_s(0) - vt$ . The equivalence of Eq. (2.4) and Eq. (2.5) relies on Galilean invariance, but there is no issue as long as the “edge effects” associated with the passage of the flux tube through the  $c\bar{c}$  wave function are

small [38]. At very large  $\gamma$ , the Lorentz contraction of the longitudinal dimension of the proton's wave function at rest indicates that “edge effects” are not small. However, that does not mean that Eq. (2.5) is the Hamiltonian of choice. As Bjorken [16] and Kancheli [17] have emphasized, a hadron boosted to high momenta has rather little resemblance to the simple Lorentz contraction of its rest frame wave function. It is supposed that the moving proton is a conglomerate of boosted vacuum fluctuations which have coupled to the boosted proton and the Lorentz-contracted object which contains the original three quarks [16,18]. The lowest momentum components of this picture – the so-called “wee” partons – are uncontracted [16,18]. Moreover, it is supposed that interactions with the wee partons should comprise the bulk of the diffractive interactions that charmonium suffers in its exit through the nucleus [39]. Discussions of boosted vacuum fluctuations are rather far away from the scope of the simple model considered here. They have been mentioned in this context only to indicate that the relevant longitudinal dimension of the nucleon which undergoes diffractive interactions with charmonium is itself a nontrivial issue. As the computational effort involved in solving the multiple scattering problem associated with Eq. (2.5) is prohibitive, Eq. (2.4) is the interaction of choice. Thus, the form of Eq. (2.4), though heuristic, is adopted as the model Hamiltonian, since it contains the physics deemed critical to transparency: an interaction which varies as the separation of the quarks, and time dilation of the  $c\bar{c}$  wave packet's evolution through the medium with energy.

Upon production at a point  $\vec{r}$  in the nucleus, the charmonium superposition “sees” a regular sequence of static nucleon flux tubes, where each nucleon has some frozen, random field orientation transverse to charmonium's direction of motion [40]. As no particular set of transverse field orientations can be preferred, an observable is the result of the average of that quantity over the statistical ensemble of all possible “snapshots.” The ensemble average, in principle, should be performed over the nucleons' orientations as well as over their relative separations. However, performing an additional ensemble average over all possible flux tube spacings – constrained to some total density – is a markedly more difficult computational problem. Consequently, the distance between the flux tubes,  $\xi^A$ , for a particular nucleus is fixed such that the internucleon spacing is given by  $D_{\text{spac}} = \tau + \xi^A = 2(3/4\pi\rho_{\text{unif}}^A)^{1/3}$ , and  $\rho_{\text{unif}}^A$  is the nucleus' uniform equivalent density,  $\rho_{\text{unif}}^A = 3A/4\pi R_{\text{eq}}^3$ , where  $R_{\text{eq}}$  is the equivalent volume radius. A schematic drawing of the geometry is shown in Fig. 2, and  $D_{\text{spac}}$  and  $\xi^A$  for various nuclei are given in Table I. Only the spacing of the flux tubes is computed from  $\rho_{\text{unif}}^A$ ; the number of nucleons that the  $c\bar{c}$  tower interacts with, given a particular production point in a particular nucleus, is determined from the nuclear thickness function, obtained from the experimentally determined charge density [44]. (In a sudden approximation, the outgoing tower of  $c\bar{c}$  states interacts with the matter density of the original nucleus.) The “crystal” picture presented relies on the expectation that, in a dense liquid with a strong short-

TABLE I. The typical nucleon-nucleon separation,  $\xi^A$ , as a function of  $A$ .  $\xi^A$  is defined as  $D_{\text{spac}} - \tau$ , where  $\tau$  is the width of a nucleon “string.”  $D_{\text{spac}}$  is the typical spacing of the nucleon centers; it is taken to be equal to  $2R_{\text{eq}}/A^{1/3}$ , where  $R_{\text{eq}}$  is the uniform-equivalent-volume radius, taken from Ref. [44].

Nucleus	$R_{\text{eq}}$ (fm)	$D_{\text{spac}}$ (fm)	$\xi^A$ (fm)
Be	3.12	3.00	1.70
Fe	4.84	2.53	1.23
Pb	6.98	2.36	1.06

range repulsion in its pair-wise forces, the inter-particle correlation function will be peaked around some average separation  $D_{\text{spac}}$ . The approximation is the insistence on a linear array. For the purposes of transparency, it would be preferable to consider a true liquid, as regularly spaced nucleons could enhance the effect of the coherent superposition of states. The picture adopted, then, is consistent with an optimal scenario.

The above discussion implicitly presumes that the photon may produce charmonium at any point in the nuclear volume; however, this picture is altered at sufficiently high photon energies, due to shadowing. Two different reaction mechanisms exist. Figure 3 presents a schematic of  $c\bar{c}$  photoproduction for (a) the “shadowed” process, i.e., via a long-lived virtual tower of hadrons [11], and for (b) the “direct” process, in which the  $c\bar{c}$  fluctuation is knocked immediately on-shell. Following Feynman [18], a real photon is a bare photon plus a virtual hadron, where the latter, according to perturbation theory, is weighted by a factor of  $1/\Delta E$ , with  $\Delta E = \sqrt{E_\gamma^2 + m_H^2} - E_\gamma$ , the energy difference of a momentum state as a hadron with mass  $m_H$  and as a photon. The factor  $1/\Delta E$  is also an estimate of the “lifetime” of a particular hadronic fluctuation, that is, crudely, the distance before the target that the conversion may occur. Table II shows  $1/\Delta E$  (in fm) for  $J/\psi$  production as a function of the photon energy  $E_\gamma$ . One may crudely judge the relative importance of the “direct” and “shadowed” contributions by comparing  $\Delta E$  with the typical nucleon separation, which is of  $O(1\text{ fm})$ . For energies less than 30 GeV, the “direct” process likely dominates, whereas the “shadowed” process would certainly seem to dominate for energies greater than 200 GeV. These considerations are essential in converting the occupation probability of a particular

TABLE II. “Lifetime” of a  $J/\psi$  fluctuation in the laboratory frame given a photon with energy  $E_\gamma$ . Note that  $\Delta E = \sqrt{E_\gamma^2 + m_{J/\psi}^2} - E_\gamma$ .

$E_\gamma$ (GeV)	$(1/\Delta E)_{J/\psi}$ (fm)
8.5	0.36
15	0.62
30	1.24
60	2.47
120	4.94
200	8.23
400	16.5

final state computed for a linear array of  $N$  flux tubes to that appropriate for a nucleus  $A$ . For the “direct” case,  $A^{\text{eff}}/A$  is given by

$$\left[ \frac{A^{\text{eff}}}{A} \right]_{J/\psi} = \frac{\int_A dz d^2\vec{b} \rho_A(z, b) \tilde{P}_{J/\psi}(N_{\text{eff}}(z, b))}{\int_A dz d^2\vec{b} \rho_A(z, b)}. \quad (2.6)$$

$\rho_A(z, b)$  is the nuclear density, and  $N_{\text{eff}}(z, b)$  is the effective number of nucleons with which the  $c\bar{c}$  tower interacts, given an initial production point  $(z, \vec{b})$ .  $z$  and  $\vec{b}$  are defined with respect to the center of the nucleus;  $z$  is the reaction coordinate of the  $c\bar{c}$  tower, parallel to the incoming photon, whereas  $\vec{b}$  is the impact parameter.  $\tilde{P}_{J/\psi}(N_{\text{eff}}(z, b))$  is the probability of observing  $J/\psi$  after  $N_{\text{eff}}$  flux tubes, normalized to its content in the initial state. With this definition,  $A^{\text{eff}}/A$  for H is 1. However, in the calculations presented here, this additional normalization will be omitted, so that “ $A^{\text{eff}}/A$ ” is well-defined for the higher-mass charmonium states as well, regardless of the initial state’s content. Note that

$$N_{\text{eff}}(z, b) \equiv \left[ \left( \frac{t_A(z, b)}{\rho_{\text{unif}}^A D_{\text{spac}}} \right) \right], \quad (2.7)$$

where  $t_A(z, b)$  is the nuclear thickness function,  $t_A(z, b) = \int_z^\infty dz' \rho(z', b)$ , and the in-line brackets in Eq. (2.7) denote “nearest integer.” Now for the completely shadowed case,  $A^{\text{eff}}/A$  is given by

$$\left[ \frac{A^{\text{eff}}}{A} \right]_{J/\psi} = \frac{\int_0^{b_{\text{max}}} b db \tilde{P}_{J/\psi}(N_{\text{eff}}|_{\text{path}})}{\int_0^{b_{\text{max}}} b db}. \quad (2.8)$$

In this limit the  $c\bar{c}$  fluctuation occurs well outside the nucleus, so that the average number of nucleons participating in the reaction is determined by averaging  $\tilde{P}_{J/\psi}$  over the possible paths across the nucleus.  $b_{\text{max}}$  is the  $b$  for which  $N_{\text{eff}}|_{\text{path}} \equiv 0$ . As before,  $\tilde{P}_{J/\psi}$  is the probability of observing  $J/\psi$  after  $N_{\text{eff}}$  flux-tube interactions (given some initial state), where  $N_{\text{eff}}|_{\text{path}}$  is the effective number of nucleons with which the  $c\bar{c}$  tower interacts over a particular path. Here

$$N_{\text{eff}}|_{\text{path}} \equiv \left[ \frac{t(-\infty, b)}{\rho_{\text{unif}}^A D_{\text{spac}}} \right]. \quad (2.9)$$

The in-line brackets in Eq. (2.9) denote “nearest integer.” Throughout this paper, as a result of the photon energies considered, the direct process is assumed to dominate and Eq. (2.6) will be used to calculate  $A^{\text{eff}}/A$ . Equation (2.8) will be employed briefly in Sec. III, in an attempt to discern the qualitative effect of this additional reaction mechanism at large photon energies. In this way, through use of Eqs. (2.6) and (2.7), the occupation probability for a particular  $c\bar{c}$  final state computed for a linear array of  $N$  flux tubes is converted to the nuclear-averaged probability  $A^{\text{eff}}/A$  for a particular nucleus  $A$ .

The survival of the  $J/\psi$  depends on the wave function of the initial photoproduced state. The photon is pointlike, so that it is presumed that the photon’s coupling to  $q\bar{q}$  is also pointlike. This means, then, that the

amplitude required for the photon to fluctuate to a particular charmonium state should be proportional to its wave function at the origin. This picture is supported by the two- and three-photon decays of the  $s$ -wave states of charmonium [45]; these decays are controlled by the charmonium state's wave function or its derivative at the origin. Thus, the photon fluctuates to a tower of  $s$ -wave vector charmonium states; the fluctuation is narrow, as the photon is pointlike. For the particular exclusive process considered, the initial fluctuation is produced more and more nearly on-shell as the photon energy increases, so that it is supposed that the medium interactions which knock the fluctuation on-shell do not disrupt its small size. Even though the fluctuation is narrow, it cannot be pointlike, as the size of this virtual state must be limited by the Compton wavelength of the charmed quark. That is, the fluctuation's  $q\bar{q}$  rms separation is such that  $\langle r_{q\bar{q}}^2 \rangle^{1/2} \geq \hbar c/m_{J/\psi} \sim 0.127$  fm. Following a "best case" scenario for transparency, the initial state at very large photon energies is parametrized as a Gaussian wave packet of form

$$\psi_i(r) = \left(\frac{\alpha_i}{\pi}\right)^{3/4} \exp\left(-\frac{\alpha_i}{2} r^2\right), \quad (2.10)$$

where  $\alpha_i \equiv 3/2\langle r_i^2 \rangle$  and  $\langle r_i^2 \rangle^{1/2} = \hbar c/m_{J/\psi}$  [46]. (As a result of interactions with the medium, the amplitude for  $l \neq 0$  states may also be finite, but this possibility is ignored, consistent with the assumption that the interactions which knock the state on-shell do not significantly affect it.)

Kopeliovich and Zakharov [14] do not assume the parametrization of Eq. (2.10) for their initial state at large photon energies. Rather, they calculate the amplitude, in the infinite momentum frame, for a photon to fluctuate to a *free*  $c\bar{c}$  pair. In this approximation, the photon-to- $c\bar{c}$  amplitude is  $\psi_{\gamma \rightarrow c\bar{c}} \propto K_0(m_c \rho)$ , where  $\vec{\rho}$  is the transverse separation of the  $c$  and  $\bar{c}$ . They explicitly include a two-gluon interaction cross section  $\sigma(\rho)$  with the nucleon, to write, in the frozen approximation,

$$\psi_i^T(\rho) \propto K_0(m_c \rho) \sigma(\rho). \quad (2.11)$$

$\psi_i^T(\rho)$  is the on-shell initial  $c\bar{c}$  wave function in the transverse coordinate. This initial wave function, although specific to the infinite momentum frame, is used directly in their evolution calculation for the  $c\bar{c}$ -medium interactions. The latter calculation is formulated in the charmonium rest frame, as it must be, due to their choice of a nonrelativistic harmonic oscillator model for charmonium. The issue of the overall consistency of this approach is not addressed. Equation (2.11) is of a transverse size comparable to that of the  $J/\psi$ , and, hence, is

rather larger than the initial state used here.

At lower energies, the initial photoproduced superposition can be affected by threshold effects. For a particular photon energy, it is presumed that the states which contribute significantly to the initial amplitude are those  $s$ -wave states which can be physically produced in quasifree kinematics with a nucleon. Given some number of states which contribute, the initial state is fixed by *Ansatz*: the smallest state which can be constructed from the available channels is chosen as the initial state (see Appendix E). This prescription could also enhance the possible effect of transparency. Alternative *Ansätze* are explored in Sec. V as well.

For near threshold energies, the frozen approximation which yields Eq. (2.11) is crudely broken, so that Kopeliovich and Zakharov [14] compute  $A^{\text{eff}}/A$  for a variety of *Ansätze*. Namely, they consider  $\psi_i^T(\rho) \propto \exp(-\rho^2/a^2)$ , where  $a = (1-3)/m_c$  and the transverse size  $\langle \rho^2 \rangle^{1/2} \sim (1-3)/m_c$ . The *Ansätze* considered in Sec. V have a somewhat larger transverse size,  $\langle \rho^2 \rangle^{1/2} \sim (2-3)/m_c$ , in their units. Kopeliovich and Zakharov do not consider threshold effects.

The electric-dipole interaction in this model does have the behavior needed for transparency, and the initial charmonium superposition becomes "small" at high photon energies. Thus, it is to be expected that the model will exhibit behavior consistent with color transparency; the interesting issue is its magnitude at the energies considered. I shall first solve the model in the limit where the charmonium's internal motion is frozen and then proceed to solve it through numerical construction of the evolution matrix.

### III. THE FROZEN LIMIT

Analytical progress can be made when the expectation value of the  $c\bar{c}$ 's relative separation is frozen in its passage through the nucleus [8]. The Hamiltonian which defines the eigenstates of  $c\bar{c}$  is

$$H_0(\vec{r}) = -\frac{(\hbar c)^2}{2\mu_c} \nabla_{\vec{r}}^2 + \frac{1}{2} \mu_c \omega^2 r^2 + C, \quad (3.1)$$

where  $\mu_c = 0.92$  GeV and  $\hbar\omega = 0.24$  GeV.  $C$  is defined such that  $m_{J/\psi} = 2m_c + E_{\text{gs}}$ ;  $E_{\text{gs}}$  is the ground state energy of Eq. (3.1) (see Sec. II). In the high energy picture adopted here, charmonium executes a straight line path through a linear array of  $N$  flux tubes, so that as a function of time, due to passage through the flux tubes, the Hamiltonian is

$$\begin{aligned} H_N(t) = & H_0(\vec{r}) - e\vec{E}_{\text{str}}^{(1)} \cdot \vec{r} \Theta(t-t_1) \Theta(t_1 + \tilde{\tau}_R - t) - e\vec{E}_{\text{str}}^{(2)} \cdot \vec{r} \Theta(t-t_2) \Theta(t_2 + \tilde{\tau}_R - t) \\ & - \dots - e\vec{E}_{\text{str}}^{(N)} \cdot \vec{r} \Theta(t-t_N) \Theta(t_N + \tilde{\tau}_R - t). \end{aligned} \quad (3.2)$$

Equation (3.2) is written in charmonium's rest frame; in this model, the electric fields uniformly illuminate the  $c\bar{c}$  wave function for a time  $\tilde{\tau}_R$ . The interaction time in the  $c\bar{c}$  rest frame is  $\tilde{\tau}_R = \tilde{\tau}/\gamma$ , where  $\gamma$  is

the usual Lorentz factor and  $\tilde{\tau}$  is the flux-tube transit time in the lab frame. The flux-tube interactions are spaced by  $\tilde{\xi}_R^A$ , where  $\tilde{\xi}_R^A = \xi^A/\gamma c$  and  $t_i = t_{i-1} + \tilde{\xi}_R^A$ ,  $t_1 = \tilde{\xi}_R^A$ . ( $\xi^A$  was defined in Sec. II, see Table I.) As

noted earlier, the flux tubes are chosen purely transverse to the charmonium's direction of motion  $z$ , so that upon introducing cylindrical coordinates  $\vec{r} = (\vec{s}, z)$ , one has  $|eE_{\text{str}}^{(i)}| = \gamma k_{\text{Regge}} \Theta(R - |\vec{s}|)$  with  $R = 0.8$  fm and  $k_{\text{Regge}} \approx 0.9$  GeV/fm. ( $\tau$ , the flux tube width in the lab frame, will be found equal to  $1.3 \pm 0.3$  fm through fitting to the highest energy photoproduction data available, and  $\tilde{\tau} = \tau/c$ .)  $\tilde{\tau}_R$  does not depend on the particular flux tube encountered as they are purely transverse to charmonium's direction of motion. The wave function  $\Psi(\vec{r}, t)$  associated with Eq. (3.2) may be written as

$$\Psi(\vec{r}, t) = g(\vec{r}, t) \sum_{j=1}^{N_{\text{top}}} e^{-\frac{iE_j t}{\hbar}} C_j \phi_j(\vec{r}). \quad (3.3)$$

Here the amplitude at  $t = 0$  is  $\psi_i(\vec{r}) \equiv \sum_{j=1}^{N_{\text{top}}} C_j \phi_j(\vec{r})$ , where  $H_0 \phi_j = E_j \phi_j$ ,  $N_{\text{top}}$  is the total number of states in the initial amplitude, and the  $C_j$  are constant coefficients. Due to the interaction, the components  $\phi_j$  of the initial amplitude are modified by the *same* phase factor  $g(\vec{r}, t)$ . Requiring that Eq. (3.3) satisfies  $i\hbar \frac{\partial}{\partial t} \Psi = H_N(t) \Psi$  in passage through the *first* flux tube yields

$$i\hbar \frac{\partial_t g}{g} = -\frac{(\hbar c)^2}{2\mu_c} \left( \frac{\nabla_{\vec{r}}^2 g}{g} + 2 \frac{(\vec{\nabla}_{\vec{r}} g) \cdot \sum_{j=1}^{N_{\text{top}}} [\exp(-iE_j t/\hbar) C_j \vec{\nabla}_{\vec{r}} \phi_j]}{g \sum_{j=1}^{N_{\text{top}}} C_j \exp(-iE_j t/\hbar) \phi_j} \right) - e\vec{E}_{\text{str}}^{(1)} \cdot \vec{r}. \quad (3.4)$$

For sufficiently high energies,  $(H_0 - E_j)g(\vec{r}, t)\phi_j(\vec{r}) \approx 0$ , as  $g(\vec{r}, t = 0) = 1$ , so that the terms with spatial derivatives of  $g$  become negligible relative to the interaction; thus, after successive interactions with  $N$  fields,  $g(\vec{r}, t)$  takes the form

$$g(\vec{r}, t > N(\tilde{\tau}_R + \xi_R^A)) = \exp\left(\frac{i\tilde{\tau}_R}{\hbar} \sum_{i=1}^N e\vec{E}_{\text{str}}^{(i)} \cdot \vec{r}\right). \quad (3.5)$$

This is the eikonal approximation, and it is valid as long as  $\gamma|\vec{k}_{\text{Regge}} \cdot \vec{r}| \gg \tau^2 k_{\text{Regge}}^2 / 2\mu_c$  and  $\gg c\tau k_{\text{Regge}} \kappa_{\text{rel}} / \mu_c$ , where  $\kappa_{\text{rel}}$  is the typical relative momentum of the free  $c\bar{c}$  eigenstates; these inequalities are satisfied if the  $c\bar{c}$  lab energy is a mere 10 GeV. However, to make the frozen approximation, that is, to require that the  $j$  components of Eq. (3.3) do not evolve relative to one another – “decorrelate” – over the width of the flux tube and subsequent evolution to the next flux tube, one must require that

$$\frac{N_{\text{top}} \Delta E D_{\text{spac}}}{\hbar c \gamma} \ll 1. \quad (3.6)$$

$N_{\text{top}} \Delta E$  is the energy difference between the top state in Eq. (3.3) and the ground state, and  $D_{\text{spac}}$ , as introduced in Sec. II, is  $\tau + \xi$ . This is clearly a more restrictive constraint: if  $N_{\text{top}} = 10$ ,  $\Delta E \sim 0.2$  GeV, and  $D_{\text{spac}} \sim 2$  fm, then Eq. (3.6) can only be reasonably well-satisfied for energies in excess of a 100 GeV. Restricting, then, the discussion to the frozen limit, the probability that the  $c\bar{c}$  initially in state  $|\psi_i\rangle$  ends up in state  $|\phi_f\rangle$  is

$$P_{f \leftarrow i}(N) = \overline{|\langle \phi_f | g(\vec{r}, t) | \psi_i \rangle|^2}, \quad (3.7)$$

where the bar denotes an average over the ensemble of all flux-tube orientations. Here I compute the probability and *then* average over the ensemble of flux-tube orientations. For fast charmonium, the orientation of the flux tube is frozen during its transit, so that computing the ensemble average of the probability is appropriate. Introducing cylindrical coordinates,  $\vec{r} = (\vec{s}, z)$ , where  $z$  is oriented along the direction of the  $c\bar{c}$ 's motion, allows one to rewrite the absolute square in Eq. (3.7) as

$$P_{f \leftarrow i}(N) = \iint d^2 \vec{s} d^2 \vec{s}' \prod_{i=1}^N \exp\left(\frac{ie\tilde{\tau}_R}{\hbar} [\vec{E}_{\text{str}}^{(i)}(s) \cdot \vec{s} - \vec{E}_{\text{str}}^{(i)}(s') \cdot \vec{s}']\right) \rho_{fi}(\vec{s}) \rho_{fi}^*(\vec{s}'), \quad (3.8)$$

where  $\rho_{fi}(\vec{s}) = \int_{-\infty}^{\infty} dz \phi_f^*(\vec{s}, z) \psi_i(\vec{s}, z)$ . The orientations of the flux tubes are all independent, so that the average over the ensemble of all possible flux-tube orientations may be performed by averaging over the orientation of *each* one of them. Letting  $\eta$  be the angle between  $|\Theta(R - s)\vec{s} - \Theta(R - s')\vec{s}'|$  and any  $\vec{E}_{\text{str}}^{(i)}$ , Eq. (3.8) becomes

$$\begin{aligned} P_{f \leftarrow i}(N) &= \iint d^2 \vec{s} d^2 \vec{s}' \rho_{fi}(\vec{s}) \rho_{fi}^*(\vec{s}') \left[ \frac{1}{2\pi} \int_0^{2\pi} d\eta \exp\left(\frac{ik_{\text{Regge}} \tau}{\hbar c} |\Theta(R - s)\vec{s} - \Theta(R - s')\vec{s}'| \cos \eta\right) \right]^N \\ &= \iint d^2 \vec{s} d^2 \vec{s}' \rho_{fi}(\vec{s}) \rho_{fi}^*(\vec{s}') J_0^N \left( \frac{k_{\text{Regge}} \tau}{\hbar c} |\Theta(R - s)\vec{s} - \Theta(R - s')\vec{s}'| \right), \end{aligned} \quad (3.9)$$

where  $J_0$  is a Bessel function of the first kind of order 0.  $\tau$ , the flux-tube width in the lab frame, has been introduced; all factors of  $\gamma$  have canceled, so that Eq. (3.9) contains no explicit energy dependence [47]. The behavior of Eq. (3.9) for large  $N$  may be determined by noting that  $NJ_0^N(x) \sim \delta(x)$  as  $N \rightarrow \infty$  [48], so that, in leading order,

$$P_{f \leftarrow i}(N) \sim \frac{4\pi\hbar c}{Nk_{\text{Regge}}\tau} \int d^2\vec{s} |\rho_{fi}(\vec{s})|^2. \quad (3.10)$$

The argument of  $J_0$  is also zero for  $s, s' > R$ , but this contribution is exponentially smaller than that given in Eq. (3.10), if  $\rho_{fi}(\vec{s})$  is nonzero. Note that if one were to average over the  $\vec{E}$  field and then to compute the survival probability, that the final result would go as  $1/N^2$ , rather than as  $1/N$  in the large  $N$  limit [19]. Equation (3.10) is quite distinct from the exponential form familiar from Glauber theory [49–51]. As explained by Nemenov [52], the exponential form results if one assumes that the nucleons of the nucleus *independently* modify the initial wave packet, that is, that sufficient time exists between successive nucleon interactions for the wave packet to decorrelate to a size typical of the stationary states. Alternatively, the exponential form results if all excited states are “lost” and cannot rescatter to the ground state. (Actually, the independent nucleon assumption is precisely consistent with this latter statement; with the expectation that similarly sized states should interact in a similar way, this assumption is roughly equivalent to Nemenov’s restatement in terms of a decorrelation time.) The time between successive nucleon interactions in the wave packet’s rest frame can be made arbitrarily short due to Lorentz dilation; thus, the propagation of the correlated wave packet and the subsequent  $1/N$  form is a relativistic effect. The distinction between Eq. (3.10) and

an exponential form was noted previously in the study of ultrarelativistic positronium scattering from metal foil [52–55]; an empirical measurement of the positronium-atom interaction cross section with  $\gamma \sim 10^3$ , however, was unable either to confirm or to rule out the prediction [56]. A confirmation would be extremely interesting, as it would demonstrate the qualitative importance of quantum-mechanical coherence effects in the final-state interactions.

The transition probability upon passage through a linear array of flux tubes is given by Eq. (3.9); however, this does not suffice to compute  $A^{\text{eff}}/A$  for a particular nucleus, which is necessary to fix  $\tau$ , the width of the flux tube. The procedure necessary to effect such a computation, and the resulting fit to high-energy photoproduction data to determine the flux-tube width  $\tau$  is described in detail in Appendix C. The flux-tube width is determined to be

$$\tau = 1.3 \pm 0.3 \text{ fm}. \quad (3.11)$$

I shall now proceed to investigate the relative production of  $J/\psi$ ,  $\chi$ , and  $\psi'$  in the frozen limit. The probabilities in Eqs. (C1)–(C3), computed from the above choice of  $\tau$ , are plotted in Fig. 4(a); the  $\chi$  yield is strongly suppressed relative to that of  $J/\psi$  and  $\psi'$ . That is, in contrast to Fig. 4(b), where  $|\psi_i\rangle = |\psi_{J/\psi}\rangle$ , the initial state is strongly localized near the origin; the node of the  $\chi$ , then, trivially explains the suppression. The initial wave function is normalized; the small values of the “survival” probabilities for  $J/\psi$ ,  $\chi$ , and  $\psi'$  indicate that most of the initial wave packet scatters to – or remains in – a higher excitation state. The  $A^{\text{eff}}/A$  for  $J/\psi$ ,  $\chi$ , and  $\psi'$  for the nuclei used in the Sokoloff experiment [35], computed from these probabilities and Eq. (2.6), are shown in Table III. In the case of H, the  $A^{\text{eff}}/A$  are given by the initial-state probabilities.  $A^{\text{eff}}/A$  for  $\chi$  pro-

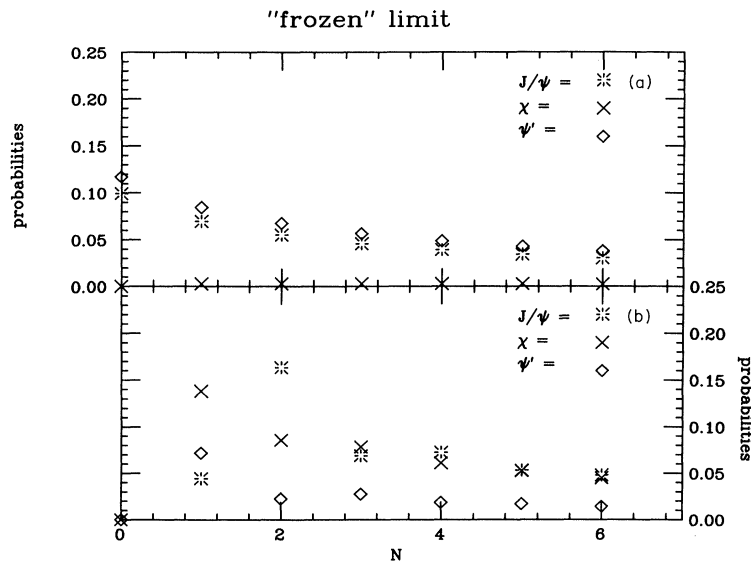


FIG. 4.  $J/\psi$ ,  $\chi$ , and  $\psi'$  probabilities with  $N$  in the frozen limit, as computed from Eqs. (C1)–(C3), where in (a) the initial state, which is taken to be of form  $\psi_i(r) = (\alpha_i/\pi)^{3/4} \exp(-\alpha_i r^2/2)$ , is determined by the Compton wavelength of the heavy quark,  $\alpha_i = 3(\hbar c)^2/2m_{J/\psi}^2$ , and in (b) the initial state is the  $J/\psi$  wave function,  $\alpha_i = \alpha_f$ .

TABLE III. “Raw”  $A^{\text{eff}}/A$  for  $J/\psi$ ,  $\chi$ , and  $\psi'$  in the “frozen” limit.

State	H	Be	Fe	Pb
$J/\psi$	$9.94 \times 10^{-2}$	$7.93 \times 10^{-2}$	$6.87 \times 10^{-2}$	$6.00 \times 10^{-2}$
$\chi$	0.	$2.76 \times 10^{-4}$	$3.58 \times 10^{-4}$	$3.97 \times 10^{-4}$
$\psi'$	$6.67 \times 10^{-2}$	$5.41 \times 10^{-2}$	$4.72 \times 10^{-2}$	$4.15 \times 10^{-2}$
and for $J/\psi$ once feeding is included...				
$J/\psi$	0.166	0.134	0.116	0.102

duction is quite small relative to that of  $J/\psi$  and  $\psi'$ ; this is merely an echo of the relative size of the  $J/\psi$ ,  $\chi$ , and  $\psi'$  probabilities. The absorption coefficients,  $\alpha$ , can be found through fitting  $A^\alpha$  to  $A^{\text{eff}}/A$ ; zero  $\alpha$  means zero absorption or production. The results are in Table IV; evidently the  $\alpha$ 's show some sensitivity to whether the H data are included in the fits. The fit for  $\tau$  includes the H data (and feeding effects from the decay of higher charmonium states, as described in Appendix C), as the fits by Sokoloff *et al.* do [35]. It is notable that feeding effects do relatively little to the  $A$  dependence of  $J/\psi$  production; the  $\alpha_{\text{no feed}}$  fit to the  $J/\psi$  data of the first row of Table III is  $\alpha_{\text{no feed}} = -9.3 \times 10^{-2}$  – a mere 3% change. The  $\alpha$ 's associated with  $\chi$  production are fit using the Be, Fe, and Pb numbers only;  $\alpha_\chi$  is greater than zero as it is produced through final-state interactions – no  $\chi$  is present in the initial state. It is interesting to note that the  $\alpha$  coefficient associated with  $\psi'$  production is less absorptive than that associated with  $J/\psi$ , contrary to the naive expectation that  $\psi'$  should suffer more absorptive interactions than  $J/\psi$  in the medium, due to its larger size. As the initial superposition is frozen in its transit through the nucleus, this result is likely sensitive to the particular initial state chosen.

The  $J/\psi$ -nucleon and  $\psi'$ -nucleon cross sections can also be computed. Semiclassically, the absorption cross section is the inelastic transition probability times the head-on area of the object. At high energies,  $\sigma^{\text{abs}}$  is approximately  $\sigma^{\text{tot}}$ , due to the preponderance of open inelastic channels (here equated to charmonium excited states). This can be seen in this model through explicit calculation of  $\sigma^{\text{el}}$ ; it is, indeed, much smaller than  $\sigma^{\text{tot}}$  [57]. The “head-on” area, which sets the

TABLE IV. Absorption coefficients  $\alpha$  in the “frozen” limit, determined by fitting  $A^\alpha$  to the  $A^{\text{eff}}/A$  given in Table III. The sign of  $\alpha$  determines whether the quantity considered decreases or increases in the medium;  $\alpha < 0$  corresponds to absorption.  $\alpha_{\text{no feed}}$  denotes the absorption coefficient associated with direct  $J/\psi$  production, and  $\alpha_{\text{feed}}$  is that associated with  $J/\psi$  production once feeding effects due to electromagnetic decay of  $\chi$  and  $\psi'$  states are included.

$\alpha$	With H data	Without H data
$\alpha_{\text{feed}}$	-0.0900	-0.0856
$\alpha_{\text{no feed}}$	-0.0930	-0.0880
$\alpha_\chi$	—	0.117
$\alpha_{\psi'}$	-0.0874	-0.0835
$\alpha_{\chi:J/\psi}$	—	0.196
$\alpha_{\psi':J/\psi}$	$6.71 \times 10^{-3}$	$5.28 \times 10^{-3}$
$\alpha_{\chi:\psi'}$	—	0.193

scale, is  $\pi R^2 \sim 20$  mb. The scale is appropriate, as  $\sigma_{pp}^{\text{tot}} \sim 2\pi R^2$ ; the experimental  $p-p$  total cross section is 40 mb. The inelastic transition probability for  $J/\psi$  is  $1 - P_{J/\psi \leftarrow 1s}(1)/P_{J/\psi \leftarrow 1s}(0)$ , so that from Eqs. (C1) and (C2) (with the above  $\tau$ ) one obtains

$$\sigma_{J/\psi-N}^{\text{abs}} = 6.0 \text{ mb} \quad \sigma_{\psi'-N}^{\text{abs}} = 5.6 \text{ mb}, \quad (3.12)$$

where the inelastic transition probability for  $\psi'$  is defined in analogy to that of  $J/\psi$ . Note that the narrow Gaussian wave packet, Eq. (2.10), has been used as the initial state. The smaller  $\psi' - N$  cross section is consistent with the previously computed absorption coefficients [58]. It is also of interest to compute the  $J/\psi$  and  $\psi'$  cross sections in the event that the initial state is either a pure  $J/\psi$  or  $\psi'$  state. Using Eq. (C1) with  $|\psi_i\rangle = |\psi_{J/\psi}\rangle$  and Eq. (3.9) with  $|\psi_i\rangle = |\psi_{\psi'}\rangle$ , one obtains

$$\sigma_{J/\psi-N}^{\text{abs}} = 19.2 \text{ mb} \quad \text{and} \quad \sigma_{\psi'-N}^{\text{abs}} = 19.8 \text{ mb}, \quad (3.13)$$

respectively. With these initial states, the relative size of the  $J/\psi$  and  $\psi'$  cross sections are now reversed. These cross sections can also be calculated in perturbation theory. For weak fields, that is, for small  $\beta$ , the  $J_0$  in Eq. (3.9) [noting Eq. (C1)] can be expanded to obtain

$$P_{J/\psi \leftarrow J/\psi}(1) = 1 - \frac{1}{2} \frac{\beta^2}{\alpha_f} [1 - e^{-X_{\text{str}}^2} (X_{\text{str}}^2 + 1)] + O\left(\frac{\beta^4}{\alpha_f^2}\right) \quad (3.14)$$

and

$$P_{\psi' \leftarrow \psi'}(1) = 1 - \frac{1}{3} \frac{\beta^2}{\alpha_f} \left[ \left( -X_{\text{str}}^6 - X_{\text{str}}^4 - \frac{7}{2} X_{\text{str}}^2 \right) e^{-X_{\text{str}}^2} + \frac{7}{2} (1 - e^{-X_{\text{str}}^2}) \right] + O\left(\frac{\beta^4}{\alpha_f^2}\right). \quad (3.15)$$

Thus, to lowest order in perturbation theory, Eqs. (3.14) and (3.15) yield

$$\sigma_{J/\psi-N}^{\text{abs}} = 54.5 \text{ mb} \quad \text{and} \quad \sigma_{\psi'-N}^{\text{abs}} = 58.7 \text{ mb}. \quad (3.16)$$

This disagrees rather dramatically with the exact numerical results of Eq. (3.13), though the cross section ratios are much closer:  $\frac{\sigma_{\psi'}^{\text{abs}}}{\sigma_{J/\psi}^{\text{abs}}}|_{\text{pert}} = 1.08$ , whereas the ratio for the exact calculation is 1.03. If  $X_{\text{str}}$  is large, the cross section ratio is equal to  $\langle r^2 \rangle_{\psi'} / \langle r^2 \rangle_{J/\psi}$ , or  $\frac{7}{3}$ . Thus,

the often-quoted  $p$ QCD cross section behavior [59,60],  $\sigma \propto \langle r^2 \rangle$ , can be realized in this model only in lowest order perturbation theory for infinitely long flux tubes; the actual parameters of the model violate this behavior rather severely.

The above calculations have been performed assuming that the photon interacts weakly with matter: the probability to produce charmonium at a point in the nucleus depends only on the nuclear density at that point. However, Table II shows that at energies above 100 GeV this cannot be a completely realistic picture; yet, changing the reaction mechanism to include shadowing is non-trivial. As a simple estimate of the effect of the inclusion of this physics,  $\tau$  is re-fit assuming that the process at 120 GeV is strongly shadowed, even though this is a crude caricature at this energy. Thus, the nuclear average given by Eq. (2.8) is used, and  $\tau$  becomes

$$\tau = 1.0 \pm 0.2 \text{ fm} . \quad (3.17)$$

$\tau$  is smaller as the effective number of nucleons with which the produced  $c\bar{c}$  must interact is larger. Evidently, the fitted  $\tau$  parameter is not very sensitive to the way in the which the nuclear average is performed—perhaps because the empirical  $A^{\text{eff}}/A$  is already rather close to 1. The “true”  $\tau$  is likely intermediate to the values deduced assuming the reaction mechanism is either due entirely to the direct process [Eq. (3.11)] or to the shadowed process [Eq. (3.17)]. The  $\tau$  found using Eq. (2.6),  $\tau = 1.3 \pm 0.3$  fm, will be used in the following sections, as I think the direct process is a better caricature of the physics at 120 GeV (see Table II). At any rate, repeating the absorption cross section estimates for the  $\tau$  of Eq. (3.17) yields, in contrast to Eq. (3.12),

$$\sigma_{J/\psi-N}^{\text{abs}} = 3.6 \text{ mb} \quad \sigma_{\psi'-N}^{\text{abs}} = 3.4 \text{ mb} , \quad (3.18)$$

which shows that the deduced cross sections are sensitive to the change in  $\tau$ , though the relative magnitude is retained. This example perhaps illustrates what would happen as the reaction mechanism changes for fixed  $\tau$ . Without shadowing, the frozen limit has no energy dependence at all, so that  $A^{\text{eff}}/A$  should saturate with energy. Yet, as energy increases, the change in reaction mechanism will cause the effective path of the produced  $c\bar{c}$  in the medium to increase and, thus, may cause  $A^{\text{eff}}/A$  to *decrease*. This trend may explain some preliminary data from NA37 at CERN on quasielastic muon production of  $J/\psi$  [61]. Certainly, the change of the reaction mechanism at high energies complicates the elucidation of transparency effects.

$$|\Psi(t > t_2)\rangle = \sum_{n,m,l} \exp(-i\omega_l^{\text{free}}(t-t_2) - i\omega_m^{\text{str}}(t_2-t_1) - i\omega_n^{\text{free}}t_1) \langle \psi_l^{\text{free}} | \psi_m^{\text{str}} \rangle \langle \psi_m^{\text{str}} | \psi_n^{\text{free}} \rangle \langle \psi_n^{\text{free}} | \Psi(t=0) \rangle | \psi_l^{\text{free}} \rangle , \quad (4.2)$$

where the free and str superscripts denote the exact  $c\bar{c}$  eigenfrequencies and eigenstates in free space and in the flux tube, respectively. The operation on  $|\Psi(t=0)\rangle$  can be repeated with  $|\Psi(t > t_2)\rangle$  to yield the evolution of the initial wave packet through a second flux tube, and so on.

#### IV. THE EVOLUTION CALCULATION

The computation of the time development of an initial superposition of physical  $c\bar{c}$  states due to interaction with the color fields of the nucleus is performed in charmonium’s rest frame: this is defined by the rest mass of the  $J/\psi$ . This definition implicitly ignores the phase differences of the states in the wave packet due to the momenta of the higher mass  $c\bar{c}$  states relative to the  $J/\psi$  [62]. Yet, unlike the previous section in which the relative propagation of the states in the wave packet was frozen in time, now the phase differences of the states due to their differing mass must be included in order to examine the wave packet’s time development. To illustrate that this approach is consistent with an assumption of moderately large  $c\bar{c}$  energies, consider the time development of the following two state system:

$$|\Psi(t)\rangle = e^{im_0t} |\psi_0\rangle + e^{i(m_0+\delta)t} |\psi_1\rangle . \quad (4.1)$$

For  $E_\gamma \gg m_0 \equiv m_{J/\psi}$ , the momenta of these states, presuming both are on-shell, after quasielastic photo-production with zero  $p_T$  and large  $x_F$ , will be  $p_0 \sim \sqrt{E_\gamma^2 - m_0^2}$  and

$$p_1 \sim \sqrt{E_\gamma^2 - (m_0 + \delta)^2} \\ \sim \sqrt{E_\gamma^2 - m_0^2} \{ 1 - m_0\delta / (E_\gamma^2 - m_0^2) + O(\delta^2) \} .$$

If  $m_0\delta / (E_\gamma^2 - m_0^2)$  is small, then it is entirely reasonable to ignore the relative momentum boosts of the states in the  $c\bar{c}$  tower and include only the phase differences arising from their varying masses. If  $m_0 \sim 3.1$  GeV,  $\delta \sim 0.25$  GeV, and  $E_\gamma \sim 12$  GeV, then  $p_1 - p_0 \sim -0.07$  GeV/ $c$  and  $(p_1 - p_0)^2 / (2m_{J/\psi}) \sim 8 \times 10^{-4}$  GeV [63]. In the rest frame – as defined here – the  $c\bar{c}$  wave packet is stationary while the fields flash on and off. The Hamiltonian which specifies the interactions of the system is given in Eq. (3.2), and a schematic drawing of the geometry is shown in Fig. 2. As in the frozen limit, the path of the evolving  $c\bar{c}$  is a straight line; the elastic scattering amplitude is forward-peaked for sufficiently high energies. In the rest frame, this geometry is manifested by flux-tube encounters which are equally spaced in time, as shown in Fig. 2. To illustrate the procedure to come, consider some initial  $c\bar{c}$  wave function  $|\Psi(t=0)\rangle$  at  $t=0$ . Then the wave function for  $t > t_2$ , after propagating to  $t = t_1$  in free space and from  $t_1$  to  $t_2$  in a flux tube, is

To begin, it is technically convenient to write the initial superposition of states in the form:

$$\langle x, y, z | \Psi(t=0) \rangle = \sum_{\zeta, n_z} C_{\zeta n_z}^{(\text{init})} \Phi_{n_z}(z) \Psi_\zeta(x, y) , \quad (4.3)$$

TABLE V. An occupation number basis —  $\zeta$  [see Eq. (D1) ff] in terms of  $n_x$  and  $n_y$ .

$\zeta$	$n_x$	$n_y$
1	0	0
2	0	1
3	1	0
4	0	2
5	1	1
6	2	0
$\vdots$	$\vdots$	$\vdots$

where  $z$  is parallel to the on-coming flow of flux tubes. As the flux tubes are transverse, the  $z$  coordinate factorizes, so that the  $\Phi_{n_z}(z)$  are the usual harmonic oscillator functions  $[-d^2/dz^2 + z^2]\Phi_{n_z}(z) = \varepsilon_{n_z}\Phi_{n_z}(z)$ , in units  $z = z_{\text{dim}}/b$ , where  $b$  is the harmonic oscillator constant.  $\zeta$  is a compact way of counting the excitations in the  $x$  and  $y$  oscillators, so that  $\zeta \equiv (n_x, n_y)$  and  $\Psi_\zeta(x, y) = \Phi_{n_x}(x)\Phi_{n_y}(y)$ . A translation between the  $\zeta$  and  $(n_x, n_y)$  representations is shown in Table V. After propagating in free space for a time  $\tilde{\xi}_R$  and in the flux tube for a time  $\tilde{\tau}_R$ , the coefficients  $C_{\zeta n_z}^{(\text{init})}$  become

$$C_{\zeta' n_z'}^{(N=1)} = \sum_{\zeta, n_z} \mathbf{T}_{\zeta' n_z'}^{\zeta n_z}(\theta_1) C_{\zeta n_z}^{(\text{init})}. \quad (4.4)$$

$\theta_1$  is the orientation of the first flux tube. The form of the “transfer matrix”  $\mathbf{T}$  is readily deduced from Eq. (4.2) when  $t = t_2$ , so that

$$\begin{aligned} \mathbf{T}_{\zeta' n_z'}^{\zeta n_z}(\theta_1) &= \delta_{n_z' n_z} e^{-i[E_\zeta \xi_A + E_{n_z}(\xi_A + \tau)]_{\hbar c \beta_{c\bar{c}} \gamma}} \\ &\times \sum_{\eta} \langle \Psi_{\zeta'} | \tilde{\Psi}_\eta \rangle \langle \tilde{\Psi}_\eta | \Psi_\zeta \rangle e^{-i\tilde{E}_\eta \tau_{\hbar c \beta_{c\bar{c}} \gamma}}. \end{aligned} \quad (4.5)$$

$E_\eta$  and  $|\tilde{\Psi}_\eta\rangle$  are the *exact* two-dimensional eigenvalues – in dimensionless units – and eigenstates of the  $c\bar{c}$  inside

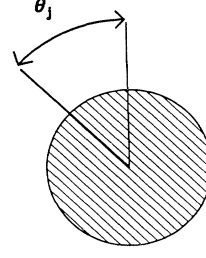


FIG. 5. “Head-on” nucleon field configuration the  $c\bar{c}$  encouters. The orientation of the first nucleon flux tube defines an axis against which the orientation of successive nucleons may be measured; here the nucleon is rotated by  $\theta_j$  with respect to that axis.

the flux tube, and  $\gamma$  is the Lorentz factor. The computation of these two-dimensional eigenvalues and eigenfunctions is described in Appendix D. They depend on the orientation of the flux tube, as illustrated in Fig. 5. Thus,  $\mathbf{T}$  itself may have some  $\theta$  dependence, as indicated. After the  $j$ th flux tube,

$$C_{\zeta' n_z'}^{(N=j)} = \sum_{\zeta n_z \dots} \mathbf{T}_{\zeta' n_z'}^{\zeta n_z}(\theta_j) \mathbf{T}(\theta_{j-1}) \dots \mathbf{T}(\theta_1) C_{\zeta n_z}^{(\text{init})}, \quad (4.6)$$

where the additional indices, which are summed over, have been suppressed. The  $C_{\zeta' n_z'}^{(N=j)}$  can be readily combined to yield the probability for  $J/\psi$ ,  $\chi$ , or  $\psi'$  production at a particular  $N$ ; however, since the time evolution has thus been computed for a fixed set of nucleon flux-tube orientations, an ensemble average over all (transverse) flux-tube orientations must still be performed in order to yield the true probability of producing  $J/\psi$ ,  $\chi$ , and  $\psi'$  states after traversing  $N$  flux tubes.  $\theta_1$  defines the orientation axis, so that the final averages are of the form:

$$P_{J/\psi}^{(N=j)} = \frac{1}{(2\pi)^{j-1}} \int_{-\pi}^{\pi} d\theta_2 \dots d\theta_j |C_{10}^{(N=j)}(0, \theta_2, \dots, \theta_j)|^2, \quad (4.7)$$

$$P_{\chi}^{(N=j)} = \frac{1}{(2\pi)^{j-1}} \int_{-\pi}^{\pi} d\theta_2 \dots d\theta_j \left[ |C_{11}^{(N=j)}(0, \theta_2, \dots, \theta_j)|^2 + |C_{20}^{(N=j)}(0, \theta_2, \dots, \theta_j)|^2 + |C_{30}^{(N=j)}(0, \theta_2, \dots, \theta_j)|^2 \right], \quad (4.8)$$

and

$$P_{\psi'}^{(N=j)} = \frac{1}{(2\pi)^{j-1}} \int_{-\pi}^{\pi} d\theta_2 \dots d\theta_j \frac{1}{3} \left[ |C_{12}^{(N=j)}(0, \theta_2, \dots, \theta_j) + C_{40}^{(N=j)}(0, \theta_2, \dots, \theta_j) + C_{60}^{(N=j)}(0, \theta_2, \dots, \theta_j) \right]^2. \quad (4.9)$$

The Monte Carlo integrals in Eqs. (4.7)–(4.9) are performed naively; that is, the integration points are chosen randomly on  $[-\pi, \pi]$ . The integrands in Eqs. (4.7)–(4.9) are rather smooth, and they differ in their dependence on  $\theta_j$ , so that the naive method is judged the most practical. It is also of interest to examine the size of the wave packet as it evolves through the nucleus. To this purpose, consider the longitudinal and transverse rms separations,  $\langle r_L^2 \rangle^{1/2}$  and  $\langle r_T^2 \rangle^{1/2}$ , such that the rms  $q\bar{q}$  separation  $\langle r^2 \rangle = \langle r_L^2 \rangle + 2\langle r_T^2 \rangle$ . It is useful to make a separation of the longitudinal and transverse sizes as the interactions with the medium are purely transverse. Thus,  $\langle r_L^2 \rangle = \langle z^2 \rangle$  and  $\langle r_T^2 \rangle = \frac{1}{2}\langle x^2 + y^2 \rangle$ . These quantities can be readily realized in terms of the  $C_{\zeta n_z}^{(N)}$  coefficients, that is,

$$\langle r_L^2 \rangle^{(N)} = \sum_{\zeta, n_z} \left[ C_{\zeta n_z}^{(N)} C_{\zeta n_z}^{*(N)} \langle \Phi_{n_z} | z^2 | \Phi_{n_z} \rangle + (C_{\zeta n_z}^{(N)} C_{\zeta n_z + 2}^{*(N)} + C_{\zeta n_z + 2}^{(N)} C_{\zeta n_z}^{*(N)}) \langle \Phi_{n_z + 2} | z^2 | \Phi_{n_z} \rangle \right] \quad (4.10)$$

and

$$\begin{aligned} \langle r_T^2 \rangle^{(N)} &= \frac{1}{2} \sum_{n_x, n_y, n_z} \left[ C_{n_x n_y n_z}^{(N)} C_{n_x n_y n_z}^{*(N)} (\langle \Phi_{n_x} | x^2 | \Phi_{n_x} \rangle + \langle \Phi_{n_y} | y^2 | \Phi_{n_y} \rangle) \right. \\ &\quad + (C_{n_x n_y n_z}^{(N)} C_{n_x+2n_y n_z}^{*(N)} + C_{n_x+2n_y n_z}^{(N)} C_{n_x n_y n_z}^{*(N)}) \langle \Phi_{n_x+2} | x^2 | \Phi_{n_x} \rangle \\ &\quad \left. + (C_{n_x n_y n_z}^{(N)} C_{n_x n_y+2n_z}^{*(N)} + C_{n_x n_y+2n_z}^{(N)} C_{n_x n_y n_z}^{*(N)}) \langle \Phi_{n_y+2} | y^2 | \Phi_{n_y} \rangle \right], \end{aligned} \quad (4.11)$$

where  $\zeta$  has been replaced by  $(n_x, n_y)$ . The matrix elements over the one-dimensional harmonic oscillator wave functions are well known. In general,

$$\langle \Phi_n | z^2 | \Phi_m \rangle = \frac{1}{\alpha_f} \sqrt{\frac{2^n n!}{2^m m!}} \{ \delta_{nm} (n + 0.5) + \delta_{nm-2} (n + 2)(n + 1) + \frac{1}{4} \delta_{nm+2} \}. \quad (4.12)$$

The evolution of the longitudinal size is trivial and, thus, is independent of the orientation of the flux tubes, so that the ensemble-averaged longitudinal size  $X_L$  is equivalent to  $\sqrt{\langle r_L^2 \rangle^{(N)}}$ . Indeed, as a useful numerical check,  $X_L$  from Eq. (4.10) can be compared against the simple form

$$X_L = \sqrt{\frac{\langle r^2 \rangle_{\text{free}}}{3\alpha_f}} \quad (4.13a)$$

with

$$\langle r^2 \rangle_{\text{free}} = \sum_{n=1}^{N_i} \left( \tilde{C}_n^2 \left[ 2n - \frac{1}{2} \right] - 2\tilde{C}_n \tilde{C}_{n-1} \sqrt{(n-1) \left( n - \frac{1}{2} \right) \cos(2\eta z_{\text{rxn}})} \right), \quad (4.13b)$$

where  $\eta = \alpha_f \hbar c / \mu_c \beta_{c\bar{c}} \gamma$ ,  $\alpha_f \equiv 3/2 \langle r_{J/\psi}^2 \rangle$ , and  $z_{\text{rxn}}$  is the reaction coordinate. This follows from Eq. (E3); the coefficients  $\tilde{C}_n$  are those of the  $t = 0$  expansion in  $s$ -wave basis functions,  $|\psi_{(n-1)00}\rangle$ .

However,  $\langle r_T^2 \rangle^{(N)}$  depends on the interactions, so that, as in Eqs. (4.7)–(4.9), Eq. (4.11) must be averaged over the ensemble of flux tube orientations. The ensemble-averaged transverse size  $X_T$  is given by

$$X_T^2(N) = \frac{1}{(2\pi)^{j-1}} \int_{-\pi}^{\pi} d\theta_2 \cdots d\theta_j \langle r_T^2 \rangle^{(N=j)}(0, \theta_2, \dots, \theta_j). \quad (4.14)$$

The calculation of the probabilities to measure  $J/\psi$ ,  $\chi$ , and  $\psi'$  and of the longitudinal and transverse sizes of the  $c\bar{c}$  wave packet during its evolution through the nucleus represents the computational core of this paper. The energy dependence of these quantities is contained in the  $\gamma$  factors in Eq. (4.5) and in  $\zeta_x$  and  $\zeta_y$  in the equation of motion for the  $c\bar{c}$  eigenstates in the flux tube, Eq. (D1). The growth of  $\gamma$  with energy means that the electric fields the stationary charmonium sees also grow, allowing the  $c\bar{c}$  to scatter to higher and higher excitation states. This makes the realization of the computation in Eq. (4.6) practically impossible at many tens of GeV. The computation is still tractable at 20 GeV, however; here the

highest excitation required in the one-dimensional basis is 20. In order to calculate the two-dimensional eigenstates and eigenfunctions in the flux tube for this degree of excitation reliably, the matrix to be diagonalized must be much larger: the highest one-dimensional excitation required in the diagonalization was 35 in order to guarantee the stability of the needed eigenstates and eigenfunctions. The high degree of excitation to which the  $c\bar{c}$  may be scattered is certainly a consequence of the neglect of all open channels. The formalism required to include the open channels due to production of  $\Lambda_c^+ + \bar{D}^0$  and other charmed baryons via flux tube rearrangements is described in Appendix D, though such complications are ignored for the purposes of the present work.

The computation of the probabilities in Eqs. (4.7)–(4.9) may be verified through comparison with the results of Eqs. (C1)–(C3) at extremely high energy. Due to the convergence problems discussed above, quantitative comparison of the results of the evolution calculation to those of the frozen limit can be carried through only at smaller values of the string tension, i.e., for  $k = 10^{-2} k_{\text{Regge}}$ . For small values of the string tension, an asymptotic series in powers of  $\beta^2/\alpha_f$  may be developed for the probabilities in the frozen limit, in place of Eqs. (C1)–(C3). Thus, expanding  $J_0(x)$  in a power series around  $x = 0$  and assuming  $|\psi_i\rangle = |\psi_{J/\psi}\rangle$  yields:

$$\begin{aligned} P_{J/\psi \leftarrow J/\psi}(N) &= 1 - \frac{N \beta^2}{2 \alpha_f} [1 - e^{-X_{\text{str}}^2} (X_{\text{str}}^2 + 1)] + \frac{1}{16} \left( \frac{N}{2} + N(N-1) \right) \frac{\beta^4}{\alpha_f^2} \\ &\quad \times \{ (-X_{\text{str}}^4 e^{-X_{\text{str}}^2} + 2[1 - e^{-X_{\text{str}}^2} (X_{\text{str}}^2 + 1)]) + 2[1 - e^{-X_{\text{str}}^2} (X_{\text{str}}^2 + 1)]^2 \} + O\left(\frac{\beta^6}{\alpha_f^3}\right) \end{aligned} \quad (4.15)$$

and

TABLE VI. Comparison of the  $J/\psi$ ,  $\chi$ , and  $\psi'$  probabilities computed with the evolution approach with those of the “frozen” limit in the case where the string tension  $k = 10^{-2} k_{\text{Regge}}$ . The evolution-approach probabilities are computed with a  $J/\psi$  energy of 300 GeV.  $2R$  is the total length of the string.

$R$ (fm)	$P$	Evolution	“Frozen”
0.80	$P_{J/\psi}$	0.999850	0.999848156027
	$P_\chi$	$1.322 \times 10^{-4}$	$1.32223560 \times 10^{-4}$
	$P_{\psi'}$	$1.3 \times 10^{-9}$	$1.324 \times 10^{-9}$
1.61	$P_{J/\psi}$	0.9998256236	0.999825639647
	$P_\chi$	$1.743602 \times 10^{-4}$	$1.74343710 \times 10^{-4}$
	$P_{\psi'}$	$5.07 \times 10^{-9}$	$5.066 \times 10^{-9}$

$$P_{\chi \leftarrow J/\psi}(N) = \frac{N}{2} \frac{\beta^2}{\alpha_f} [1 - e^{-X_{\text{str}}^2} (X_{\text{str}}^2 + 1)]^2 - \frac{1}{4} \left( \frac{N}{2} + N(N-1) \right) \frac{\beta^4}{\alpha_f^2} \times [1 - e^{-X_{\text{str}}^2} (X_{\text{str}}^2 + 1)] [-X_{\text{str}}^4 e^{-X_{\text{str}}^2} + 2\{1 - e^{-X_{\text{str}}^2} (X_{\text{str}}^2 + 1)\}] + O\left(\frac{\beta^6}{\alpha_f^3}\right). \quad (4.16)$$

Whereas

$$P_{\psi' \leftarrow J/\psi}(N) = \frac{1}{12} \left( \frac{N}{2} + N(N-1) \right) \frac{\beta^4}{\alpha_f^2} [X_{\text{str}}^4 e^{-X_{\text{str}}^2} - \{1 - e^{-X_{\text{str}}^2} (X_{\text{str}}^2 + 1)\}]^2 + O\left(\frac{\beta^6}{\alpha_f^3}\right), \quad (4.17)$$

with  $X_{\text{str}} = \sqrt{\alpha_f} R$ . The results of the evolution calculation and the frozen limit for  $N = 1$  are tabulated in Table VI as a function of  $R$ , where for this test  $\tau = 0.970546$  fm,  $\xi^A = 0$ , and  $E_{J/\psi} = 300$  GeV. The numbers are quoted as per their estimated accuracies; convergence is more difficult to realize for the smaller  $R$ , as the potential’s sharp cutoff in  $R$  requires many basis functions to produce accurate flux tube eigenvalues and eigenfunctions. The  $O(\beta^6/\alpha_f^3)$  corrections to the asymptotic forms have also been computed and included in the tabulated numbers; they are of order  $10^{-12}$  for the above parameters. A particular partial sum of any of the asymptotic series given in Eqs. (4.15)–(4.17) will agree more closely with the “true” result as  $k$  decreases; thus, the slight discrepancies seen in the  $R = 1.61$  comparison need not arise from round-off error in the evolution calculation. Indeed, the comparison at  $R = 1.61$  fm is quite good; this simultaneously assures the numerical accuracy of the evolution calculations and guarantees, if the calculation were tractable, that the  $A$ -dependence of  $A^{\text{eff}}/A$  from the evolution matrix approach at extremely high energies would agree with that of the frozen limit.

## V. RESULTS

The evolution matrix approach described in the previous section permits computation of the final-state interactions, given an initial wave packet of on-shell charmonium states, from  $J/\psi$  threshold to the high energy limit. This is merely a statement of principle, however; for rea-

sons of practicality, the parameters of the model limit the largest energy which may be considered in this approach to tens of GeV. In order to convert the probabilities obtained earlier to physically meaningful observables, it is necessary (i) to make some model for the production amplitude, and (ii) to average over all possible production points in the nucleus to obtain  $A^{\text{eff}}/A$ . Point (ii) has been described previously: for the low energies considered here, shadowing cannot be significant; thus, the computation of  $A^{\text{eff}}/A$  proceeds from Eq. (2.6). Point (i) is rather more problematic. Certainly, at lower energies, the initial photoproduced superposition of  $c\bar{c}$  states must be affected by threshold effects. For a particular photon energy, the states which should contribute significantly to the initial amplitude are those which can be physically produced in quasifree kinematics with a nucleon; that is, the mass of any  $\psi_n$  that satisfies the following equation is included:

TABLE VII. The number of open  $c\bar{c}$  channels as a function of the initial photon momentum  $p_\gamma$ .  $p_{\text{max}}$  is the maximum  $J/\psi$  momentum for the given  $p_\gamma$  if  $p_T = 0$ .

$p_\gamma$ (GeV/c)	$N_{\text{open}}$	$p_{\text{max}}$ (GeV/c)
8.5	1	7.17
12	2	11.4
15	3	14.6
20	5	19.7
25	7	24.8

$$p_\gamma - \frac{1}{2M_N} M_{\psi_n}^2 = \frac{1}{M_N} \left\{ \sqrt{(M_{\psi_n}^2 + \eta^2 p_\gamma^2 + p_T^2)[M_N^2 + (1-\eta)^2 p_\gamma^2 + p_T^2]} - \eta(1-\eta)p_\gamma^2 + p_T^2 \right\}, \quad (5.1)$$

where  $p_T = 0$  and  $\eta \in [0, 1]$  as the momentum of the  $n$ th  $c\bar{c}$  state is  $p_{\psi_n} \equiv \eta p_\gamma$ . As argued in Sec. II, it is assumed that this amplitude is composed solely of  $l = 0$  states – only these states have finite amplitude at the origin. (Again, any  $l \neq 0$  admixtures are neglected.) Table VII gives the number of states which satisfy this constraint as a function of the initial photon momentum  $p_\gamma$ . Table VII also reports the maximum  $J/\psi$  momentum which satisfies Eq. (5.1) for a particular  $p_\gamma$ ; this  $p_{\max}$  is used to compute the  $\beta_{c\bar{c}}$  and  $\gamma$  input to the evolution calculation.

The number of states which should contribute to the initial amplitude at a particular energy is not sufficient to determine its shape. To explore this freedom, I shall now consider three different *Ansätze* for the initial state  $|\psi_i\rangle$ . The first is to construct an initial state with expansion coefficients  $C_n$  proportional to the charmonium wave function's at the origin; that is,  $C_n \propto \Psi_{(n-1)00}(0)$ , so that  $|\psi_i\rangle = \sum_{n=1}^{N_i} C_n |\Psi_{(n-1)00}\rangle$ . Thus,

$$C_n \propto \sqrt{\frac{\Gamma(n+1/2)}{\Gamma(n)}}, \quad (5.2)$$

which, unfortunately, is divergent in  $n$ . The  $\delta$ -function expansion is not well posed in this basis, so that this initial-state choice is discarded. A second option is to consider the expansion of  $|\psi_i(r)\rangle = (\alpha_i/\pi)^{3/4} \exp(-\alpha_i r^2/2)$ , the initial state assumed at very high energies, on the  $|\Psi_{(n-1)00}\rangle$  hadronic basis. This offers a smooth parametrization as a function of  $N_i$  to the initial wave function chosen at high energies. The coefficients,  $C_n$ , have the form

$$C_n \equiv \langle \Psi_{(n-1)00} | \Psi_i \rangle \propto \left( \frac{\alpha_i}{\alpha_f} \right)^{3/4} \left( \frac{2}{\alpha_i/\alpha_f + 1} \right)^{3/2} \times \sqrt{\frac{\Gamma(n+1/2)}{\Gamma(n)\Gamma(3/2)}} \left( \frac{\alpha_i - \alpha_f}{\alpha_i + \alpha_f} \right)^{n-1}. \quad (5.3)$$

Another alternative is to determine the initial wave packet by choosing the amplitudes of the  $|\Psi_{(n-1)00}\rangle$  states such that the narrowest possible state for a particular truncation  $N_i$  is obtained. The numerical realization of this approach is presented in Appendix E. These latter two alternatives are compared as a function of truncation in Fig. 6, and the rms  $q\bar{q}$  separation of the wave function in each approach with truncation is shown in Table VIII. The shapes of the two different *Ansätze* are not particularly different, so that the minimum-size *Ansatz* is chosen; this parametrization of the threshold effects' energy dependence is consistent with a "best case" scenario for transparency. Although the logic of this choice is clear, the experimental data which can either confirm or rule out such a choice is meager. One confrontation with experiment is afforded by the work of Camerini *et al.* [64]. At a photon energy of 21 GeV (assuming elastic  $J/\psi$  and  $\psi'$  production), they extract the cross-section ratio

$$\frac{d\sigma(\psi(3100))/dt}{d\sigma(\psi(3700))/dt} \Big|_{t_{\min}} = 6.8 \pm 2.4 \rightarrow 5.6 \pm 2.2 \quad (5.4)$$

upon assuming that the average branching ratio of  $\psi'$  into either  $e$  or  $\mu$  pairs is 1%, where  $t_{\min} = 0.069(\text{GeV}/c)^2$  for  $J/\psi$  and  $0.164(\text{GeV}/c)^2$  for  $\psi'$ . The second value

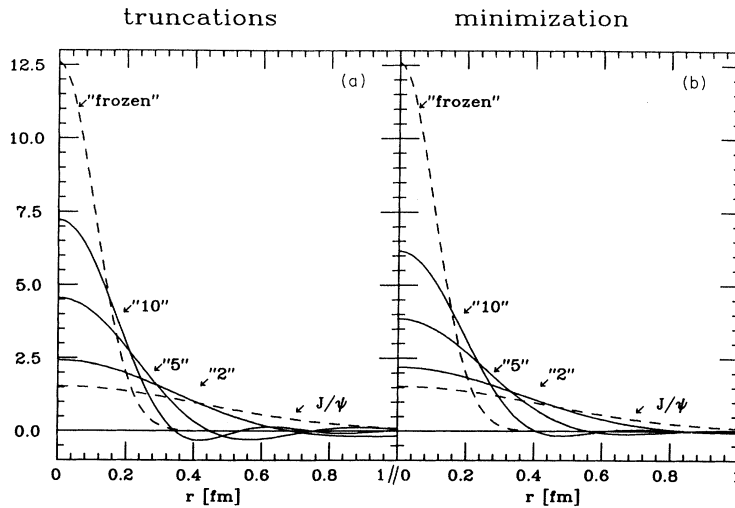


FIG. 6. Various initial state *Ansätze* as a function of the number of terms in the  $|\psi_{n-100}\rangle$  basis. Truncations of the frozen-limit *Ansatz* are shown in (a), whereas the minimum-size state for a given number of terms is shown in (b). The  $J/\psi$  and frozen-limit wave functions are also indicated.

TABLE VIII. Root-mean-square separations and  $J/\psi : \psi'$  ratios for the *Ansätze* considered as a function of  $N_i$ , the number of terms in the initial state. “trunc” refers to the truncations of the initial-state *Ansatz* in the “frozen” limit, whereas “min” refers to the minimum-size prescription.

$N_i$	$(\sqrt{\langle r^2 \rangle})_{\text{trunc}}$ (fm)	$(P_{J/\psi} : P_{\psi'})_{\text{trunc}}$	$(\sqrt{\langle r^2 \rangle})_{\text{min}}$ (fm)	$(P_{J/\psi} : P_{\psi'})_{\text{min}}$
2	0.494	0.849	0.406	4.44
3	0.470	0.849	0.346	2.16
4	0.446	0.849	0.307	1.57
5	0.423	0.849	0.278	1.31
10	0.319	0.849	0.203	0.930

reported in Eq. (5.4) results when the 1991 Particle Data Booklet value for the average branching ratio of  $\psi' \rightarrow e^+e^-$  and  $\psi' \rightarrow \mu^+\mu^-$ ,  $0.82 \pm 0.15\%$ , is used. They estimate inelastic contributions to be around 20 – 30%, and  $t_{\text{min}}$  is not small, so that the usefulness of Eq. (5.4) is perhaps unclear. Nevertheless, it is of interest to compute  $|\langle \Psi_{J/\psi} | \Psi_i \rangle| / |\langle \Psi_{\psi'} | \Psi_i \rangle|^2$  for the *Ansätze* considered; this ratio is tabulated in Table VIII. For the *Ansatz* which consists of a truncation of the expansion of  $\exp(-\alpha_i r^2/2)$ , the  $J/\psi : \psi'$  ratio is independent of  $N_i$ ; that is,  $|\langle \Psi_{000} | \Psi_i \rangle| / |\langle \Psi_{100} | \Psi_i \rangle|^2 = \frac{2}{3}[\alpha_i + \alpha_f / (\alpha_i - \alpha_f)]^2$ . Although the difficulties which bar ready interpretation of the  $J/\psi : \psi'$  measurement in Eq. (5.4) have been stated, it is clear that neither *Ansatz* proposed for use at 20 GeV compares favorably with the measured ratio. This may simply imply that the initial state at 20 GeV does not differ appreciably in size from that of the  $J/\psi$  and that the minimum-state *Ansatz* is overly optimistic. Nevertheless, I shall proceed to explore the consequences of such an initial-state choice.

Given the narrowest-state *Ansatz* for the initial state,

one can proceed to compute the probabilities of measuring  $J/\psi$ ,  $\chi$ , and  $\psi'$  as a function of the initial photon energy and number of states  $N_i$  in the initial state. Table VII shows the number of channels open for a particular  $E_\gamma$ , as per the criterion given in Eq. (5.1). In order to examine the sensitivity of the final-state interactions to  $N_i$  and  $E_\gamma$ , the following cases will be examined: ( $N_i = 1, E_\gamma = 8.5$  GeV), ( $N_i = 1, E_\gamma = 12$  GeV), ( $N_i = 1, E_\gamma = 20$  GeV), ( $N_i = 2, E_\gamma = 12$  GeV), ( $N_i = 2, E_\gamma = 20$  GeV), and ( $N_i = 5, E_\gamma = 20$  GeV). Figures 7–12 show the  $J/\psi$ ,  $\chi$ , and  $\psi'$  probabilities in the  $c\bar{c}$  wave packet, as well as its longitudinal and transverse size, as a function of the reaction coordinate  $z$  for Be, Fe, and Pb nuclei. It should be emphasized that the computations for the various nuclei are distinct, as the differing  $\xi_A$ 's (due to the differing uniform equivalent densities) alter the development of the wave packet between interactions with successive nucleons. The probabilities are all plotted together, though the probabilities for a particular nucleus are readily identified, as they are spaced by multiples of  $D_{\text{spac}}$  (see Table I). Contrary to

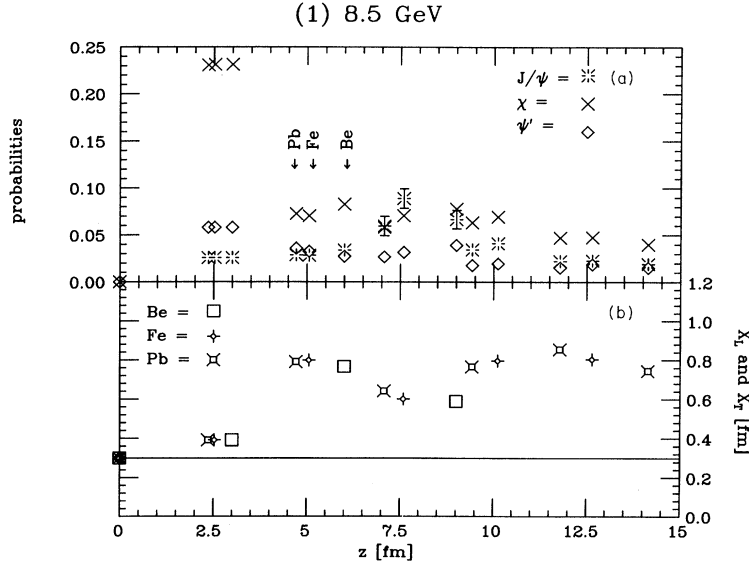


FIG. 7.  $J/\psi$ ,  $\chi$ , and  $\psi'$  probabilities (a), and the  $c\bar{c}$  wave packets' longitudinal and transverse size (b) as a function of the reaction coordinate  $z$  in the case where the initial-state wave function is that of the  $J/\psi$  and the photon energy is 8.5 GeV. The calculations for Be, Fe, and Pb are superimposed on each other, though they are readily identified since they are spaced by different values of  $D_{\text{spac}}$ , as tabulated in Table I. Here the longitudinal size  $X_L$  is trivial and is shown by the solid line in (b). The transverse size  $X_T$  is shown by the plotted symbols; the rms  $c\bar{c}$  separation in the charmonium wave packet is given by  $\langle r^2 \rangle^{1/2} \equiv (X_L^2 + 2X_T^2)^{1/2}$ . The size of the error bar from the Monte Carlo average over the nucleon field orientations is typically contained within the size of the plot symbol; the error bars of the exceptions are plotted.

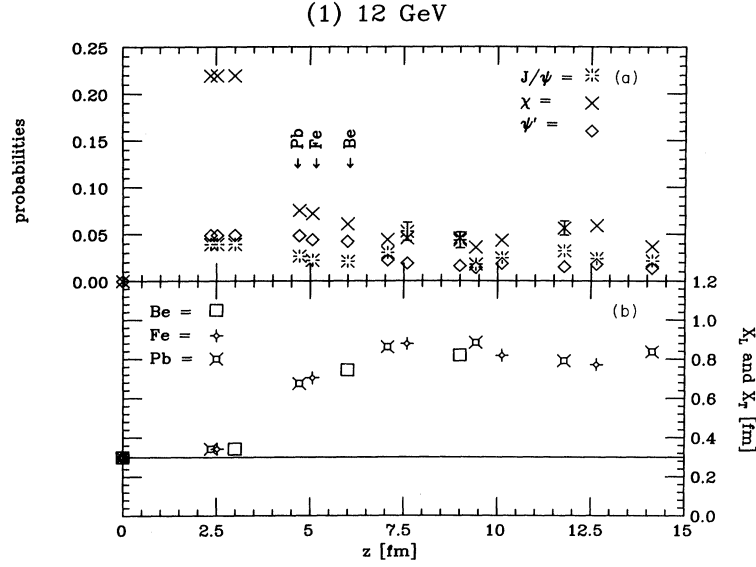


FIG. 8.  $J/\psi$ ,  $\chi$ , and  $\psi'$  probabilities (a), and the  $c\bar{c}$  wave packets' longitudinal and transverse size (b) as a function of the reaction coordinate  $z$  in the case where the initial-state wave function is that of the  $J/\psi$  and the photon energy is 12 GeV. See Fig. 7.

the high energy limit, the probability of producing  $\chi$  is now much enhanced relative to the  $J/\psi$  and  $\psi'$  survival probabilities. The  $\chi$  enhancement is quite natural, given the parity-odd interaction Hamiltonian; the  $\chi$  suppression in the frozen limit is due to the initial-state choice. To untangle what happens as  $E_\gamma$  increases, consider the  $N_i = 1$  initial state ( $J/\psi$  only) incident on a single nucleon as  $E_\gamma$  varies. Here the probabilities are independent of  $D_{\text{spac}}$  in the first time step, as the initial state is a pure state. The  $J/\psi$  occupation probability evidently

increases with  $E_\gamma$  for  $E_\gamma = 8.5$  to 20 GeV. This is a consequence of Lorentz dilation – the interaction time in the  $c\bar{c}$  rest frame scales by  $1/\gamma$  – though it is not trivial, as the interaction strength also scales with  $\gamma$ . Moreover, it should be noted that this effect cannot persist with increasing energy, as at  $E_\gamma = 20$  GeV, the  $J/\psi$  occupation probability exceeds that of the frozen limit, i.e., Eq. (3.9) with  $|\psi_i\rangle = |\psi_{J/\psi}\rangle$ . The absolute and relative magnitudes of the probabilities are controlled by the development of the wave packet in the interaction basis during

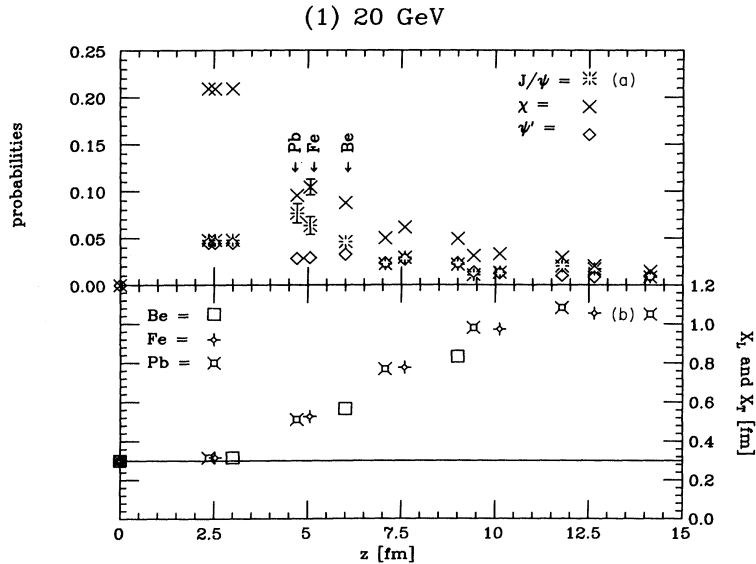


FIG. 9.  $J/\psi$ ,  $\chi$ , and  $\psi'$  probabilities (a), and the  $c\bar{c}$  wave packets' longitudinal and transverse size (b) as a function of the reaction coordinate  $z$  in the case where the initial-state wave function is that of the  $J/\psi$  and the photon energy is 20 GeV. See Fig. 7.

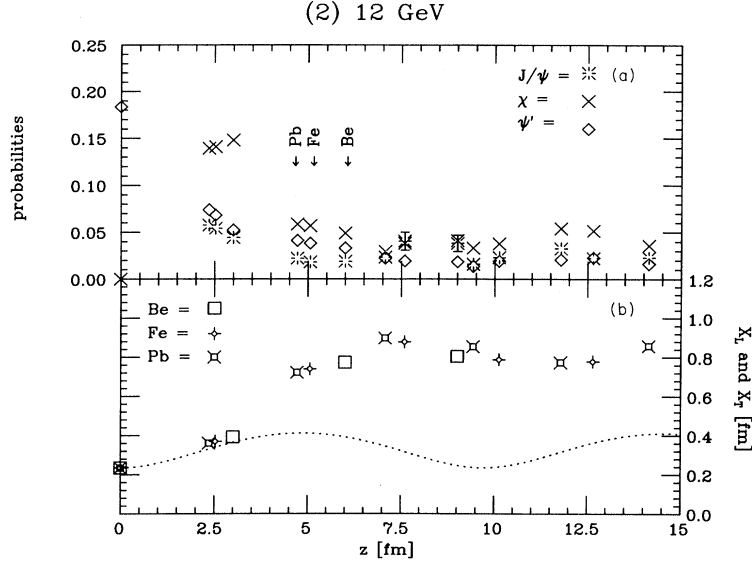


FIG. 10.  $J/\psi$ ,  $\chi$ , and  $\psi'$  probabilities (a), and the  $c\bar{c}$  wave packets' longitudinal and transverse size (b) as a function of the reaction coordinate  $z$  in the case where the initial-state wave function is the minimum-size wave packet composed of  $J/\psi$  and  $\psi'$  states only and the photon energy is 12 GeV. The calculations for Be, Fe, and Pb are superimposed on each other, though they are readily identified since they are spaced by different values of  $D_{\text{spac}}$ , as tabulated in Table I. Here the longitudinal size  $X_L$  is given by Eq. (4.13) and is shown by the dotted line in (b). The transverse size  $X_T$  is shown by the plotted symbols; the rms  $c\bar{c}$  separation in the charmonium wave packet is given by  $\langle r^2 \rangle^{1/2} \equiv (X_L^2 + 2X_T^2)^{1/2}$ . The size of the error bar from the Monte Carlo average over the nucleon field orientations is typically contained within the size of the plot symbol; the error bars of the exceptions are plotted.

charmonium's passage through the flux tube. Perhaps the energy dependence of the experimental  $\sigma_{J/\psi N}^{\text{tot}}$  can serve as a model constraint, as the energy dependence of this quantity should be connected to that of the  $J/\psi$  survival probability. It is well-known that the *total* hadron-nucleon cross sections vary weakly with energy, showing

a logarithmic rise as the energy increases. In the case of  $J/\psi$ , this latter energy-dependence is inferred, assuming vector-meson dominance, from  $d\sigma/dt|_{t=0}[\gamma N \rightarrow \psi N]$  data, implying a 40% increase in  $\sigma_{\text{tot}}^{J/\psi N}$  from 60 to 300 GeV [65]. Unfortunately, the energies amenable to study here cannot confront this data, and the assumptions im-

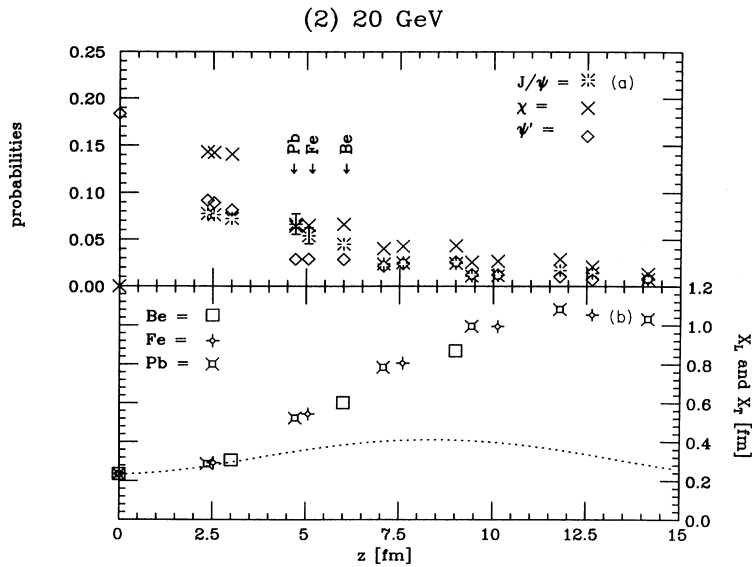


FIG. 11.  $J/\psi$ ,  $\chi$ , and  $\psi'$  probabilities (a), and the  $c\bar{c}$  wave packets' longitudinal and transverse size (b) as a function of the reaction coordinate  $z$  in the case where the initial-state wave function is the minimum-size wave packet composed of  $J/\psi$  and  $\psi'$  states only and the photon energy is 20 GeV. See Fig. 10.

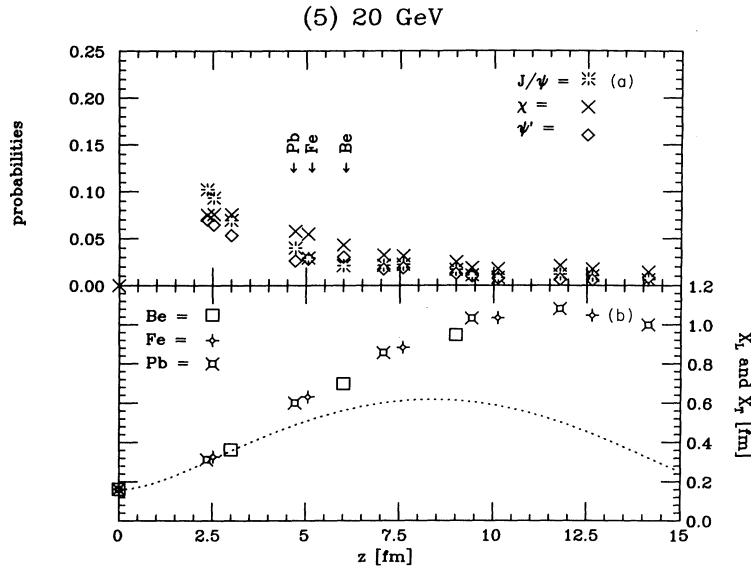


FIG. 12.  $J/\psi$ ,  $\chi$ , and  $\psi'$  probabilities (a), and the  $c\bar{c}$  wave packets' longitudinal and transverse size (b) as a function of the reaction coordinate  $z$  in the case where the initial-state wave function is the minimum-size wave packet composed of 5  $|\psi_{n00}\rangle$  states and the photon energy is 20 GeV. See Fig. 10.

plicit in this application of vector-meson dominance become suspect at lower energies. Proceeding with the results in Figs. 8–12, and comparing the  $J/\psi$ ,  $\chi$ , and  $\psi'$  probabilities after passage through a single flux tube for  $N_i \neq 1$ , it is evident that the relative magnitudes of these probabilities are quite sensitive to the initial state. At 20 GeV, the ratio of  $J/\psi$  and  $\psi'$  probabilities is greater or lesser than 1 depending on  $N_i$ .

In subsequent nucleon interactions, the precise superposition of  $c\bar{c}$  states between the flux tubes is critical in determining the  $J/\psi$ ,  $\chi$ , and  $\psi'$  probabilities. In order to make studying the probabilities plotted in Figs. 7–12 more meaningful, these figures also show the longitudinal and transverse rms  $c\bar{c}$  separations associated with those probabilities. The evolution of the longitudinal coordinate with  $z$  is trivial, but the wave packet's transverse size is generated by interactions with the medium: the final-state interactions systematically act to “push out” the wave packet. There is, moreover, a correlation between the transverse size and the  $J/\psi$  survival probability measured there – as an illustration, the dip in  $X_T$  for Be and Fe in the  $N_i = (1)$ ,  $E_\gamma = 8.5$  GeV case corresponds to a jump in the  $J/\psi$  probability. The oscillations in  $X_T$  manifest at 8.5 GeV damp out as  $E_\gamma$  increases, and increasing the photon energy does ultimately result in a larger  $c\bar{c}$  wave packet. Yet, for a fixed initial state, increasing  $E_\gamma$  acts to decrease the wave packet's transverse size for some finite distance  $z_{\text{fin}}$  after the production point; only at large  $z$  does the wave packet become bigger than at the lower energy. This can be readily understood, as the higher energy means that the  $c\bar{c}$  can be knocked into higher states of excitation, which certainly have larger rms separations. At a fixed energy, the initial size of the packet is determined by  $N_i$ , yet the transverse size for large  $z$ , e.g.,  $z > 10$  fm at  $E_\gamma = 20$

GeV, seems to be quite independent of  $N_i$ , almost as if the developing wave packet has only a finite memory of its initial state. The observation of a decreased  $X_T$  and an increased  $J/\psi$  survival probability for some fixed  $z$  and initial state as  $E_\gamma$  increases offers qualitative support for the color transparency hypothesis; it will be seen later that the retention of *all* excited  $c\bar{c}$  states in the evolution between the flux tubes, that is, the coherence of the final-state interactions, is responsible for this effect. Even if some “weakening” of the final-state interactions can be seen, the ultimate behavior of the extracted absorption coefficients from the computed nuclear average as  $E_\gamma$  increases is unclear. Before proceeding with the above probabilities and computing  $A^{\text{eff}}/A$  for  $J/\psi$ ,  $\chi$ , and  $\psi'$  production, it is useful to examine the role of coherence effects in producing the previously described behavior.

Figures 13–15 compare the “full” calculation of the final-state interactions with one in which the number of states in the free evolution between nucleons is truncated to  $n = 2$ , where  $n$  denotes the maximum excitation of a single oscillator in the  $|\Psi_{n_x n_y n_z}\rangle$  basis. The logic of this is to gauge the sensitivity of the results – in a crude way – to the lack of open channels and to understand what changes their inclusion might yield. The comparison is made for the  $N_i = 1$  case ( $J/\psi$  only) for Fe as a function of  $N$ , the number of nucleons through which the  $c\bar{c}$  wave packet passes, for  $E_\gamma$  ranging from 8.5 to 20 GeV. Both the probabilities and  $X_T$  are plotted for each calculation, so as to allow simultaneous comparison. What is quite striking is how much larger the  $J/\psi$ ,  $\chi$ , and  $\psi'$  probabilities are in the “full” calculation than in the truncated case as  $N$  increases. It is also noteworthy that this behavior is manifest even though the wave packet's transverse size may be much larger in the “full” calculation

than in the truncated one – this is true for all the energies studied. Evidently the correlation between survival probability and  $X_T$  noted earlier is only meaningful if all possible intermediate states are included. The truncated calculation is constructed so that its  $X_T$  is the  $n = 2$  portion of the “full” calculation’s transverse size; the  $X_T$  of the truncated calculation varies only weakly with  $N$  and  $E_\gamma$ . There is a miniscule shift towards smaller  $X_T$  in the truncated calculation for  $N = 1$  as  $E_\gamma$  increases, but the more palpable change in the full  $X_T$  with  $E_\gamma$  is due to the inclusion of higher mass  $c\bar{c}$  states. It is interesting to note that the  $J/\psi$  survival probability in the full calculation at  $N = 5$  is rather insensitive to the change of energy, even though  $X_T$  varies markedly; evidently, the higher mass charmonium states, though important in determining  $X_T$ , do eventually decouple from the ground state. The  $J/\psi$  survival probability with  $N$  is larger for the  $n = 2$  calculation than if no coherence effects were included at all, as in the event of no coherence,  $P_{J/\psi}(N) = [P_{J/\psi}(1)]^N$ ; thus, the increase in the  $J/\psi$  survival probability as the number of intermediate states increases for large  $N$  alters the weakening of the final-state interactions seen in a quantitative, rather than qualitative, manner. It must be emphasized that the effect of the  $n = 2$  truncation on the computed  $A^{\text{eff}}/A$  is not clear for the lower energy cases, as the  $N = 2$   $J/\psi$  probabilities are larger for the truncated cases, though  $A^{\text{eff}}/A$  would be expected to be smaller for  $E_\gamma = 20$  GeV, as the truncated  $J/\psi$  survival probabilities are systematically smaller than those of the full calculation. Thus,

a “real world” calculation in which inelastic channels are included, so that the free propagation of the  $n > 2$  states is strongly damped, may offer a weaker change in  $A^{\text{eff}}/A$  with energy. What this calculation suggests is quite different from the popular picture: usually one speaks of the interactions with the nucleus which lead to multiple particle production as “stripping away” the color nonsinglet components of the initial state, leaving a small, color-singlet state to propagate through and interact weakly with the medium [66]. This calculation shows the effect of the open channels – leading to  $\pi$  production, say – to be rather more subtle; it is certainly not clear that their inclusion enhances the effect of transparency. These statements lack significance in the absence of a quantitative calculation of  $A^{\text{eff}}/A$  for the probabilities obtained in the “full” calculation; thus, these calculations are discussed next.

Using the probabilities plotted in Figs. 7–12,  $A^{\text{eff}}/A$  [from Eq. (2.6)] is computed for Be, Fe, and Pb nuclei using the fits to the experimental charge densities as tabulated in Landolt-Börnstein [44]. The results are shown in Table IX. As before, the  $A^{\text{eff}}/A$  tabulated under the “H” column give the probabilities of  $J/\psi$ ,  $\chi$ , or  $\psi'$  in the initial state. The errors in  $A^{\text{eff}}/A$  due to the uncertainties in the Monte Carlo averages have been calculated using the standard formulas for the propagation of errors; these errors are typically in the fourth significant figure.  $A^{\text{eff}}/A$  for  $J/\psi$  is much larger than that for  $\chi$  and  $\psi'$ , though this is a consequence of the initial-state *Ansätze* used. This is illustrated when one compares the  $A^{\text{eff}}/A$  for  $\chi$  with that

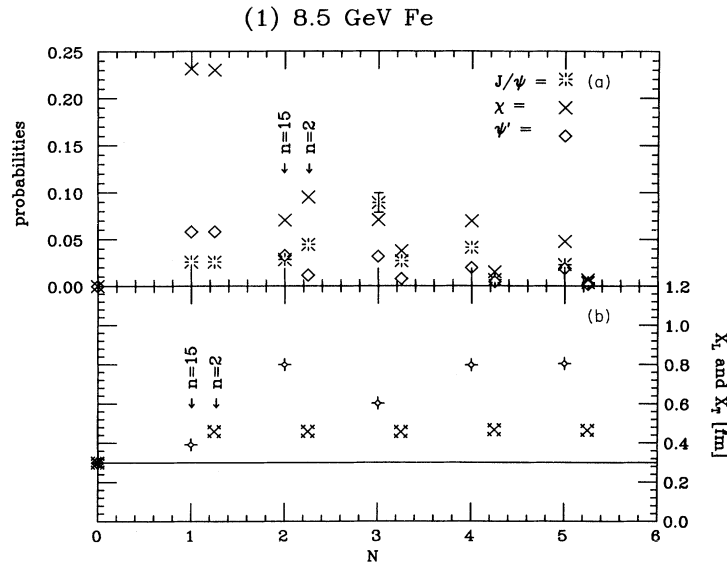


FIG. 13. Illustration of the importance of coherence effects in the computation of  $J/\psi$ ,  $\chi$ , and  $\psi'$  probabilities (a), and the  $c\bar{c}$  wave packets’ longitudinal and transverse size (b) as a function of the number of nucleons  $N$ , in the case where the initial state wave function is that of the  $J/\psi$  and the photon energy is 8.5 GeV. The computation is performed with the  $\xi_A$  of Fe, as given in Table I. The “full” calculation is shown at integer  $N$ , where the maximum single oscillator excitation required is  $n = 15$ , whereas the calculation in which only the free states with  $n \leq 2$  are allowed to propagate between nucleons are off-set a quarter unit to the right. Here the longitudinal size  $X_L$  is trivial and is shown by the solid line in (b). The transverse size  $X_T$  is shown by the plotted symbols; the rms  $c\bar{c}$  separation in the charmonium wave packet is given by  $\langle r^2 \rangle^{1/2} \equiv (X_L^2 + 2X_T^2)^{1/2}$ . The size of the error bar from the Monte Carlo average over the nucleon field orientations is typically contained within the size of the plot symbol; the error bar of the exception is plotted.

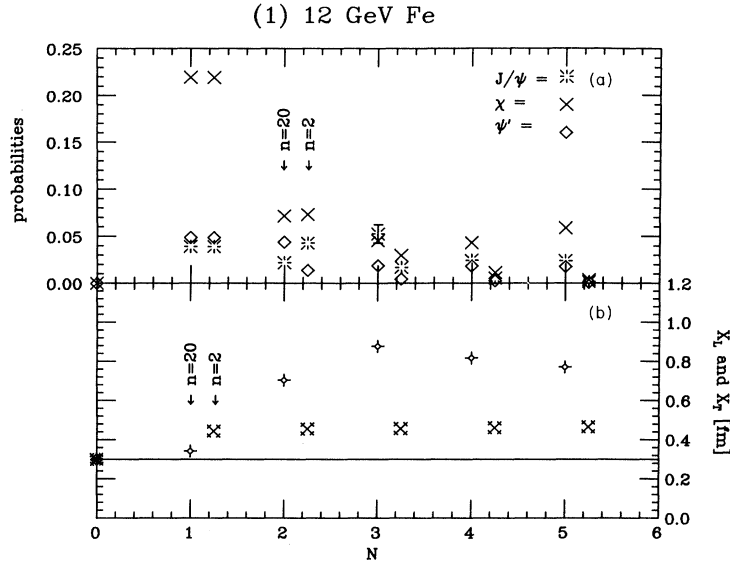


FIG. 14. Illustration of the importance of coherence effects in the computation of  $J/\psi$ ,  $\chi$ , and  $\psi'$  probabilities (a), and the  $c\bar{c}$  wave packets' longitudinal and transverse size (b) as a function of the number of nucleons  $N$ , in the case where the initial state wave function is that of the  $J/\psi$  and the photon energy is 12 GeV. The computation is performed with the  $\xi_A$  of Fe, as given in Table I. The "full" calculation is shown at integer  $N$ , where the maximum single oscillator excitation required is  $n = 20$ , whereas the calculation in which only the free states with  $n \leq 2$  are allowed to propagate between nucleons are off-set a quarter unit to the right. See Fig. 13.

for  $\psi'$  at  $E_\gamma = 20$  GeV for  $N_i = 1, 2$ , and 5. If  $N_i = 1$ , the  $A^{\text{eff}}/A$  for  $\chi$  exceeds that for  $\psi'$  – this is natural as the Hamiltonian is parity-odd – whereas if the  $\psi'$  probability is finite in the initial state, the  $A^{\text{eff}}/A$  of  $\psi'$  exceeds that of  $\chi$ . Given these  $A^{\text{eff}}/A$  and their errors, the absorption coefficients  $\alpha$ , defined through the parametriza-

tion  $A^{\text{eff}}/A \propto A^\alpha$ , can be determined for  $J/\psi$ ,  $\chi$ , and  $\psi'$  by making a least-squares fit.  $\alpha$  has been computed not only for direct  $J/\psi$  production, but also once feeding from  $\chi$  and  $\psi'$  states are taken into account. As noted previously, the degree to which feeding contaminates the observation of  $J/\psi$  depends on the resolution

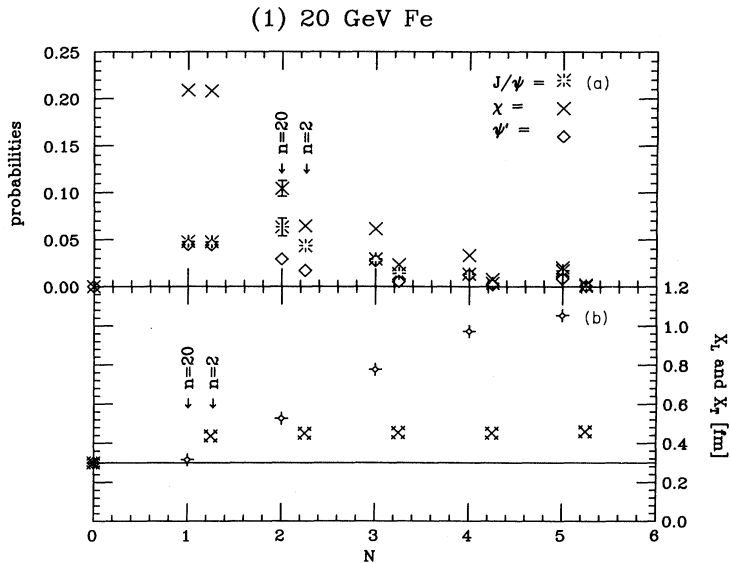


FIG. 15. Illustration of the importance of coherence effects in the computation of  $J/\psi$ ,  $\chi$ , and  $\psi'$  probabilities (a), and the  $c\bar{c}$  wave packets' longitudinal and transverse size (b) as a function of the number of nucleons  $N$ , in the case where the initial state wave function is that of the  $J/\psi$  and the photon energy is 20 GeV. The computation is performed with the  $\xi_A$  of Fe, as given in Table I. The "full" calculation is shown at integer  $N$ , where the maximum single oscillator excitation required is  $n = 20$ , whereas the calculation in which only the free states with  $n \leq 2$  are allowed to propagate between nucleons are off-set a quarter unit to the right. See Fig. 13.

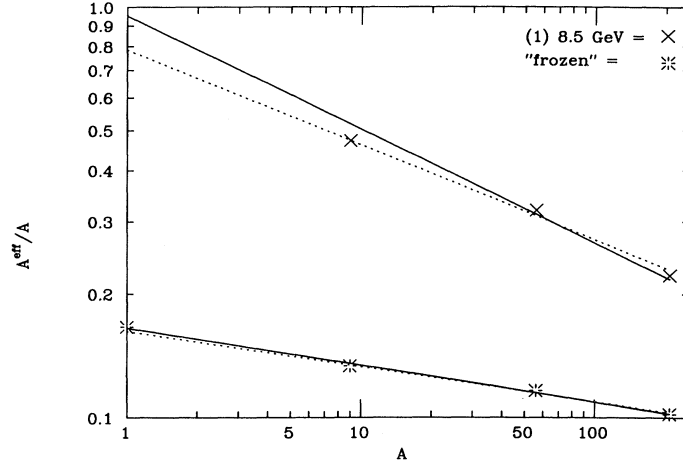


FIG. 16.  $A^{\text{eff}}/A$  vs  $A$  for  $J/\psi$  with feeding effects in the frozen limit and for the  $N_i = 1$ ,  $E_\gamma = 8.5$  GeV case. The solid lines show the least-squares fits to the calculated  $A^{\text{eff}}/A$  if the H data is included in the fits, whereas the dotted lines show the fit if the H data is *not* included.

of the experiment; as before, these effects are included naively, as per Eq. (C4), in order to gauge the maximum size of the effect. In Table X, the  $\alpha$ 's for  $J/\psi$  production, with and without feeding effects, are shown for the various cases considered. The fits to determine the absorption coefficients are performed with and without the inclusion of the H data; the relative sizes of the  $\alpha$ 's are retained, though Table X illustrates that the overall size of the absorption coefficients are rather sensitive to its inclusion. This evident disparity arises since no final-state

interactions are required to produce the H data. This is shown in Fig. 16, which compares  $A^{\text{eff}}/A$  and the fit with and without H data for  $J/\psi$  production with feeding in the frozen limit and in the  $N_i = 1$ ,  $E_\gamma = 8.5$  GeV case. The final-state interactions are quite large in the lower energy case; hence, the greater disparity upon the inclusion of the H data. The fit without H data fits the remaining  $A^{\text{eff}}/A$ 's much better; thus, only the absorption coefficients fitted in this way will be considered in the discussion and tables to come. In studying the  $\alpha$ 's in

TABLE IX. "Raw"  $A^{\text{eff}}/A$  for  $J/\psi$ ,  $\chi$ , and  $\psi'$  as a function of  $N_i$  and  $E_\gamma$  for H, Be, Fe, and Pb. Here the minimum-size prescription is used for  $N_i \geq 2$ .

State	H	Be	Fe	Pb
$N_i = 1 \quad E_\gamma = 8.5 \text{ GeV}$				
$J/\psi$	1	0.439	0.284	0.190
$\chi$	0	0.105	0.103	$9.30 \times 10^{-2}$
$\psi'$	0	$2.80 \times 10^{-2}$	$3.14 \times 10^{-2}$	$2.95 \times 10^{-2}$
$N_i = 1 \quad E_\gamma = 12 \text{ GeV}$				
$J/\psi$	1	0.441	0.281	0.187
$\chi$	0	$9.65 \times 10^{-2}$	$9.46 \times 10^{-2}$	$8.56 \times 10^{-2}$
$\psi'$	0	$2.63 \times 10^{-2}$	$2.90 \times 10^{-2}$	$2.84 \times 10^{-2}$
$N_i = 1 \quad E_\gamma = 20 \text{ GeV}$				
$J/\psi$	1	0.448	0.289	0.195
$\chi$	0	$9.70 \times 10^{-2}$	0.100	$8.36 \times 10^{-2}$
$\psi'$	0	$2.33 \times 10^{-2}$	$2.53 \times 10^{-2}$	$2.34 \times 10^{-2}$
$N_i = 2 \quad E_\gamma = 12 \text{ GeV}$				
$J/\psi$	0.816	0.365	0.236	0.159
$\chi$	0	$6.66 \times 10^{-2}$	$6.51 \times 10^{-2}$	$5.98 \times 10^{-2}$
$\psi'$	0.184	0.104	$8.08 \times 10^{-2}$	$6.33 \times 10^{-2}$
$N_i = 2 \quad E_\gamma = 20 \text{ GeV}$				
$J/\psi$	0.816	0.380	0.248	0.171
$\chi$	0	$6.67 \times 10^{-2}$	$(6.72 \pm .01) \times 10^{-2}$	$6.01 \times 10^{-2}$
$\psi'$	0.184	0.115	$8.57 \times 10^{-2}$	$6.40 \times 10^{-2}$
$N_i = 5 \quad E_\gamma = 20 \text{ GeV}$				
$J/\psi$	0.418	0.207	0.146	0.106
$\chi$	0	$3.72 \times 10^{-2}$	$4.17 \times 10^{-2}$	$3.95 \times 10^{-2}$
$\psi'$	0.318	0.160	0.111	$7.85 \times 10^{-2}$

TABLE X.  $\alpha_{\text{feed}}$  and  $\alpha_{\text{no feed}}$  computed from fitting the  $A^{\text{eff}}/A$  of Table IX to  $A^\alpha$  as a function of the number of terms in the initial state,  $N_i$ , and the photon energy  $E_\gamma$ .  $\alpha_{\text{no feed}}$  is the absorption coefficient associated with direct  $J/\psi$  production, whereas  $\alpha_{\text{feed}}$  includes the contributions to  $J/\psi$  production from electromagnetic decay of  $\chi$  and  $\psi'$ . The sensitivity of the fits to the inclusion of the H-data is shown.

$(N_i)$	$E_\gamma$ (GeV)	$\alpha_{\text{feed}}$	$\alpha_{\text{no feed}}$	$\alpha_{\text{feed}}$	$\alpha_{\text{no feed}}$
		With H data		Without H data	
(1)	8.5	-0.277	-0.306	-0.231	-0.257
(1)	12	-0.282	-0.309	-0.241	-0.270
(1)	20	-0.277	-0.302	-0.232	-0.251
(2)	12	-0.276	-0.301	-0.232	-0.259
(2)	20	-0.266	-0.289	-0.225	-0.243
(5)	20	-0.246	-0.252	-0.202	-0.202

Table X, it is evident that they can *oscillate* with energy. This is so for the  $N_i = 1$  case *and* for the “optimum” case in which one considers the narrowest state composed of the open channels at a given energy. Yet, in both cases the  $\alpha$ 's without feeding effects are smaller at 20 GeV than they are at 8.5 GeV. These trends are meaningful; the errors in the  $\alpha$ 's are typically in the fifth significant figures. However, the total magnitude over which the absorption coefficients vary is not large – the change is barely 20% in the largest case – that is, from the  $N_i = 1$ ,  $E_\gamma = 8.5$  GeV to the  $N_i = 5$ ,  $E_\gamma = 20$  GeV cases. The naive inclusion of feeding effects tend to blur these effects markedly, though presumably these can be largely controlled by the resolution of the experiment. The trend towards smaller  $\alpha$ 's upon inclusion of feeding effects can be readily understood: the depopulation of the  $J/\psi$  channel with  $N$  is compensated by the production of  $\chi$  and  $\psi'$ , so that the  $J/\psi$  probability as a function of  $N$  is flatter.

In order to understand how coherence effects impact the  $\alpha$ 's reported in Table X, the absorption coefficients for  $J/\psi$  production without feeding in the  $N_i = 1$  case are computed when *no* coherence effects are included. Thus,  $P_{J/\psi}(N) = [P_{J/\psi}(1)]^N$  is used in the computation of  $A^{\text{eff}}/A$  as per Eq. (2.6). The resulting  $\alpha_{\text{incoh}}$  are shown in Table XI, where they are compared with the absorption coefficients of the full calculation.  $\alpha_{\text{incoh}}$  changes very weakly with energy, thus confirming the hypothesis that any significant change in  $\alpha$  with energy is due to coherence effects, a.k.a. “color transparency.” Even though the variation in  $\alpha_{\text{no feed}}$  over the interval  $E_\gamma \in [8.5, 20]$  GeV is not particularly large, it should be emphasized

TABLE XI. The sensitivity of the  $J/\psi$  absorption coefficients to coherence effects.  $\alpha_{\text{no feed}}$  and  $\alpha_{\text{feed}}$  are defined as in Table X; here  $\alpha_{\text{incoh}}$  denotes the absorption coefficient for direct  $J/\psi$  production when excited charmonium states are not allowed to scatter back to the  $J/\psi$  channel. The line labeled “frozen” repeats the calculations of the high energy limit reported in Table IV with the substitution  $|\psi_i\rangle = |\psi_{J/\psi}\rangle$ .

$(N_i)$	$E_\gamma$ (GeV)	$\alpha_{\text{feed}}$	$\alpha_{\text{no feed}}$	$\alpha_{\text{incoh}}$
(1)	8.5	-0.231	-0.257	-0.299
(1)	12	-0.241	-0.270	-0.296
(1)	20	-0.232	-0.251	-0.295
(1)	“frozen”	-0.205	-0.224	-0.295

that it is enormous compared to the “baseline” computation, as offered by  $\alpha_{\text{incoh}}$ .

As the trend in  $\alpha_{\text{no feed}}$  with energy is not especially sensitive to the initial state, it is useful to examine the absorption coefficients of  $\chi$  and  $\psi'$  and their ratios to  $J/\psi$  for the cases studied previously. These  $\alpha$ 's are tabulated in Table XII; note that  $A^{\text{eff}}/A$  for  $\psi' : J/\psi$ , for example, is simply the  $A^{\text{eff}}/A$  for  $\psi'$  divided by that of  $J/\psi$ . Again, as previously, the error in a quantity is not explicitly reported if it does not appear in the first three significant figures. A positive  $\alpha$  indicates that that state is produced in final-state interactions. These absorption coefficients are rather more sensitive to the initial state. A measurement of  $\alpha_\chi$  and  $\alpha_{\psi'}$  (or of  $\alpha_{\psi':J/\psi}$  and  $\alpha_{\chi:\psi'}$ ) might be quite interesting: Table XII shows that one of these quantities changes sign whenever a different initial state is considered.

As most experiments report a  $J/\psi$ -nucleon total cross section in addition to the measured  $A$  dependence, it is of interest to examine the  $J/\psi$ - and  $\psi'$ -nucleon cross sections in the context of this model. The absorption cross section, is defined as earlier, so that  $\sigma_{J/\psi}^{\text{abs}} = (\pi R_{\text{str}}^2)[1 - P_{J/\psi}(1)/P_{J/\psi}(0)]$  and  $\sigma_{\psi'}^{\text{abs}} = (\pi R_{\text{str}}^2)[1 - P_{\psi'}(1)/P_{\psi'}(0)]$ . (Here  $\sigma^{\text{abs}}$  is also approximately  $\sigma^{\text{tot}}$  [57].) At any rate, these cross sections are tabulated in Table XIII, for the initial states and photon energies studied previously. The  $J/\psi$ -nucleon cross sections are quite large and vary only moderately with energy. The  $\psi'$  absorption cross sections are actually *smaller* than those for  $J/\psi$ . This may seem non-intuitive since  $\psi'$  is larger than  $J/\psi$ , but this is partially a consequence of the initial-state *Ansätze* employed. To demonstrate this, Tables XIV and XV examine these same cross sections for a variety of *Ansätze*. That is, in Table XIV, initial states with fixed  $J/\psi : \psi'$  ratios and varying sizes are employed to decouple the cross sections' dependence on these two quantities. Since the minimum  $J/\psi : \psi'$  ratio for the functional form used in Table XIV is 2:3, Table XV examines the cross sections for *Ansätze* composed only of  $J/\psi$  and  $\psi'$  with varying  $J/\psi : \psi'$  ratios. Upon examination of Table XIV, it is apparent that the  $J/\psi$  and  $\psi'$  absorption cross sections depend more strongly on the  $J/\psi : \psi'$  ratio than on the initial-state size. Comparing with Table XV, one concludes that decreasing this ratio increases the size of  $\sigma_{\psi'}^{\text{abs}}$  relative to  $\sigma_{J/\psi}^{\text{abs}}$ . It is amusing that the pure  $\psi'$  state has a smaller

TABLE XII. Absorption coefficients for  $\chi$  and  $\psi'$  states, their ratio, and their ratios to  $J/\psi$  as a function of  $N_i$  and  $E_\gamma$ , determined by fitting  $A^\alpha$  to the  $A^{\text{eff}}/A$  given in Table IX.

State	$\alpha_\chi$	$\alpha_{\psi'}$	$\alpha_{\psi':J/\psi}$	$\alpha_{\chi:J/\psi}$	$\alpha_{\chi:\psi'}$
(1) 8.5	$-(2.92 \pm 0.03) \times 10^{-2}$	$(3.18 \pm 0.02) \times 10^{-2}$	0.288	0.226	$-(6.25 \pm 0.04) \times 10^{-2}$
(1) 12	$-(2.42 \pm 0.01) \times 10^{-2}$	$(2.96 \pm 0.03) \times 10^{-2}$	0.299	0.236	$-(6.28 \pm 0.04) \times 10^{-2}$
(1) 20	$-(3.51 \pm 0.06) \times 10^{-2}$	$(5.81 \pm 0.21) \times 10^{-3}$	0.273	0.227	$-(4.37 \pm 0.07) \times 10^{-2}$
(2) 12	$-(2.87 \pm 0.02) \times 10^{-2}$	-0.150	0.106	0.229	0.123
(2) 20	$-(2.45 \pm 0.05) \times 10^{-2}$	-0.176	$(7.23 \pm 0.02) \times 10^{-2}$	0.226	0.155
(5) 20	$(2.53 \pm 0.07) \times 10^{-2}$	-0.221	$-(1.31 \pm 0.01) \times 10^{-2}$	0.235	0.249

absorption cross section than the pure  $J/\psi$  state; here, though, the spatial shape of  $\psi'$  – due to its radial node – allows it to have a larger overlap with the wave functions in the flux tube basis. Perhaps, then, the previously noted correlation between the wave function's transverse size and the  $J/\psi$  survival probability is not readily generalizable to the excited states in the  $c\bar{c}$  tower. Minimally, it would seem naive to assume that  $\psi'$  should interact more strongly with the nuclear medium than  $J/\psi$  simply because of its larger size. In the event of an initial mixed state, the implications for the relative survival of  $J/\psi$  and  $\psi'$  are complicated still further.

Thus far, only the behavior of the  $J/\psi$  and  $\psi'$  cross sections as defined by the model have been discussed. In practice, however, experimentalists *infer* a value for the total  $J/\psi$ -nucleon cross section from the measured  $A$  dependence. For example, Anderson *et al.* [67] measured the ratio of  $A^{\text{eff}}/A$ 's for  $J/\psi$  production from Be and Ta with a photon bremsstrahlung beam of 20 GeV endpoint energy. From this, they inferred a  $J/\psi$ -nucleon total cross section of  $3.5 \pm 0.8$  mb using the nuclear-optics model of Gottfried and Yennie [68] (see Appendix B), in which  $A^{\text{eff}}/A$  is given by

$$\frac{A^{\text{eff}}}{A} = \frac{2\pi}{A} \int_0^\infty b db \int_{-\infty}^\infty dz \rho(z, b) e^{-\sigma_{J/\psi N}^{\text{tot}} t_A(z, b)}, \quad (5.5)$$

where all the nucleons in the nucleus are assumed to be able to participate in the process.  $t_A(z, b)$  is the nuclear thickness function, as defined previously. Unfortunately, the form given in Eq. (5.5) is not justifiable merely on the basis of the Glauber theory, as the exponential form

TABLE XIII.  $J/\psi$  and  $\psi'$  absorption cross sections as a function of  $N_i$  and  $E_\gamma$ , computed from the  $J/\psi$  and  $\psi'$  survival probabilities after passage through a single nucleon. As the initial wave packet is assumed to propagate a distance  $\xi_A$  before its interaction with a nucleon, the cross sections for the  $N_i \geq 2$  cases depend on the  $\xi_A$  chosen. Here  $\xi_A$  for Be,  $\xi_A = 1.70$  fm, is used.

$(N_i)$	$E_\gamma$ (GeV)	$\sigma_{J/\psi}^{\text{abs}}$ (mb)	$\sigma_{\psi'}^{\text{abs}}$ (mb)
(1)	8.5	19.6	—
(1)	12	19.3	—
(1)	20	19.1	—
(2)	12 [Be]	19.0	7.1
(2)	20 [Be]	18.3	11.2
(5)	20 [Be]	16.8	16.7

is only appropriate if the number of nucleons the  $J/\psi$  encounters after creation at a point  $(z, \vec{b})$  is very large. Thus, in order to compare my previously calculated absorption cross sections with those inferred from the calculated  $A$  dependence, I shall adopt the form

$$\frac{A^{\text{eff}}}{A} = \frac{2\pi}{A} \int_0^\infty b db \int_{-\infty}^\infty dz \rho(z, b) (1-w)^{N_{\text{eff}}(z, b)} \quad (5.6)$$

for  $A^{\text{eff}}/A$ , which is consistent with the basic assumptions of the Glauber theory.  $w$  is the inelastic transition probability, so that the inferred absorption cross section  $\sigma_{G1}$  is  $\sigma_{G1} = (\pi R_{\text{str}}^2)w$  [69].  $N_{\text{eff}}(z, b)$  is defined by Eq. (2.7). Following the procedure of Anderson *et al.*, but using Eq. (5.6), the inferred cross sections  $\sigma_{G1}$  are extracted from  $[A^{\text{eff}}/A]_{\text{Be}}/[A^{\text{eff}}/A]_{\text{Pb}}$  for the cases tabulated in Table IX for direct  $J/\psi$  production. These results are tabulated in Table XVI, along with the cross sections computed directly from the model. As the Glauber theory assumes that all nucleon interactions are independent, the agreement between  $\sigma_{J/\psi}^{\text{abs}}$  and  $\sigma_{G1}$  for the row marked “no coherence” is necessary.  $\sigma_{G1}$  essentially tracks the behavior of  $\alpha_{\text{no feed}}$ , as in Table X, with energy; the exception is the  $N_i = 2, E_\gamma = 12$  GeV case. As  $\alpha_{\text{no feed}}$  is only very slightly larger than that of the  $N_i = 1, E_\gamma = 8.5$  GeV case, it is not surprising that the  $\sigma_{G1}$  extracted from two of the  $A^{\text{eff}}/A$ 's in the fit should yield a slightly smaller cross section. As  $\sigma_{G1}$  follows the behavior of  $\alpha_{\text{no feed}}$  quite closely, its calculation offers no further insight; moreover, if one's goal is the determination of the  $J/\psi$ -nucleon cross section, this approach – in the exclusive process studied here – does not seem to be useful, though it could offer a means of determining the cross section's lower bound.

It should be mentioned, in passing, that the model in Eq. (5.5) has been used as a starting point for semiclassical models of transparency (see, for example, Refs. [13,19]). In these models,  $\sigma_{J/\psi N}^{\text{tot}} t_A(z, b)$  is replaced by

$$\int_{\text{path}} dz \sigma^{\text{eff}}(\vec{p}, z) \rho_A(z), \quad (5.7)$$

where the effective  $c\bar{c}$ -nucleon cross section,  $\sigma^{\text{eff}}(\vec{p}, z)$ , introduced to mock-up the weaker interactions of the  $J/\psi$  in a “narrow” wave packet, depends on the  $c\bar{c}$ 's momentum and its distance after the production point. The point is that Eq. (5.5) is derived assuming that the  $J/\psi$ -nucleon interactions are *independent*, so that any quantum-mechanical coherence effects in the final-state

TABLE XIV.  $J/\psi$ - and  $\psi'$ -nucleon absorption cross sections as a function of  $E_\gamma$  for a variety of initial state *Ansätze*. Here the *Ansätze* considered are truncations with  $N_i$  terms of a  $1s$  harmonic oscillator wave function with scale factor  $\alpha_i$ , so that the cross sections' dependence on the  $J/\psi : \psi'$  ratio and the initial-state size can be decoupled. The scale factor for the initial state *Ansatz* used in the “frozen” limit is  $92.37 \text{ fm}^{-2}$ . The  $\xi^A$  used in these calculations is that of Be,  $\xi^A = 1.70 \text{ fm}$ .

$\alpha_i \text{ (fm}^{-2}\text{)}$	$(N_i)$	$J/\psi:\psi'$	$\langle r_i^2 \rangle^{1/2} \text{ (fm)}$	$\sigma_{J/\psi}^{\text{abs}}$ and $\sigma_{\psi'}^{\text{abs}}$ (mb)		$\sigma_{J/\psi}^{\text{abs}}$ and $\sigma_{\psi'}^{\text{abs}}$ (mb)	
				at		at	
				$E_\gamma = 12 \text{ GeV}$		$E_\gamma = 20 \text{ GeV}$	
92.37	(2)	0.849	0.494	19.9	17.6	16.7	16.0
92.37	(5)	0.849	0.423	19.8	15.6	15.0	19.1
92.37	(6)	0.849	0.401	19.8	14.5	14.8	19.7
12.	(2)	4.98	0.406	19.0	13.9	18.4	10.5
12.	(5)	4.98	0.354	19.4	12.9	18.4	11.1

interactions have been neglected. As the possibility of weakened final-state interactions arise from these effects, the usefulness of Eq. (5.7) as an effective single-channel description of transparency is unclear.

## VI. CONCLUSIONS

The final-state interactions of photoproduced charmonium with the nucleus have been calculated in a QCD-inspired model as a function of photon energy for the exclusive process in which quasielastically photoproduced  $J/\psi$  carries off the maximum momentum consistent with momentum conservation (large  $x_F$ , zero  $p_T$ ). Color transparency can be understood in this context as arising from the coherent interference between the final-state interactions of a spatially small superposition of photoproduced  $c\bar{c}$  states. In the language promulgated by Gribov and others, the phenomenon may be restated in terms of the inclusion of all the “Glauber corrections due to inelastic screening” [1,3], i.e., via transitions from  $\psi' \leftrightarrow J/\psi$ , etc.

This work represents a departure from conventional descriptions of hadronic final-state interactions in two different ways. First, the assumption of a spatially small initial state means that the initial amplitude is a complicated superposition of charmonium eigenstates, rather than an amplitude for  $J/\psi$  production alone. Second, the propagation of the small *superposition* of states through the nuclear medium implies that quantum mechanical co-

herence effects in the final-state interactions cannot be, and are not, neglected. The Glauber formalism commonly used to treat hadronic final-state interactions assumes that the projectile interacts independently with the nucleons of the nucleus, ignoring these coherence effects.

The calculation of  $A^{\text{eff}}/A$  with energy shows the overall change of  $A^{\text{eff}}/A$  to be less than 20% in the energy range  $E_\gamma = 8.5$  to 20 GeV, even though many of the model's aspects enhance the effect of transparency. Moreover, in the energy range considered,  $A^{\text{eff}}/A$  may *oscillate* with energy (see Table X). The overall change of  $A^{\text{eff}}/A$  is not large, yet the relative effect can be enormous. That is, a computation “without transparency” yields less than a 2% change in  $A^{\text{eff}}/A$  in the same energy range, where “without transparency” means that the initial superposition is the  $J/\psi$  eigenstate and that only the  $J/\psi$  state is retained in the propagation of the  $c\bar{c}$  wave packet between nucleons (see Table XI). This comparison is a unique feature of this work: the energy dependence of  $A^{\text{eff}}/A$  with and without transparency is computed in the same model. Although the change of  $A^{\text{eff}}/A$  in the energy range considered is not large, this work supports the use of the empirical behavior of  $A^{\text{eff}}/A$  with energy as a signature of transparency. Another interesting result of this paper is that an increase in  $A^{\text{eff}}/A$  with energy, albeit much weaker, can be seen even if the initial superposition is just the  $J/\psi$  eigenstate. Even if the initial state is an eigenstate, the final-state interactions themselves will produce a superposition of states, which will oscillate in

TABLE XV.  $J/\psi$ - and  $\psi'$ -nucleon absorption cross sections as a function of  $E_\gamma$  for initial-state *Ansätze* composed of  $J/\psi$  and  $\psi'$  only. The wave-function coefficients are assumed to be positive definite, so that the  $J/\psi : \psi'$  ratio specifies the state. For the entries marked “—”, the absorption cross section is not defined, as the probability for that state increases upon interaction with the nucleon. The  $\xi^A$  used in these calculations is that of Be,  $\xi^A = 1.70 \text{ fm}$ .

$J/\psi:\psi'$	$\langle r_i^2 \rangle^{1/2} \text{ (fm)}$	$\sigma_{J/\psi}^{\text{abs}}$ and $\sigma_{\psi'}^{\text{abs}}$ (mb)		$\sigma_{J/\psi}^{\text{abs}}$ and $\sigma_{\psi'}^{\text{abs}}$ (mb)	
		at		at	
		$E_\gamma = 12 \text{ GeV}$		$E_\gamma = 20 \text{ GeV}$	
0.	0.793	—	18.2	—	17.9
0.01	0.763	—	18.2	—	17.8
0.25	0.617	15.0	18.1	12.9	17.0
4.	0.406	19.0	14.8	18.3	11.7
100.	0.479	19.3	—	19.0	—

TABLE XVI.  $J/\psi$  absorption cross sections as a function of  $N_i$  and  $E_\gamma$ , compared with the  $J/\psi$ -nucleon cross sections in the Glauber approach, *inferred* from the ratio of  $A^{\text{eff}}/A$  for Be and for Pb from Table IX for direct  $J/\psi$  production. The line marked “frozen” uses the  $A^{\text{eff}}/A$  of the high energy limit, as reported in Table III. As described in Table XIII, the  $N_i \geq 2$  results depend on  $\xi^A$ , so that the absorption cross sections for both Be and Pb are reported. In the case marked “no coherence,” the excited charmonium states are not allowed to scatter back to the  $J/\psi$  channel.

$(N_i)$	$E_\gamma$ (GeV)	$[A^{\text{eff}}/A]_{\text{Be}}/[A^{\text{eff}}/A]_{\text{Pb}}$	$\sigma_{J/\psi}^{\text{abs}}$ (mb)	$\sigma_{\text{GI}}$ (mb)
(1)	8.5 [no coherence]	2.57	19.6	19.6
(1)	8.5	2.31	19.6	16.2
(1)	12	2.36	19.3	16.9
(1)	20	2.30	19.1	16.1
(2)	12 [Be,Pb]	2.29	19.0, 18.7	16.0
(2)	20 [Be,Pb]	2.23	18.3, 18.2	15.1
(5)	20 [Be,Pb]	1.95	16.8, 15.1	11.7
	“frozen”	1.32	6.0	4.2

time, with a period (in the wave packet’s rest frame) determined by the level spacing of the hadron spectrum (see Figs. 7–9). In the laboratory frame, this period dilates, so that “snapshots” taken in the laboratory frame at a distance  $d$  from the initial interaction point at successively increasing momenta show the wave packet at earlier and earlier moments in its rest-frame expansion. Thus, as a nucleus is of finite size, it “sees” more of the initial state as the momentum increases. This illustrates the essential role of the final-state interactions in yielding transparency. It should be emphasized, however, that the computed change in  $A^{\text{eff}}/A$  depends critically on the choice of the initial state.

In the event that color transparency is observed in this process, what does it mean? This model shows significant variations in  $A^{\text{eff}}/A$  with energy (see Table XI), yet perturbation theory does a dismal job of predicting its cross sections even at high energies, though, for the specific exclusive process considered here, the momentum transfers are never large. Thus, an observation of color transparency in this process does not simultaneously validate the application of  $p$ QCD, since this model study serves as a specific counterexample. However, one could perhaps imagine other processes in which the validity of  $p$ QCD and the existence of color transparency could be more closely tied. What is true, though, is that transparency, if observed, makes a subnucleonic picture of the nuclear medium and of the particles produced in it essential. That is, transparency’s existence relies on an interaction which depends on the relative separation of a projectile’s *quarks*. Thus, its existence could be regarded as a concrete example of the elusive “quark signatures” long sought in nuclear physics.

The possible existence of transparency in this process can also be regarded as a “weak” test of QCD, or, rather, of charge screening; both QCD and QED have this property. That is, the correlation observed between the wave packet’s transverse size  $X_T$  and the  $J/\psi$  survival probability for a *given* initial state is a consequence of charge screening. The comparison of the survival probabilities for  $J/\psi$  and  $\psi'$  when *Ansätze* of varying size and  $c\bar{c}$  state composition are used demonstrates the fallacies in applying color-screening intuition too freely (see Tables XIV and XV).

This model study, in which many of the approximations involved are consistent with “maximizing” transparency, yields a relatively small variation in  $A^{\text{eff}}/A$  for  $J/\psi$  with energy, though this variation is much larger than that of the baseline calculation, in which no coherence effects are included in the final-state interactions. Certainly, the absolute magnitudes of the absorption coefficients are very sensitive to the inclusion of coherence effects, though I would not regard the absolute magnitudes of the  $A^{\text{eff}}/A$  computed in this model as predictive. That is, through ignorance, the overall interaction scale has been specified by the choice of  $\tau$ , which was fit to the  $A$  dependence of the Sokoloff data [35]. This is basically a reasonable procedure: the cause for concern is generated by both the uncertainty in the experiment –  $x_F$  is not measured – and in the initial state. Thus, the variations in  $A^{\text{eff}}/A$  are regarded as being of greater significance. What is important is that this model study demonstrates the feasibility of an  $A$ -dependence study with  $E_\gamma$  in determining the existence of transparency, as the baseline calculation in the energy range studied is quite flat. Moreover, the model demonstrates how the  $A$  dependence of  $A^{\text{eff}}/A$  for  $J/\psi$  production may *oscillate* with energy, simply because of quantum mechanical effects. Such oscillations can never be obtained in a semiclassical picture [13,19]. Perhaps this contributes to the oscillation in  $A^{\text{eff}}/A$  noted in the  $(p,2p)$  data at Brookhaven [70]. In this model, such oscillations can occur only at relatively low energies; any oscillations in the wave packet’s transverse size damp out with energy, as seen here through explicit numerical calculation. Indeed, in the absence of a change in reaction mechanism, this model – and indeed all other transparency models – shows a “saturation” of  $A^{\text{eff}}/A$  at very high energies. In the event of a change in the reaction mechanism at high energies, as discussed at the end of Sec. III, this prediction will not hold; this may explain the energy dependence of some early data from NA37 [61].

The comprehensive study of the  $J/\psi$ ,  $\chi$ , and  $\psi'$  systematics with  $A$  and  $E_\gamma$  in this model demonstrate that the absorption coefficients associated with  $\chi$  and  $\psi'$  propagation through the nucleus are much more sensitive to the unknowns of the production process, i.e., the initial-state *Ansätze*, than that associated with  $J/\psi$ . This could

be extremely useful in unraveling the physics of the production process. Moreover, irrespective of the absorption coefficients, the overall magnitude of  $\chi$  production relative to that of  $J/\psi$  and  $\psi'$  is indicative of the initial-state composition and its interactions with energy, with  $\chi$  production becoming strongly suppressed at high energies.

In this model, the  $J/\psi$ -nucleon total cross section is well determined. Thus, one has the opportunity to compare the total cross section *inferred* from the computed  $A$  dependence, the usual empirical procedure, with the actual  $J/\psi$ -nucleon cross section defined by the model. This comparison shows that the Glauber analysis is quite misleading, yielding  $J/\psi$ -nucleon cross sections rather smaller than those of the actual model. However, at least for the cases studied, it does serve as a lower bound. The empirical extractions of the  $J/\psi$ -nucleon total cross section, both from the measured  $A$  dependence and from invoking vector-meson dominance, using the forward elastic cross section  $d\sigma(\gamma + N \rightarrow J/\psi + N)/dt|_{t=0}$ , are compared in Appendix B. As the VMD extraction is from a H target, it is not affected by the possible existence of coherence effects in the final-state interactions, and, thus, hopefully should serve as a more reliable estimate of the  $J/\psi$ -nucleon cross section. However, the cross sections derived from VMD are rather smaller than those deduced from the measured  $A$  dependence at a comparable energy scale, quite the opposite of the behavior shown in this model. This disparity could be explained either by uncertainty in the  $\gamma$ -vector-meson coupling constant needed for the VMD analysis, or by a novel dependence in the nuclear absorption with  $x_F$ , since the model comparison is performed for  $x_F \rightarrow 1$ , whereas  $x_F$  is not measured in the  $A$ -dependence experiments. Indications of changing physics with  $x_F$  have been noted in hadroproduction measurements of  $J/\psi$  off nuclear targets, though such effects have not been studied in photoproduction [71,66,72]. It could also imply that the initial state grows in size with energy (implying “color opacity”), but this seems nonintuitive, as the photon’s coupling to  $c\bar{c}$  in the forward diffractive process should be pointlike, as consistent with the  $\gamma\gamma$  and  $\gamma\gamma\gamma$  decays of  $c\bar{c}$ .

In order to effect the described calculations, many simplifications have been made. It is useful to reiterate some of these simplifying assumptions and, thus, point the way for further work. First, this entire work has assumed that the physics of the production step can be factorized from that of the final-state interactions. Although some separation of time scale may exist, it is clear that in order to construct a complete description of the process, including the production step, this factorization assumption must be broken, as final-state interactions must act to knock the initial hadronic fluctuation on-shell. This is an essential piece of physics: the states of the  $c\bar{c}$  tower must be produced in such a way that the remaining nuclear fragments are identical, so that the coherence effects may exist. Although this is ultimately important to understanding transparency, it is thought unimportant for the phenomenological study undertaken here. However, what may be important phenomenologically is the inclusion of open channels, such as  $\bar{D}\Lambda_c$  or  $\pi$  production. It is highly impractical to include all these channels explicitly,

so that some appropriate optical model to describe the loss of states to the open channels must be constructed. There are also some computational simplifications: the  $c\bar{c}$ -flux-tube interaction is assumed to illuminate the  $c\bar{c}$  wave function uniformly, the flux tubes are treated as if they are purely transverse, and they are assumed to be equally spaced, in order to simplify the Monte Carlo integrations. If all the underlying model parameters were well known, then the Herculean computational effort involved in relaxing these last restrictions would perhaps be justified; however, that is not currently the case. Moreover, as the variation in  $A^{\text{eff}}/A$  for  $J/\psi$  production is relatively small with energy, the results would not seem to demand such improvements. It seems more instructive to try to use the results of the current calculations to construct some reasonable, few-channel, effective description of transparency, so that the calculations can be extended to higher energies. The change of the reaction mechanism with energy, that is, the onset of shadowing, can then be modeled explicitly.

In conclusion, an explicit microscopic model has been constructed and solved in a numerically exact manner in order to explore the role of coherence effects in the final-state interactions of charmonium with the nuclear medium and their impact on the phenomenology of the  $A$  dependence of quasielastic  $J/\psi$ ,  $\chi$ , and  $\psi'$  photoproduction with energy. It is to be emphasized that these effects have been computed only in the  $p_T = 0$ ,  $x_F \rightarrow 1$  limit. The overall variation of  $A^{\text{eff}}/A$  for  $J/\psi$  production for the energy range  $E_\gamma = 8.5$  to 20 GeV is small, though it is much larger than its variation when no coherence effects are included. However, as the overall effect is small, it is possible that larger energies will be required to observe transparency. Regardless, this model study supports the feasibility of elucidating the existence of color transparency from the energy variation of the nuclear dependence of  $J/\psi$  production in this exclusive limit.

#### ACKNOWLEDGMENTS

I am grateful to J. W. Negele for useful advice on certain of the problem’s numerical aspects, and to P. Geiger and J. D. Walecka for helpful comments and support. I also thank J. D. Walecka for readings of the manuscript, and for suggestions helpful in improving its clarity. I thank F. Gross and J. W. Van Orden for providing access to the Cray YMP at Florida State University, which made the calculations presented here possible. It is a pleasure to acknowledge the hospitality of H. A. Weidenmüller at the Max-Planck-Institut für Kernphysik in Heidelberg, where this work was initiated; I was supported by the BMFT under Contract No. 06-HD-710 during that period. I gratefully acknowledge support from the DOE under Contract No. DE-AC05-84ER40150 and from the AAUW Educational Foundation.

#### APPENDIX A: ON IDENTIFYING THE EXCLUSIVE PROCESS

To isolate the exclusive process discussed here, it is necessary to measure both  $x_F$  and  $p_T$  of the produced  $c\bar{c}$

particles; thus, it is also necessary to perform any measurements with a photon tagger. However, for extremely high energies, it might be more practical to consider a measurement of quasielastic electro- or muoproduction of  $c\bar{c}$  in place of photoproduction. The purpose now is merely to emphasize that the quasielastic process with small  $p_T$  and large  $x_F$  discussed here can be isolated experimentally and, thus, is not an idle theoretical construct. The difficulty is that as the energy increases, the coherent peak begins to dominate the small  $p_T$  region overwhelmingly. Thus, cuts in  $p_T$  must be performed to remove any coherent contamination, yet one must guarantee that the production is still predominately elastic. In a study of  $J/\psi$  photoproduction from H at a mean energy of  $\langle E_\gamma \rangle \sim 105$  GeV, Denby *et al.* have determined the  $p_T$  dependence of elastic and inelastic  $J/\psi$  production [73]. Placing the lowest  $p_T$  bin of the Sokoloff experiment,  $0.15 \text{ (GeV}/c)^2 < p_T^2 < 0.55 \text{ (GeV}/c)^2$ , on the Denby data yields a ratio of 2 : 1 for the elastic relative to inelastic events [35,73]. Thus, it should prove possible to isolate the exclusive process studied here.

#### APPENDIX B: INFERRED $J/\psi$ -NUCLEON TOTAL CROSS SECTIONS

In Sec. V the Glauber method of determining the total  $J/\psi$ -nucleon cross section from the measured  $A$  dependence was evaluated in the context of this model. The objective here is to examine different experimental determinations of the total  $J/\psi$ -nucleon cross section, in order to see what consistency may exist between the varying approaches. In fact, there exist just two: using Glauber theory to infer the cross section from the measured  $A$  dependence or invoking vector-meson dominance and the optical theorem (assuming the real part of the scattering amplitude to be zero) to infer the cross section from the forward-elastic cross section,  $d\sigma(\gamma + N \rightarrow J/\psi + N)/dt|_{t=0}$  [51].

It is not difficult to review the world's data: there exist merely two experiments which measure the  $A$  dependence of  $J/\psi$  photoproduced in nuclei. The first, the previously discussed measurement of Anderson *et al.* at SLAC, uses Eq. (5.5) and their measurement  $\sigma(\text{Be})/\sigma(\text{Ta}) = 1.21 \pm 0.07$  to infer a total  $J/\psi$ -nucleon cross section of  $\sigma_{J/\psi-N} = 3.5 \pm 0.8$  mb [67]. Unfortunately, they use an uniform density approximation in place of integration over the experimental charge densities. Correcting this error, and it is such, as Be is primarily surface, yields  $\sigma_{J/\psi-N} = 4.5 \pm 1.5$  mb. Yet, as discussed prior to Eq. (5.5), the exponential form itself is not well motivated for finite nuclei. Replacing Eq. (5.5) with the model given by Eq. (5.6) shifts the central value to 3.7 mb, which is close to the result originally reported! The other experiment is that of Sokoloff *et al.* at Fermilab [35]; they report a  $\sigma_{J/\psi-N}$  of 1 – 2 mb, even though their  $p_T$ -averaged  $A$  dependence is the same as that of Anderson *et al.* Thus, they should have reported a cross section comparable to that of the Anderson data; for the smallest  $p_T$  bin, for which the absorption coefficient is slightly larger, Eq. (5.6) yields  $\sigma_{J/\psi-N} \sim 4.2$  mb. It is interesting that two experiments at such different energy

scales ( $\langle E_\gamma \rangle \approx 120$  GeV versus an end-point energy of 20 GeV) should have nearly identical  $A$  dependences. However, the comparison is clouded, as the SLAC measurement is performed for a  $p_T$  of 1.65 GeV/ $c$ , whereas the Fermilab experiment integrates over the  $p_T$  spectrum. Moreover,  $x_F$  is not measured.

Many more experiments exist which invoke VMD and the optical theorem to extract the total  $J/\psi$ -nucleon cross section from  $\frac{d\sigma(\gamma+N \rightarrow J/\psi+N)}{dt}|_{t=0}$ . Typically the sizes of these cross sections are 1–2 mb; in particular, the experiment of Binkley *et al.* at  $\langle E_\gamma \rangle \sim 150$  GeV reports a total cross section of  $\sigma_{J/\psi-N} = 1.5 \pm 0.2$  mb [65]. The cross sections from the VMD and  $A$ -dependence methods are *distinct*; what is striking, moreover, is that the VMD cross sections are *smaller* than those inferred from the  $A$  dependence. The above model study shows how the cross section inferred from the  $A$  dependence can be markedly smaller than the true  $J/\psi$ -nucleon cross section in the exclusive limit studied. This points up the oddness of the empirical situation: the VMD approach does purport to measure the total cross section associated with the elastic process discussed here, and the cross section inferred from the  $A$  dependence with small  $p_T$  should also arise mainly from elastic production of  $J/\psi$ . Yet, the relative sizes of the two cross sections are different from those of the model study. The possible causes of this disparity are various, though they are all interesting. First, the VMD approach could simply be wrong, or that the vector-meson coupling constant is inferred in an inappropriate way. Second, as the  $A$ -dependence measurements do not measure  $x_F$ , there could be a novel dependence on this quantity. Third, perhaps the appropriate initial-state *Ansatz* at a photon energy of a 100 GeV or so is much *larger* in size than that of a pure  $J/\psi$  state, though this seems nonintuitive. Conservatively, it seems entirely fair to echo the comment of Brodsky and Mueller and say that the  $J/\psi$ -nucleon cross section has not yet been determined [12].

#### APPENDIX C: DETERMINATION OF THE FLUX TUBE WIDTH $\tau$

In this section the computation of  $A^{\text{eff}}/A$  and the resulting fit of the model to high-energy photoproduction data to extract the flux-tube width  $\tau$  is described. In order to compute  $A^{\text{eff}}/A$ , the specific reaction geometry must be discussed, and the initial-state input in Eq. (3.9) must be fixed as well. As mentioned in Sec. II, there are two possible reaction mechanisms at high energies – a shadowed and a direct process (see Fig. 3). The energies at which shadowing becomes important are estimated in Sec. II (see Table II); for the purposes of this work, this alternative reaction mechanism is essentially ignored, so that the nuclear-averaged probability  $A^{\text{eff}}/A$ , for  $J/\psi$  production, is given by Eq. (2.6). The probability  $\hat{P}_{J/\psi}(N_{\text{eff}})$  in both Eqs. (2.6) and (2.8) can now be determined. As discussed previously,  $|\psi_i\rangle$  is chosen as a Gaussian wave packet where the  $q\bar{q}$  rms separation is that of the Compton wavelength of the heavy quark, that is,  $\psi_i(r) = (\alpha_i/\pi)^{3/4} \exp(-\alpha_i r^2/2)$ , with  $\alpha_i \equiv 3/2\langle r_i^2 \rangle$  and  $\langle r_i^2 \rangle^{1/2} = \hbar c/m_{J/\psi}$ . Given this  $|\psi_i\rangle$  and Eq. (3.9), the probability as a function of  $N$  that  $J/\psi$  is produced is

$$P_{1s \leftarrow 1s}(N) = \frac{8}{\pi} \left( \frac{\beta^2}{\alpha_i + \alpha_f} \right) \left( \frac{\alpha_i \alpha_f}{\beta^4} \right)^{\frac{3}{2}} \int_0^\infty s ds \int_0^\infty s' ds' e^{-\frac{\alpha_i + \alpha_f}{2\beta^2} (s^2 + s'^2)} \\ \times \int_0^\pi dx J_0^N \left( (\Theta_s s^2 + \Theta_{s'} s'^2 - 2\Theta_s \Theta_{s'} s s' \cos x)^{\frac{1}{2}} \right). \quad (\text{C1})$$

Here  $\beta \equiv k_{\text{Regge}} \tau / \hbar c$ ,  $\alpha_f \equiv 3/2 \langle \tau_{J/\psi}^2 \rangle = \omega \mu_c / \hbar c^2$ ,  $\Theta_s \equiv \Theta(X_{\text{str}} - \sqrt{\alpha_f} s / \beta)$ , and  $\Theta_{s'} \equiv \Theta(X_{\text{str}} - \sqrt{\alpha_f} s' / \beta)$ , where  $X_{\text{str}} = \sqrt{\alpha_f} R$ . For  $\psi'$ ,

$$P_{2s \leftarrow 1s}(N) = \frac{16}{3\pi} \left( \frac{\beta^2}{\alpha_i + \alpha_f} \right) \left( \frac{\alpha_i \alpha_f}{\beta^4} \right)^{\frac{3}{2}} \int_0^\infty s ds \int_0^\infty s' ds' e^{-\frac{\alpha_i + \alpha_f}{2\beta^2} (s^2 + s'^2)} \\ \times \left[ \frac{3}{2} - \frac{\alpha_f}{\alpha_i + \alpha_f} - \frac{\alpha_f}{\beta^2} s^2 \right] \left[ \frac{3}{2} - \frac{\alpha_f}{\alpha_i + \alpha_f} - \frac{\alpha_f}{\beta^2} s'^2 \right] \int_0^\pi dx J_0^N \left( (\Theta_s s^2 + \Theta_{s'} s'^2 - 2\Theta_s \Theta_{s'} s s' \cos x)^{\frac{1}{2}} \right). \quad (\text{C2})$$

For  $\chi$ , summing over all final  $m$ -states using  $\sum_m Y_{1m}^*(\theta, \varphi) Y_{1m}(\theta', \varphi') = \frac{3}{4\pi r r'} \{z z' + s s' \cos(\varphi - \varphi')\}$  yields

$$P_{2p \leftarrow 1s}(N) = \frac{16}{\pi} \left( \frac{\alpha_f}{\alpha_i + \alpha_f} \right) \left( \frac{\alpha_i \alpha_f}{\beta^4} \right)^{\frac{3}{2}} \int_0^\infty s ds \int_0^\infty s' ds' e^{-\frac{\alpha_i + \alpha_f}{2\beta^2} (s^2 + s'^2)} \\ \times \int_0^\pi dx \cos x J_0^N \left( (\Theta_s s^2 + \Theta_{s'} s'^2 - 2\Theta_s \Theta_{s'} s s' \cos x)^{\frac{1}{2}} \right). \quad (\text{C3})$$

The probability in Eq. (C1) is not, however, the probability of *observing*  $J/\psi$ . In principle, electromagnetic decays from higher charmonium states must also be included. In hadroproduction experiments, these corrections can be quite large; for example, Lemoigne *et al.* have observed in 185 GeV/c  $\pi^-$ -Be interactions that 30.5% of the observed  $J/\psi$  production comes from the  $\chi_1$  and  $\chi_2$  states [74]. As  $\chi$  states are not to be directly photoproduced, the role of  $\chi$  states should be less important here. Nevertheless, the feeding of the  $J/\psi$  channel by higher  $c\bar{c}$  states could be significant, and, thus, the  $J/\psi$  probability input to Eq. (2.6) and Eq. (2.8) takes these effects into account. That is,

$$\tilde{P}_{J/\psi}(N) = P_{J/\psi \leftarrow 1s}(N) + P_{\chi \leftarrow 1s}(N) \times \Gamma_{\chi \rightarrow J/\psi + \gamma} \\ + P_{\psi' \leftarrow 1s}(N) \times \Gamma_{\psi' \rightarrow J/\psi + \text{anything}}. \quad (\text{C4})$$

Typically, the decays will cause the  $J/\psi$ 's which arise from higher charmonium states to have finite  $p_T$  or to have slightly less momentum; however, for large momenta of the parent particles, the daughter  $J/\psi$ 's with small  $p_T$  will be indistinguishable from those produced directly. The effect of the decays, then, depends on the resolution of the experiment. The kinematic factors are ignored here in order to see simply the maximum size of the effect. The branching ratios used are taken from the 1991 Particle Data Book;  $\Gamma_{\psi' \rightarrow J/\psi + \text{anything}} = 0.57$ , whereas  $\Gamma_{\chi \rightarrow J/\psi + \gamma} = 0.1667$  was obtained by making a  $(2J+1)$ -weighted average over the reported branching ratios for the  $\chi_0$ ,  $\chi_1$ , and  $\chi_2$  states. Feeding of the  $J/\psi$  channel from  $\psi'$  via an intermediate  $\chi$  state is ignored as the product of branching ratios is  $\sim 0.01$ . One might worry that the produced  $\chi$  and  $\psi'$  might decay before exiting the nucleus: however, even in the case of  $\chi_0$  with its full

width of  $W = 14 \pm 5$  MeV, this is highly unlikely as  $\hbar c \beta_{c\bar{c}} \gamma / W \gg R_{pb} \sim 7$  fm even for  $E_{J/\psi} \sim 8$  GeV, so that the form given in Eq. (C4) is justified. Feeding from still higher charmonium states to either  $J/\psi$ ,  $\chi$ , or  $\psi'$  is conceptually possible, but unmeasured; thus, only the  $J/\psi$  probability is presumed modified by feeding effects.

Given the form for  $\tilde{P}_{J/\psi}$  in Eq. (C4), and Eqs. (2.6), (2.7), and (C1)–(C3), one can now determine  $\tau$ , the flux-tube width in the laboratory frame. The direct process, Eq. (2.6), is assumed to dominate at these energies, though this is unclear (see Table II). This assumption will be examined more carefully later.  $\tau$ , which is assumed energy independent, is determined by fitting  $A^{\text{eff}}/A$  from Eq. (2.6) to the highest-energy photoproduction data available. This is provided by an experiment at Fermilab by Sokoloff *et al.* which measured the relative yield of  $J/\psi$  from real photons in the energy range of 80–190 GeV ( $\langle E_\gamma \rangle \approx 120$  GeV) incident on H, Be, Fe, and Pb targets [35]. Their resolution in  $p_T$  allows them to extract the  $A$  dependence of both coherent and incoherent production. (In “coherent” photoproduction, the nucleus recoils in its ground state as a result of the production of the  $c\bar{c}$ .) Fitting their yields *per nucleus* to the power law form  $\sigma_{\text{incoh}} = \sigma_{\text{incoh}}^0 A^{\tilde{\alpha}_{\text{incoh}}}$ , they report

$$\tilde{\alpha}_{\text{incoh}} = 0.94 \pm 0.02 \pm 0.02 \quad p_T^2 > 0.15 (\text{GeV}/c)^2, \quad (\text{C5})$$

where the cut on  $p_T$  has been made to avoid severe contamination by the coherent peak. Note that  $A^{\text{eff}}/A \equiv A^{\tilde{\alpha}_{\text{incoh}} - 1} \equiv A^\alpha$  is adopted throughout this paper. The  $A$  dependence of incoherent production is also determined for various bins in  $p_T$ :

$$\tilde{\alpha}_{\text{incoh}} = \begin{cases} 0.91 \pm 0.03, & 0.15 \text{ (GeV}/c)^2 < p_T^2 < 0.55 \text{ (GeV}/c)^2, \\ 0.92 \pm 0.04, & 0.55 \text{ (GeV}/c)^2 < p_T^2 < 1 \text{ (GeV}/c)^2, \\ 0.99 \pm 0.04, & p_T^2 > 1 \text{ (GeV}/c)^2. \end{cases} \quad (\text{C6})$$

Denby *et al.* have previously determined that low- $p_T^2$   $J/\psi$  production is elastic ( $\gamma + N \rightarrow \psi + N$ ), whereas for  $p_T^2 > 1 \text{ (GeV}/c)^2$  it is mainly inelastic ( $\gamma + N \rightarrow \psi + N + X$ ) [73]. Thus, variations in  $\tilde{\alpha}_{\text{incoh}}$  with  $p_T^2$  may indicate that elastic and inelastic  $J/\psi$  production have differing  $A$  dependences, which could be relevant to understanding transparency. Unfortunately, it is also true that the effective photon energy also varies with the  $p_T$  bin. Here the photon energy is ill-determined, so that the  $p_T^2 > 1 \text{ (GeV}/c)^2$  bin originates from a larger share of high-energy photons, perhaps explaining the apparently different  $A$  dependence in this bin. At any rate, the measurement which is closest to the one desired is that of the smallest  $p_T$  bin,  $0.15 \text{ (GeV}/c)^2 < p_T^2 < 0.55 \text{ (GeV}/c)^2$ . A similar bin in  $p_T$  placed on the Denby *et al.* photo-production data from H with a mean energy of  $E_\gamma \sim 105 \text{ GeV}$  yields a ratio of 2 : 1 for the elastic relative to inelastic events [73]. Even if the production is primarily elastic, one can not guarantee that the subsequent interactions are also elastic. For that, a measurement of  $x_F$  and  $p_T^2$  is required (see Appendix A), though no such data is available. Fitting  $A^{\text{eff}}/A$  computed from Eqs. (2.6) and

(C4) to the measured  $A$  dependence in this bin yields – as reported in Sec. II –

$$\tau = 1.3 \pm 0.3 \text{ fm}, \quad (\text{C7})$$

where the error bars result from repeating the fitting procedure for the upper and lower bounds of the experimental  $\tilde{\alpha}_{\text{incoh}}$ . The fitting procedure uses realistic nuclear charge densities as tabulated in Landolt-Börnstein [44], and  $D_{\text{spac}}$  for the various nuclei is given in Table I. Clearly, the stronger absorption requires the larger  $\tau$ .

#### APPENDIX D: COMPUTATION OF THE FLUX TUBE EIGENFUNCTIONS

Here the numerical computation of the eigenenergies and eigenfunctions of the  $c\bar{c}$  in the nucleon flux tube is described. As the flux tubes are purely transverse, the flux-tube basis is nontrivial only in two dimensions. Labelling the transverse dimensions by  $x$  and  $y$  yields the following equation of motion:

$$\left[ -\partial_x^2 - \partial_y^2 + x^2 + y^2 - 2(\zeta_x x + \zeta_y y) \Theta(X_{\text{str}} - (x^2 + y^2)^{1/2}) \right] \Psi_\eta(x, y) = \tilde{E}_\eta \Psi_\eta(x, y), \quad (\text{D1})$$

where dimensionless units such that  $x = x_{\text{dim}}/b$  have been introduced.  $b$  is the usual harmonic oscillator constant,  $\sqrt{\hbar/\omega\mu_c}$ , so that  $\zeta_x = [\gamma b^3 k_{\text{Regge}} \mu_c / (\hbar c)^2] \cos \theta$ , whereas  $\zeta_y = \zeta_x \tan \theta$  and  $X_{\text{str}} = R/b$ . Labeling the eigenenergies and eigenfunctions by  $\eta$  is a compact way of denoting the occupation of the  $x$  and  $y$  oscillators; Table V shows the translation from the  $\eta$  [ $\zeta$ ] to the  $(n_x, n_y)$  representation. To solve Eq. (D1), let

$$\Psi_\eta(x, y) = \sum_{\tilde{\eta}} C_{\eta\tilde{\eta}} \Phi_j(x) \Phi_m(y), \quad (\text{D2})$$

where  $\tilde{\eta} = (j, m)$  and  $\eta = (i, n)$ . The  $\Phi$ 's are one-dimensional harmonic-oscillator wave functions, i.e.,  $[-d^2/dx^2 + x^2]\Phi_i(x) = \varepsilon_i \Phi_i(x)$ . Thus, the elements of the matrix  $C_{\eta\tilde{\eta}}$  are the overlap functions between the free and flux-tube eigenfunctions needed to calculate the evolution matrix through a flux tube, Eq. (4.5). One proceeds by inserting Eq. (D2) in Eq. (D1) and multiplying by  $\int_{-\infty}^{\infty} dx \Phi_i(x) \int_{-\infty}^{\infty} dy \Phi_n(y)$  to yield

$$\sum_{\tilde{\eta}} C_{\eta\tilde{\eta}} \left[ (\varepsilon_j + \varepsilon_m) \delta_{\eta\tilde{\eta}} - 2\zeta_x I_{\eta\tilde{\eta}}^{(x)} - 2\zeta_y I_{\eta\tilde{\eta}}^{(y)} \right] = \tilde{E}_\eta C_{\eta\tilde{\eta}}, \quad (\text{D3})$$

with

$$I_{\eta\tilde{\eta}}^{(x)} \equiv \iint_{(x^2+y^2)^{1/2} \leq X_{\text{str}}} dx dy \Phi_i(x) x \Phi_j(x) \Phi_n(y) \Phi_m(y) \quad (\text{D4a})$$

and

$$I_{\eta\tilde{\eta}}^{(y)} \equiv \iint_{(x^2+y^2)^{1/2} \leq X_{\text{str}}} dx dy \Phi_i(x) \Phi_j(x) \Phi_n(y) y \Phi_m(y). \quad (\text{D4b})$$

Equation (D3) can be readily solved for  $C_{\eta\tilde{\eta}}$ . Thus, a two-dimensional matrix problem has been reduced to a one-dimensional one with matrices of size  $(n_x^{\text{max}} + 1)(n_x^{\text{max}} + 2)/2$ , where  $n_x^{\text{max}}$  denotes the highest excitation state of the one-dimensional oscillators. This method readily generalizes to  $n$  dimensions, at the price of solving an ever larger one-dimensional problem. The largest value of  $n_x^{\text{max}}$  needed is 35, so that the matrix inversion problem is still practicable. It can now be seen why the flux tube's field configuration was chosen to have a circular profile. For this geometry,  $I_{\eta\tilde{\eta}}^{(x)}$  and  $I_{\eta\tilde{\eta}}^{(y)}$  are independent of the flux tube's orientation  $\theta$  and need be calculated only once; however, Eq. (D3) has to be recom-

puted at every point in the Monte Carlo average over the flux tubes' orientations. The computational saving of having theta-independent  $I_{\eta\bar{\eta}}$ 's is needed for tractability.

The computation of the  $C_{\eta\bar{\eta}}$ 's can be tested in the limit when  $X_{\text{str}}$  grows large. In this limit, the two-dimensional eigenvalue problem decouples, and each one-dimensional wave function is a harmonic-oscillator wave function with a shifted coordinate. The computed  $\tilde{E}_\eta$  and  $C_{\eta\bar{\eta}}$ 's can be compared to

$$\tilde{E}_\eta = i + n + 1 - (\zeta_x^2 + \zeta_y^2)/2 \quad (\text{D5})$$

and

$$\begin{aligned} C_{\eta\bar{\eta}} &\equiv \iint dx dy \Phi_j(x) \Phi_m(y) \tilde{\Psi}_\eta(x, y) \\ &\equiv \langle y_j | \tilde{y}_i \rangle_x \langle y_m | \tilde{y}_n \rangle_y \end{aligned} \quad (\text{D6})$$

where

$$\langle y_j | \tilde{y}_i \rangle_x = \exp\left(-\frac{1}{4}\zeta_x^2\right) \left(\frac{1}{2^{j+i} j! i!}\right)^{\frac{1}{2}} \begin{cases} 2^j j! (-\zeta_x)^{i-j} L_j^{i-j}(\zeta_x^2/2), & j \leq i \\ 2^i i! (-\zeta_x)^{j-i} L_i^{j-i}(\zeta_x^2/2), & j \geq i. \end{cases} \quad (\text{D7})$$

The  $L_i^{j-i}$  are generalized Laguerre polynomials, and replacing  $\zeta_x$  by  $\zeta_y$  yields  $\langle y_j | \tilde{y}_i \rangle_y$ . The  $\tilde{E}_\eta$  and  $C_{\eta\bar{\eta}}$  given in Eqs. (D5) and (D6) are reproduced quantitatively by the solutions to Eq. (D3) for large  $X_{\text{str}}$ .

The flux-tube eigenfunctions generated by Eq. (D1) exclude the existence of open channels, though they certainly exist in reality, either via  $q\bar{q}$  pair production to produce  $D\bar{D}$  or via rearrangement of the quarks in the flux tube to produce  $\bar{D}\Lambda_c$  or  $\bar{D}\Sigma_c$ . To explain this notation, it should be noted that isospin breaking effects are ignored, so that  $\Sigma_c^0$ ,  $\Sigma_c^+$ , and  $\Sigma_c^{++}$  are degenerate, as are  $\bar{D}^0$  and  $D^-$ . Pair production effects are rather more difficult to include as the free  $c\bar{c}$  spectrum must be modified as well. Thus, merely the modification of the  $c\bar{c}$  eigenfunctions in the flux tube to include "string flips" is discussed here, so that Eq. (D1) becomes

$$\begin{aligned} -\frac{\hbar^2}{2\mu_c} \nabla_{\vec{r}}^2 \Psi + \left(\frac{1}{2}\mu_c \omega^2 r^2 - e\vec{E}_{\text{str}} \cdot \vec{r}\right) \Psi + f_{\Lambda_c}(r)\phi_1 + f_{\Sigma_c}(r)\phi_2 &= E\Psi \\ -\frac{\hbar^2}{2\mu_{\bar{D}\Lambda_c}} \frac{1}{r} \partial_r^2 (r\phi_1) + \frac{l_{\Lambda_c}(l_{\Lambda_c} + 1)\hbar^2}{2\mu_{\bar{D}\Lambda_c} r^2} \phi_1 + f_{\Lambda_c} \Psi &= (E - E_{\Lambda_c})\phi_1 \\ -\frac{\hbar^2}{2\mu_{\bar{D}\Sigma_c}} \frac{1}{r} \partial_r^2 (r\phi_2) + \frac{l_{\Sigma_c}(l_{\Sigma_c} + 1)\hbar^2}{2\mu_{\bar{D}\Sigma_c} r^2} \phi_2 + f_{\Sigma_c} \Psi &= (E - E_{\Sigma_c})\phi_2, \end{aligned} \quad (\text{D8})$$

where  $E$  is defined relative to  $2m_c + C$ ,  $E_{\Lambda_c} = m_{\bar{D}} + m_{\Lambda_c} - m_N - 2m_c - C$ , and  $E_{\Sigma_c} = m_{\bar{D}} + m_{\Sigma_c} - m_N - 2m_c - C$ .  $\phi_1$  and  $\phi_2$  are the relative wave functions of the  $\bar{D}\Lambda_c$  and  $\bar{D}\Sigma_c$  systems, respectively. The mass difference  $m_{\Lambda_c} + m_{\bar{D}} - m_N - m_{J/\psi}$  is  $\sim 150$  MeV, so that the channel mixing cannot be regarded as weak. The channel couplings  $f_\Lambda$  and  $f_\Sigma$ , which are real, depend on the relative orientation of the  $c\bar{c}$  and nucleon flux tubes and increase monotonically with  $r$ , though their functional form is not well-constrained. As the produced  $\bar{D}\Lambda_c$  and  $\bar{D}\Sigma_c$  result from a "short-circuit" of the nucleon flux tube, it is reasonable to treat them as free particles. Thus, the following one-channel reduction can be effected:

$$\begin{aligned} -\frac{\hbar^2}{2\mu_c} \nabla_{\vec{r}}^2 \Psi + \left(\frac{1}{2}\mu_c \omega^2 r^2 - e\vec{E}_{\text{str}} \cdot \vec{r}\right) \Psi + f_\Lambda G_{l_\Lambda, k_\Lambda}^0 f_\Lambda \Psi \\ + f_\Sigma G_{l_\Sigma, k_\Sigma}^0 f_\Sigma \Psi = E\Psi, \end{aligned} \quad (\text{D9})$$

where  $G_{l_\Lambda, k_\Lambda}^0$  and  $G_{l_\Sigma, k_\Sigma}^0$  are the free Green function's associated with  $\bar{D}\Lambda$  and  $\bar{D}\Sigma$  production, respectively. That is,

$$G_{l_\Lambda, k_\Lambda}^0(r, r') = -\frac{1}{k_\Lambda} \hat{j}_{l_\Lambda}(k_\Lambda r_<) \hat{h}_{l_\Lambda}^+(k_\Lambda r_>) \quad (\text{D10})$$

with  $k_\Lambda = \sqrt{2\mu_{\bar{D}\Lambda}(E - E_\Lambda)/\hbar^2}$ .  $\hat{j}_l$  is the spherical Riccati-Bessel function of order  $l$ , whereas  $\hat{h}_l^+$  is the spherical Riccati-Hankel function. Unfortunately, Eq. (D9) is not only nonlocal, it also fails to be separable in either spherical or Cartesian coordinates. Thus, the decoupling of the  $z$  coordinate, so convenient earlier, no longer exists. Solving Eq. (D9) is quite nontrivial; perhaps a phenomenological approach to the inclusion of open channels would prove more practical, e.g., via an optical model potential with an imaginary part.

#### APPENDIX E: CONSTRUCTION OF THE INITIAL STATE

As discussed in Sec. V, the initial state used as input for the evolution calculation is constructed by minimizing the size of the wave packet for a fixed number of basis states. That is, presuming this initial state to be composed only of  $|\Psi_{n00}\rangle$  states, one wishes to determine the coefficients  $C_n^{(N_{\text{mix}})}$  such that

$$\langle \Psi_i | r^2 | \Psi_i \rangle = \sum_{n, m=1}^{N_{\text{mix}}} C_m^{*(N_{\text{mix}})} C_n^{(N_{\text{mix}})} \langle \Psi_{m-100} | r^2 | \Psi_{n-100} \rangle \quad (\text{E1})$$

is minimized, subject to the constraint that  $\sum_{n=1}^{N_{\text{mix}}} |C_n^{N_{\text{mix}}}|^2 = 1$ . This can be immediately realized as  $\mathbf{MC} = \lambda C$ , where  $M_{mn} = \langle \Psi_{m-100} | r^2 | \Psi_{n-100} \rangle$ ; the eigenvector associated with the smallest eigenvalue  $\lambda_{\text{min}}$  consists of the desired  $C_n$ 's. Now

$$\Psi_{n00}(r) = \sqrt{2}\alpha_f^{3/4} \sqrt{\frac{n!}{\Gamma(n+3/2)}} L_n^{(\frac{1}{2})}(\alpha_f r^2) \times \exp(-\alpha_f r^2/2) \quad (\text{E2})$$

so that

$$\langle \Psi_{m-100} | r^2 | \Psi_{n-100} \rangle = \frac{1}{\alpha_f} \begin{cases} \delta_{m,n} [\frac{3}{2} + 2n] - \delta_{m,n-1} \sqrt{n(n+\frac{1}{2})} - \delta_{n,m-1} \sqrt{(n+1)(n+\frac{3}{2})}, & m, n \geq 1 \\ \delta_{m,0} \frac{3}{2} - \delta_{0,m-1} \sqrt{\frac{3}{2}}, & \text{otherwise.} \end{cases} \quad (\text{E3})$$

The generated  $C_n$ 's must be decomposed on the Cartesian basis  $|\Phi_{n_x n_y n_z}\rangle$  in order to generate the starting coefficients  $C_{\zeta n_z}^{(\text{init})}$  [ $\zeta = (n_x, n_y)$ ] as given in Eq. (4.3).  $\langle \Phi_{n_x n_y n_z} | \Psi_{n00} \rangle$  can be readily computed, so that

$$\langle \Phi_{n_x n_y n_z} | \Psi_{n00} \rangle = \begin{cases} D_{n_x n} D_{n_y n} D_{n_z n}, & \text{if } n_x, n_y, n_z \text{ are even and } \frac{n_x}{2}, \frac{n_y}{2}, \frac{n_z}{2} \leq n \\ 0, & \text{otherwise,} \end{cases} \quad (\text{E4})$$

where

$$D_{n_x n} = (-1)^{\frac{n_x}{2}} \left( \frac{1}{\sqrt{2}\pi^{5/4}} \sqrt{\left( \frac{n_x!}{\Gamma(n_x + 3/2)} \right)} \right)^{\frac{1}{3}} \sqrt{\left( \frac{2^{n_x}}{n_x!} \right)} \Gamma\left( \frac{1}{2} + \frac{n_x}{2} \right) \quad (\text{E5})$$

and, for completeness, where

$$\Phi_{n_x}(x) = \alpha_f^{\frac{1}{4}} \sqrt{\left( \frac{1}{\sqrt{\pi} 2^{n_x} n_x!} \right)} H_{n_x}(\sqrt{\alpha_f} x) \exp(-\alpha_f x^2/2). \quad (\text{E6})$$

Thus, the  $C_{\zeta n_z}^{(\text{init})}$  to be used as input to the evolution calculation are generated.

- 
- [1] Al. B. Zamolodchikov, B. Z. Kopeliovich, and L. I. Lapidus, *Pis'ma Zh. Eksp. Teor. Fiz.* **33**, 612 (1981) [*JETP Lett.* **33**, 595 (1981)].
- [2] G. Bertsch, S. J. Brodsky, A. S. Goldhaber, and J. G. Gunion, *Phys. Rev. Lett.* **47**, 297 (1981).
- [3] V. N. Gribov, *Zh. Eksp. Teor. Fiz.* **56**, 892 (1969) [*Sov. Phys. JETP* **29**, 483 (1969)]; J. Pumplin and M. Ross, *Phys. Rev. Lett.* **21**, 1778 (1968). See also N. N. Nikolaev, *Usp. Fiz. Nauk* **134**, 369 (1981) [*Sov. Phys. Usp.* **24**, 531 (1981)].
- [4] S. J. Brodsky, in *Proceedings of the Thirteenth International Symposium on Multiparticle Dynamics*, edited by W. Kittel, W. Metzger, and A. Stergiou (World Scientific, Singapore, 1982), p. 963.
- [5] A. Mueller, in *Proceedings of the Seventeenth Rencontre de Moriond, Moriond, 1982*, edited by J. Tran Thanh Van (Editions Frontieres, Gif-sur-Yvette, France, 1982), p. 13.
- [6] E. L. Berger and D. Jones, *Phys. Rev. D* **23**, 1521 (1981).
- [7] This has been remarked upon in a different language by H. I. Miettinen and J. Pumplin, *Phys. Rev. Lett.* **42**, 204 (1979).
- [8] J. Hüfner, B. Povh, and S. Gardner, *Phys. Lett. B* **238**, 103 (1990).
- [9] E. Quack, *Nucl. Phys.* **B364**, 321 (1991).
- [10] J.-P. Blaizot, R. Venugopalan, and M. Prakash, *Phys. Rev. D* **45**, 814 (1992).
- [11] Y. Nambu, *Phys. Rev.* **106**, 1366 (1957); J. J. Sakurai, *Ann. Phys.* **11**, 1 (1960); M. Gell-Mann and F. Zachariassen, *Phys. Rev.* **124**, 953 (1961).
- [12] S. J. Brodsky and A. H. Mueller, *Phys. Lett. B* **206**, 685 (1988).
- [13] G. R. Farrar, L. L. Frankfurt, M. I. Strikman, and H. Liu, *Phys. Rev. Lett.* **64**, 2996 (1990).
- [14] B. Z. Kopeliovich and B. G. Zakharov, *Phys. Rev. D* **44**, 3466 (1991).
- [15] B. K. Jennings and G. A. Miller, *Phys. Rev. D* **44**, 692 (1991).
- [16] J. D. Bjorken, in *Hadron Final States in Deep Inelastic Processes*, edited by K. Korner, *Lecture Notes in Physics* Vol. 56 (Springer, New York, 1976), p. 93.
- [17] O. V. Kancheli, *Pis'ma Zh. Eksp. Teor. Fiz.* **18**, 465 (1973) [*JETP Lett.* **18**, 274 (1973)]; **22**, 491 (1975) [**22**, 237 (1975)].
- [18] R. P. Feynman, *Photon-Hadron Interactions* (Addison-Wesley, New York, 1972), p. 109.
- [19] L. Frankfurt and M. Strikman, *Prog. Part. Nucl. Phys.* **27**, 135 (1991).
- [20] B. Z. Kopeliovich, *Fiz. Elem. Chastits At. Yadra* **21**, 117 (1990) [*Sov. J. Part. Nucl.* **21**, 49 (1990)].
- [21] E. Eichten, K. Gottfried, T. Kinoshita, K. D. Lane, and T. M. Yan, *Phys. Rev. D* **21**, 203 (1980). See also E. Eichten *et al.*, *ibid.* **17**, 3090 (1978), and references therein.
- [22] W. Buchmüller and S.-H. H. Tye, *Phys. Rev. D* **24**, 132 (1981).

- [23] S. Godfrey and N. Isgur, Phys. Rev. D **32**, 189 (1985).
- [24] J. Kogut and L. Susskind, Phys. Rev. D **12**, 2821 (1975).
- [25] The  $J/\psi$  rms  $q\bar{q}$  separation is reported to be 0.47 fm by Eichten *et al.* in Ref. [21]. Repeating their numerical calculations for  $\langle r^2 \rangle^{\frac{1}{2}}$ , I find  $\langle r^2 \rangle_{J/\psi}^{\frac{1}{2}} = 0.38$  fm and  $\langle r^2 \rangle_{\psi'}^{\frac{1}{2}} = 0.76$  fm rather than the reported values of 0.47 fm and 0.96 fm, even though I reproduce their mass eigenstate spacings quantitatively. A variational calculation for the ground state with an exponential or Gaussian *Ansatz* yields a rms  $q\bar{q}$  separation of 0.41 fm or 0.37 fm, respectively, for  $J/\psi$ ; one would expect that the exact rms  $q\bar{q}$  separation for  $J/\psi$  should lie between these two values. My calculations are also quite close to the values reported by Godfrey and Isgur, Ref. [23], that is, 0.37 fm and 0.69 fm for  $J/\psi$  and  $\psi'$ , respectively.
- [26] J. W. Flower and S. W. Otto, Phys. Lett. **160B**, 128 (1985).
- [27] J. Flower, Nucl. Phys. **B289**, 484 (1987).
- [28] N. Isgur and J. Paton, Phys. Rev. D **31**, 2910 (1985).
- [29] A strictly uniform field bounded by a circular region cannot be confined entirely within the boundary, as Gauss's law requires that the parallel component of the electric field be continuous at the surface. However, the numerical difference between matrix elements computed with the "true" field and the one which is purely uniform should be small – especially when the  $c\bar{c}$  state is small with respect to the size of the nucleon.
- [30] Comparing best fits of the "Y" vs "Δ" models of confinement yields an estimate of the geometry of the ground state baryon. From geometrical considerations, Dosch and Müller find (see Ref. [31])
- $$1 \leq \frac{V_Y^{\text{conf}}}{V_\Delta^{\text{conf}}} \leq \frac{2}{\sqrt{3}} \sim 1.155$$
- for all string configurations, where  $V_Y^{\text{conf}} = b \sum_{i=1}^3 |\vec{r} - \vec{r}_{\text{junction}}|$  and  $V_\Delta^{\text{conf}} = \frac{1}{2} b \sum_{i<j} r_{ij}$ . The lower limit is realized for a quark-diquark configuration, whereas the upper limit is realized when all the quarks are equidistant from each other. Flower's (see Ref. [27]) fits of his lattice simulations to the "Y" and "Δ" models support the equidistant quark arrangement with  $b_Y^{qqq} \approx b^{qq} \approx 0.18$  GeV<sup>2</sup>, and the recent relativized quark model work of Capstick and Isgur (see Ref. [32]) qualitatively supports this picture, with  $V_Y^{\text{conf}}/V_\Delta^{\text{conf}} = 1.099$  and  $b_Y^{qqq} = 0.15$  GeV<sup>2</sup>.
- [31] H. G. Dosch and V. Müller, Nucl. Phys. **B116**, 470 (1976).
- [32] S. Capstick and N. Isgur, Phys. Rev. D **34**, 2809 (1986).
- [33] This string tension will be used to determine the flux-tube width  $\tau$ ; however, in principle, the existence of a finite string width modifies the string tension. I will not bother to iterate these two quantities to self-consistency, as the precision of the model does not warrant it.
- [34] An estimate of the dressing of the  $qqq$  "bag" by virtual  $q\bar{q}$  pairs is outside the scope of this qualitative model.
- [35] M. D. Sokoloff *et al.*, Phys. Rev. Lett. **57**, 3003 (1986). These are the highest-energy photoproduction data available.
- [36] A. Di Giacomo, M. Maggiore, and Š. Olejník, Phys. Lett. B **236**, 199 (1990).
- [37] The  $J = 1$ ,  $s$ -wave  $c\bar{c}$  states (e.g.,  $J/\psi$ ,  $\psi'$ ), though, have zero magnetic dipole moment.
- [38] The claim is that the momentum of charmonium is low enough that edge effects in the passage of a flux tube through charmonium may be neglected (putting aside the parton model arguments for the moment), but yet high enough that the fields of the flux tubes may be taken to be purely transverse. For the energy range  $E_\gamma = 8.5$  to 20 GeV, the momentum of  $J/\psi$  ranges from 7.2 to 19.7 GeV for the exclusive process considered, so that  $\gamma$  ranges 2.5 to 6.4. Thus, the magnitude of the transverse electric field is 2.5 times that of the longitudinal field at the lowest energy considered. At this energy the width of the nucleon flux tube is the same size as the  $c\bar{c}$  wave function. At the highest energy considered, the flux-tube width is half the size of the  $c\bar{c}$  wave function. The approximations made seem roughly reasonable.
- [39] H. I. Miettinen and J. Pumplin, Phys. Rev. D **18**, 1696 (1978).
- [40] Although this application is novel, flux-tube models of nuclear matter do exist in the literature (see Refs. [41–43]). In this work there is no attempt to demonstrate that the flux-tube nucleus is either self-bound or that its energy saturates with increasing density. Although these issues are obviously essential to nuclear structure physics, they are irrelevant here: in the large  $x_F$  limit, the nucleus is an inert object.
- [41] C. J. Horowitz, E. Moniz, and J. W. Negele, Phys. Rev. D **31**, 1689 (1985).
- [42] C. J. Horowitz and J. Piekarewicz, Nucl. Phys. **A536**, 669 (1992).
- [43] P. J. S. Watson, Nucl. Phys. **A494**, 543 (1989); A. B. Migdal and P. J. S. Watson, Phys. Lett. B **252**, 32 (1990).
- [44] H. R. Collard, L. R. B. Elton, and R. Hofstadter, *Nuclear Radii*, group I, volume 2 in *Landolt-Börnstein Numerical Data and Functional Relationships in Science and Technology*, edited by H. Schopper (Springer-Verlag, Berlin, 1967).
- [45] F. E. Close, *An Introduction to Quarks and Partons* (Academic Press, London, 1979), p. 354ff.
- [46] The reader is reminded that the minimum-uncertainty wave packet is of Gaussian form.
- [47] This was previously noticed, for flux tubes of infinite length, by J. Hüfner, B. Povh, and S. Gardner, Phys. Lett. B **238**, 103 (1990). They report a  $1/N$  behavior in large  $N$  as well.
- [48] I thank S. Koonin for this observation.
- [49] R. Glauber, "High Energy Collision Theory," in *Lectures in Theoretical Physics, Boulder, 1958*, edited by W. E. Brittin and L. G. Dunham (Interscience, New York, 1959), p. 315.
- [50] J. D. Walecka, unpublished lecture notes.
- [51] T. H. Bauer, R. D. Spital, D. R. Yennie, and F. M. Pipkin, Rev. Mod. Phys. **50**, 261 (1978).
- [52] L. L. Nemenov, Yad. Fiz. **34**, 1306 (1981) [Sov. J. Nucl. Phys. **34**, 726 (1981)].
- [53] V. L. Lyuboshitz and M. I. Podgoretskiĭ, Zh. Eksp. Teor. Fiz. **81**, 1556 (1981) [Sov. Phys. JETP **54**, 827 (1981)].
- [54] A. S. Pak and A. V. Tarasov, Yad. Fiz. **45**, 145 (1987) [Sov. J. Nucl. Phys. **45**, 92 (1987)].
- [55] B. G. Zakharov, Yad. Fiz. **46**, 148 (1987) [Sov. J. Nucl. Phys. **46**, 92 (1987)].
- [56] L. G. Afanas'ev *et al.*, Yad. Fiz. **50**, 7 (1989) [Sov. J. Nucl. Phys. **50**, 4 (1989)].
- [57] The contribution to  $\frac{P_{f \leftarrow i}(1)}{P_{f \leftarrow i}(0)}$  from elastic scattering can be computed via

$$\begin{aligned}
P_{f\leftarrow i}^{\text{el}}(1) &= |\langle \phi_f | \left[ 1 - \exp \left( i \frac{e\vec{\tau}_R}{\hbar} \vec{E}_{\text{str}} \cdot \vec{r} \right) \right] | \psi_i \rangle|^2 \\
&= |\langle f | i \rangle|^2 - 2 \langle f | i \rangle \int d^2 \vec{s} J_0 \left( \frac{k_{\text{Regge}} \tau}{\hbar c} \Theta(R-s) s \right) \rho_{fi}(\vec{s}) \\
&\quad + \iint d^2 \vec{s} d^2 \vec{s}' J_0 \left( \frac{k_{\text{Regge}} \tau}{\hbar c} |\Theta(R-s) \vec{s} - \Theta(R-s') \vec{s}'| \right) \rho_{fi}(\vec{s}) \rho_{fi}(\vec{s}').
\end{aligned}$$

Here the wave functions are assumed real. For the initial-state wave function used in Eq. (3.12), with the model parameters,  $\sigma_{J/\psi-N}^{\text{el}} = 0.04$  mb, whereas for  $|\psi_i\rangle = |\psi_{J/\psi}\rangle$ ,  $\sigma_{J/\psi-N}^{\text{el}} = 0.56$  mb. Note that  $\sigma_{J/\psi-N}^{\text{el}} \equiv \pi R_p^2 \left( \frac{P_{f\leftarrow i}(1)}{P_{f\leftarrow i}(0)} \right) P_{f\leftarrow i}^{\text{el}}(1)$ . Both of the above cross sections are much smaller than the corresponding absorption cross sections, Eqs. (3.12) and (3.13).

- [58] The possibility that  $\sigma_{J/\psi-N}^{\text{abs}}$  may exceed  $\sigma_{\psi'-N}^{\text{abs}}$  has also been noted by J.-P. Blaizot, R. Venugopalan, and M. Prakash, Phys. Rev. D **45**, 814 (1992).
- [59] F. E. Low, Phys. Rev. D **12**, 163 (1975).
- [60] S. Nussinov, Phys. Rev. Lett. **34**, 1286 (1975); Phys. Rev. D **14**, 246 (1976).
- [61] C. Mariotti, NMC Collaboration, at the Lepton-Photon Conference, 1991 (unpublished). I thank N. N. Nikolaev for communicating their results to me.
- [62] Indeed, the higher mass  $c\bar{c}$  states should be off-shell with momentum equal to that of the  $J/\psi$  in order for the coherence effects discussed to be included; yet, the initial wave packet is modeled by an on-shell set of states. The point is to demonstrate that this assumption is inconsequential at moderately high energies.
- [63] For this case, relaxing the  $E \gg m_{J/\psi}$  assumption yields a shift of  $\Delta p^2 / (2m_{J/\psi}) \sim 7 \times 10^{-3}$  GeV, which is still

negligible relative to  $\delta$ . The corrections due to nonrelativistic boosts can become quite nontrivial for highly excited states; yet, these corrections always grow smaller as  $E_\gamma$  increases.

- [64] U. Camerini *et al.*, Phys. Rev. Lett. **35**, 483 (1975).
- [65] M. Binkley *et al.*, Phys. Rev. Lett. **48**, 73 (1982).
- [66] S. J. Brodsky and P. Hoyer, Phys. Rev. Lett. **63**, 1566 (1989).
- [67] R. L. Anderson *et al.*, Phys. Rev. Lett. **38**, 263 (1977).
- [68] K. Gottfried and D. R. Yennie, Phys. Rev. **182**, 1595 (1969).
- [69] I believe the cross section in Eq. (5.5) should be the absorption cross section; however, as  $\sigma^{\text{abs}} \approx \sigma^{\text{tot}}$  (see Ref. [57]), the distinction is not very important. In the concluding discussion, I shall suppress this issue entirely, and merely refer to the “total cross section.” This point has also been recently noticed by A. Kohama, K. Yazaki, and R. Seki, Nucl. Phys. **A536**, 716 (1992).
- [70] A. S. Carroll *et al.*, Phys. Rev. Lett. **61**, 1698 (1988).
- [71] J. Badier *et al.*, Z. Phys. C **20**, 101 (1983).
- [72] R. Vogt, S. J. Brodsky, and P. Hoyer, Nucl. Phys. **B360**, 67 (1991).
- [73] B. H. Denby *et al.*, Phys. Rev. Lett. **52**, 795 (1984).
- [74] Y. Lemoigne *et al.*, Phys. Lett. **113B**, 509 (1982).